8-2016

Electron Transport to Photosystem I by Soluble Carriers: Evolution of the Interacting Pair

Khoa Dang Nguyen
University of Tennessee, Knoxville, knguyen4@vols.utk.edu

To the Graduate Council:

I am submitting herewith a dissertation written by Khoa Dang Nguyen entitled "Electron Transport to Photosystem I by Soluble Carriers: Evolution of the Interacting Pair." I have examined the final electronic copy of this dissertation for form and content and recommend that it be accepted in partial fulfillment of the requirements for the degree of Doctor of Philosophy, with a major in Biochemistry and Cellular and Molecular Biology.

Barry D. Bruce, Major Professor

We have read this dissertation and recommend its acceptance:

Gladys Alexandre, Engin Serpersu, Paul Frymier, Brad Binder

Accepted for the Council:

Carolyn R. Hodges

Vice Provost and Dean of the Graduate School

(Original signatures are on file with official student records.)

Electron Transport to Photosystem I by Soluble Carriers: Evolution of the Interacting Pair

A Dissertation Presented for the
Doctor of Philosophy
Degree
The University of Tennessee, Knoxville

Khoa Dang Nguyen
August 2016

This dissertation is dedicated to
my loving mother - Tram Ho,
my grandparents - Thanh Ho and Sanh Pham,
along with my aunts and uncles who raised me.

Without my family's endless love and support,
this would not be possible.

Acknowledgements

Thank you to all who believed in me and gave me a chance. A special thanks to my committee members, Dr. Barry Bruce, Dr. Brad Binder, Dr. Paul Frymier, Dr. Gladys Alexandre, and Dr. Engin Serpersu for all their guidance and support throughout my graduate career at UT.

Abstract

Oxygenic photosynthesis is driven via sequential action of Photosystem II (PSII) and (PSI) reaction centers via the Z-scheme. Both of these pigment–membrane protein complexes are found in cyanobacteria, algae, and plants. PSI, unlike PSII, is remarkably stable and does not undergo limiting photo-damage. This stability, as well as other fundamental structural differences, makes PSI the most attractive reaction centers for applied photosynthetic applications. These applied applications exploit the efficient light harvesting and high quantum yield of PSI where the isolated PSI particles are redeployed providing electrons directly as a photocurrent or, via a coupled catalyst to yield H_2. Here, we explore the reduction rate of photo-oxidized PSI with various natural and artificial electron donors. The electron transfer rate from various donors to oxidized PSI has been measured for a wide range of photosynthetic organisms encompassing cyanobacteria, algae, and plants, mainly by transient absorption spectroscopy. We utilize a Joliot-type, LED-driven, pump-probe spectrometer, along with molecular biology, genomics, and bioinformatics approaches to further investigate the relationship of this ever-evolving interacting pair with their electron transfer rates. We also implement our expanding biochemistry toolkit in hopes to increase this rate for applied photosynthesis applications, where it has become a bottle-neck for many bio-energy related bio-hybrid devices.

Table Of Contents

Page

List of Tables

Chapter 1: Introduction and Literature Review

Chapter 3: Electrostatic Mutants of Cytochrome - PSI Pair

Chapter 4: Other Cytochrome/PSI Strategies for Applied Photosynthesis

Chapter 5: Differential PsaF Recognition via Western Blot

List of Figures

Chapter 1: Introduction and Literature Review

Chapter 2: Materials and Methods

Chapter 3: Electrostatic Mutants of Cytochrome - PSI Pair

Chapter 4: Other Cytochrome/PSI Strategies for Applied Photosynthesis

Chapter 5: Differential PsaF Recognition via Western Blot

Chapter 1

Introduction and Literature Review

A. Overview of Photosynthetic Electron Transport

Oxygenic Organisms

Oxygenic photosynthesis is the primary reaction that converts solar energy into chemical energy for almost all life on Earth carried out by cyanobacteria, green algae, and plants. This process is debated to have started several hundred million years before the Great Oxygenation Event (GOE), which occurred about 2.4 billion years ago (Holland 2006, Lyons, Reinhard et al. 2014).

In cyanobacteria, algae and plants, this process of photosynthesis releases oxygen, making it oxygenic photosynthesis. Although there are some differences between oxygenic photosynthesis in plants, algae, and cyanobacteria, the overall process is quite similar in these organisms, as they have evolved from one another. The light reaction of photosynthesis is driven by the trans-membrane complexes of Photosystem I (PSI) and Photosystem II (PSII), which use the trapped sunlight to excite the primary donors (P_{700} and P_{680}, respectively) leading to the linear electron transfer reactions in the thylakoid membrane (Blankenship 2010). Water splitting is facilitated by the excitation of the P_{680} chlorophyll in PS II by a photon of light, leading to the generation of O_2, a proton, and an electron (Figure 1-1A). Electrons are then carried my membrane soluble plastoquinones, reduced to plastoquinol, to the Cytochrome b_6f complex where protons are pumped from the stroma to the

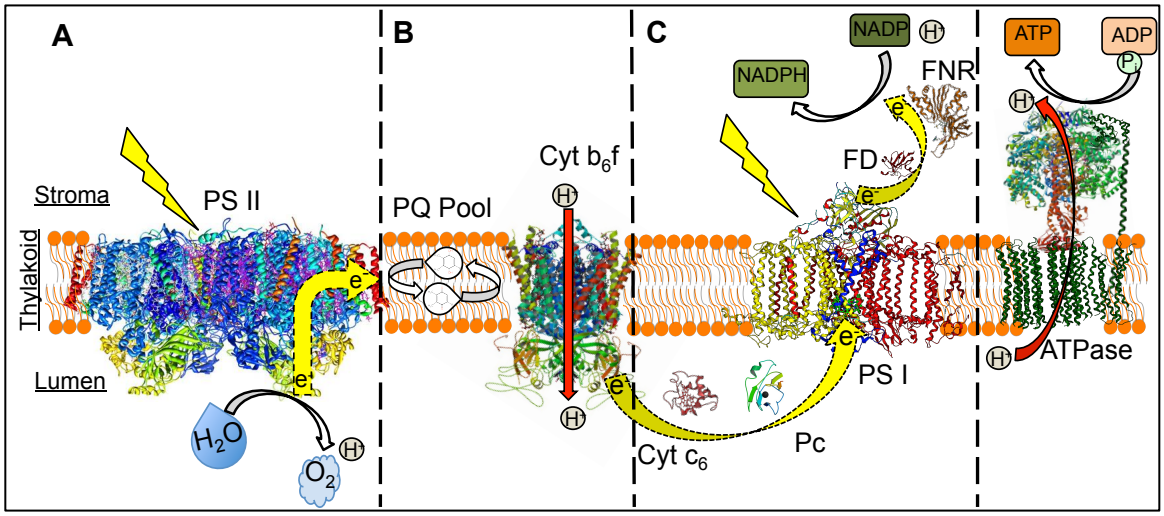

Figure 1-1. Electron (e^-) transport chain in thylakoid membranes.

A) Water splitting is facilitated by the excitation of the P_{680} chlorophyll in Photosystem II (PSII) by a photon of light, leading to the generation of O_2, a proton, and an electron. B) Electrons are then carried my membrane soluble plastoquinones (PQ Pool), reduced to plastoquinol, to the Cytochrome b_6f (Cyt b_6f) complex where protons are pumped from the stroma to the lumen. C) Lumen soluble metallo-proteins, cytochrome c_6 (cyt c_6) or plastocyanin (PC) then shuttle electrons from the Riske center of Cyt b_6f to the special pair chlorophylls P_{700} of Photosystem I (PSI). Upon photon excitation, electrons at P_{700} are funneled through PSI to the iron-sulfur centers on the stromal end, leading to the eventual reduction of NADP to NADPH.

lumen (Figure 1-1B) (Blankenship 2010). Lumen soluble metallo-proteins (cyt c_6 or PC) then shuttle electrons from the Cytb_6f complex to the special pair chlorophylls P_{700} of PSI (Figure 1-1C). Upon photon excitation, electrons at P_{700} are funneled through PSI to the iron-sulfur centers on the stromal end, leading to the eventual reduction of NADP to NADPH by FNR(Blankenship 2010).

Photosystem II

Photosystem II is a large and complex redox enzyme composed of at least 17 protein subunits and a large number of cofactors specialized in light harvesting, photo-protection, and electron and proton transfer reactions including water oxidation. Water oxidation occurs at the PSII tetra-manganese cluster (Mn_4CaO_5), where four electrons are extracted from two water molecules, with the release of four protons into the thylakoid lumen and O_2 as a byproduct (Cardona, Sedoud et al. 2012, Dau, Zaharieva et al. 2012, Muh, Glockner et al. 2012, Perez Navarro, Ames et al. 2013). The reaction center cofactors involved in charge separation and water oxidation are coordinated by a pair of homologous protein subunits, known as D1 (PsbA) and D2 (PsbD).

The D1 protein provides most of the ligands to the Mn_4CaO_5 cluster where water oxidation occurs (Ferreira, Iverson et al. 2004, Kawakami, Umena et al. 2011). Electrons that are released from water, reduce P_{680} which are then, with another photon of light, sent to reduce the primary electron acceptors of PSII, Q_A and Q_B, on the stromal side of the membrane. Once it has accepted two electrons, Q_B is released from PSII into the plastoquinone pool and reduced plastoquinol docks to the Qo site of Cyt b_6f.

Cytochrome b_6f

The cytochrome b_6f complex is one of the three integral oligomeric membrane protein complexes involved in linear or noncyclic electron transport in the chloroplast thylakoid and cyanobacterial membrane systems that participate in oxygenic photosynthesis. It is located between PSII and PSI both electrochemically and in the pathways of electron transport (Cramer and Trebst 1991, Szczepaniak, Huang et al. 1991). Its photosynthetic electron transfer reactions can also occur in the dark. It is phylogenetically related to the cytochrome bc_1complex of mitochondria and photosynthetic bacteria (Widger, Cramer et al. 1984, Widger, Cramer et al. 1984), with which there are many structure-function similarities. From the cytochrome b_6f complex, electrons are shuttled by a soluble metalloprotein to the lumenal side of PSI.

Photosystem I

PSI catalyzes the sunlight-driven trans-membrane electron transport with the oxidation of a soluble carrier (plastocyanin/cytochrome c_6) in the inner side of the thylakoid membrane (lumen) and the reduction of ferredoxin (FD) in the stroma. PSI is the most efficient photoelectric complex in nature with the quantum efficiency of nearly 100%, so that every photon absorbed by PSI is used for electron excitation (Ben-Shem, Frolow et al. 2004, Ben-Shem, Frolow et al. 2004, Nelson and Yocum 2006, Amunts, Drory et al. 2007, Amunts and Nelson 2009, Amunts, Toporik et al. 2010).

PSI also plays important roles in photosynthetic acclimation to the changing environment mainly by participating in PSI cyclic electron transfer (CET), state

transitions and adjustment of photosystem stoichiometry. In addition, oxygenic organisms can redistribute excitation energy between PSI and PSII by state transitions (Bellafiore, Barneche et al. 2005, Grieco, Tikkanen et al. 2012). During short-term adaptations of photosynthesis to changes of light quality, phycobilisome in cyanobacteria and light harvesting complex (LHC) II in the green lineage can relocate between PSI and PSII to balance the distribution of the absorbed light energy (Minagawa 2011, Rochaix 2011, Kana, Kotabova et al. 2014, Mullineaux 2014, Rochaix 2014). State transitions are controlled by redox state of plastoquinone in cyanobacteria: reduction of plastoquinone triggers adaptation to "state II" in which more energy is transferred to PSI, while oxidation of plastoquinone triggers energy transfer to PSII (Mullineaux and Allen 1990, Mullineaux 2014). However, no mutants related to state transitions have been identified in cyanobacteria so far. In the algae Chlamydomonas and plants, the regulation of redox state of plastoquinone pool on state transitions is clearly more established as compared to cyanobacteria (Pesaresi, Pribil et al. 2011, Rochaix 2011, Grieco, Tikkanen et al. 2012). Under conditions when PSII is preferentially excited, the plastoquinone pool becomes reduced, which favors the binding of plastoquinone to the Q_0 site of the Cyt b_6f complex and leads to the activation of LHCII phosphorylation by Stt7/ STN7 kinase. The phosphorylated LHCII migrates to PSI, thus increasing the cross-section of the PSI antenna (Depege, Bellafiore et al. 2003, Bellafiore, Barneche et al. 2005, Bonardi, Pesaresi et al. 2005).

Photosystem I participates in photosynthetic acclimation processes by being involved in cyclic electron transfer and state transitions for sustaining efficient

photosynthesis. The PSI complex is highly conserved from cyanobacteria to higher plants and contains the light harvesting complex and the reaction center complex. The assembly of the PSI complex is highly complicated and involves the concerted assembly of multiple subunits and hundreds of cofactors (Amunts, Toporik et al. 2010).

The biochemical and physiological functions of PSI depend on the complex structure of PSI in which many protein subunits and cofactors are precisely assembled (Figure 1-2). PSI represents one of the largest and most complex macromolecular assemblies in nature and the basic structure of PSI has been conserved from cyanobacteria to higher plants during the course of evolution (Nelson and Yocum 2006, Jensen, Bassi et al. 2007). The X-ray crystal structures of PSI from cyanobacteria and higher plants have been determined at 2.5A and 3.3A resolutions, respectively (Fromme, Jordan et al. 2001, Jordan, Fromme et al. 2001, Amunts, Drory et al. 2007, Amunts, Toporik et al. 2010). While most of the cyanobacterial PSI complex functions as a trimer, in which each monomer contains 12 subunits and 127 cofactors(Fromme, Jordan et al. 2001, Jordan, Fromme et al. 2001). The PSI complex from higher plants functions as a large monomer containing at least 19 subunits and nearly 200 cofactors (Amunts, Drory et al. 2007, Amunts, Toporik et al. 2010). Of these subunits at least five are chloroplast encoded

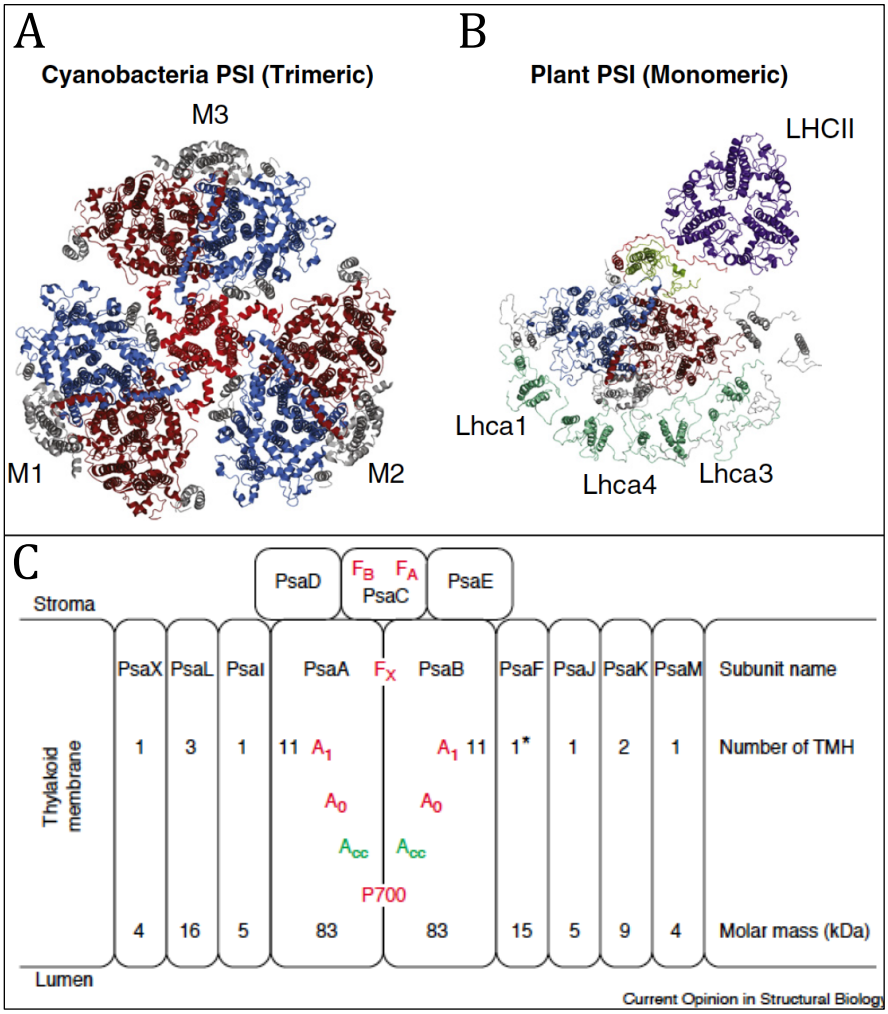

Figure 1-2. Photosystem I (PSI) Structures.

A) PSI from cyanobacteria (*Thermosynechococcus elongatus* ,PDB ID: 1JB0). M1-3 denote individual monomers comprising the native trimer. Major subunits are shown: PsaA(burgundy), PsaB(blue), PsaL(red), and other subunits (gray). B) PSI from plant (*Pisum sativum* PDB ID: 2O01). LHCI subunits are shown in teal (Lhca1-4) and LHCII in violet. Major subunits are shown: PsaA(burgundy), PsaB(blue),PsaL(olive), PsaH(red), and other subunits (gray). C) Schematic description of the subunit composition of PSI in cyanobacteria. Under each subunit name (PsaA-PsaF, PsaI-M, PsaX), the number of TMHs within each subunit and the molar mass (kDa) of the subunit are indicated. Cofactors of the ETC are shown in red (P_{700}, A_0, A_1, F_X, F_A, F_B). *A) and B) were from (Nguyen and Bruce 2014). C) was from (Saenger, W., P. Jordan and N. Krauss 2002).

(PsaA, -B, -C, -I and -J) and six nuclear-encoded polypeptides (PsaD, -E, -F, -G, -H and -K) (Shen, Antonkine et al. 2002, Shen, Zhao et al. 2002).

Of the PSI subunits, two large subunits PsaA and PsaB form a heterodimer that constitutes the core of the reaction center and harbors the electron transport chain. PsaC contains [4Fe–4S] clusters F_A and F_B and also participates in the electron transfer reactions. While the small PsaC, PsaD and PsaE subunits in the stromal side are essential for the binding of ferredoxin, the PsaF and PsaN subunits are involved in the interaction with plastocyanin/cytochrome c_6 in the lumen(Farah, Frank et al. 1995, Haldrup, Naver et al. 1999, Naver, Haldrup et al. 1999, Jensen, Gilpin et al. 2000). The other small integral subunits are either important for the stability of the complex in cyanobacteria or involved in the interaction with LHCI and LHCII in higher plants(Jensen, Gilpin et al. 2000, Ihalainen, Jensen et al. 2002).

PsaC has been described as a ferredoxin-like protein (Newman and Gray 1988). It however contains two domains which are absent from 2[4Fe-4S] ferredoxins; an internal loop between the two [4Fe-4S] cluster binding motifs and a C-terminal extension. These additional sequences have been proposed to interact with the PsaA/B heterodimer and the PsaD subunit, respectively (Naver, Scott et al. 1996). PsaC has been shown to be essential for *in-vivo* assembly of PSI in *Chlamydomonas reinhardtii* (Takahashi, Goldschmidt-Clermont et al. 1991). The PsaD and PsaE subunits are located on the stromal side of PSI and interact with PsaC (Jansson, Andersen et al. 1996). PsaD is required for stable assembly of PsaC and PsaE in PSI complex reconstitution assays (Zhao, Warren et al. 1990, Li, Zhao et al. 1991). Other chemical cross-linking assays revealed a direct interaction between

PsaD and Fd (Zanetti and Merati 1987, Zilber and Malkin 1988, Andersen, Scheller et al. 1992, Lelong, Setif et al. 1994). Inactivation of PsaD demonstrated its role for efficient Fd reduction(Chitnis, Reilly et al. 1989, Chitnis, Reilly et al. 1989, Xu, Jung et al. 1994). PsaE has also been shown to interact with ferredoxin:NADP1-oxidoreductase as well as Fd and to be required for Fd reduction(Andersen, Scheller et al. 1992, Rousseau, Setif et al. 1993, Sonoike, Hatanaka et al. 1993, Xu, Jung et al. 1994).

The PsaF subunit provides a docking site for plastocyanin and Cyt c_6 on the lumenal side of PSI, and is required for their fast photo-oxidation in *C. reinhardtii*, but not in cyanobacteria (Xu, Odom et al. 1994, Xu, Yu et al. 1994, Farah, Frank et al. 1995, Drepper, Hippler et al. 1996, Hippler, Reichert et al. 1996, Hippler, Riedel et al. 1996). Interaction between the transmembrane domain of PsaF and the stromal subunit PsaE has been reported (Xu, Yu et al. 1994, Jansson, Andersen et al. 1996).

Although the current literature and knowledge of the PSI structure and function has advanced, how these subunits and cofactors are assembled into a functional complex in the thylakoid membrane is largely unknown (Schlodder, Hussels et al. 2011). Understanding the PSI complex assembly process will lead to the understanding of its high efficiency of energy transformation and its potential application in biomimetic solar-to-fuel system. Compared to the PSII assembly process, PSI assembly is much faster, making it very difficult to isolate the assembly intermediate complex (Schlodder, Hussels et al. 2011). Data collected from genetics, structural biology, and in-vitro reconstitution studies from various oxygenic

organisms has yielded a preliminary understanding of PSI assembly procedure (Schlodder, Hussels et al. 2011).

B. Cyanobacteria and Thylakoid Ultrastructure (Cyanobacteria vs. Plastids)

The ability to perform oxygenic photosynthesis was passed on to algae and higher plants by an endosymbiotic event that turned a cyanobacterium into a cell organelle, the chloroplast. The photosynthetic machinery of both, cyanobacteria and chloroplasts, is located on a special internal membrane system, the thylakoids. Thanks to the unique architecture of this membrane cyanobacteria and chloroplasts convert solar energy into chemical energy with an efficiency significantly better than any man-made photovoltaic system. Therefore, the ability of the cell to build and alter this membrane system is essential for oxygenic photosynthesis.

The additional compartment that the thylakoid network creates in cyanobacterial cells and in chloroplasts is an important feature that distinguishes these from bacteria performing anoxygenic photosynthesis. In these latter organisms, the internal membranes are invaginations still continuous with the plasma membrane (Olive, Wollman et al. 1981, Hagemann, Gad'on et al. 1995). In mature chloroplasts and in cyanobacteria it is assumed that the thylakoids are no longer connected to the inner envelope or the plasma membrane, respectively, because no such continuum can be observed in electron microscopic pictures.

In cyanobacteria and many algae, thylakoids consist mainly of single layers formed by long lamellae. The structure of the thylakoid membrane in a fully mature chloroplast is more complex. In early electron microscopic studies a model for the thylakoid structure as a huge intertwined network of stroma lamellae connecting grana stacks was proposed which still stand today with little alterations (Small and Anderson 1988). Grana are short, disc-shaped lamellae closely packed to form stacks. These stacks are interconnected by stroma lamellae which also form prolonged extensions into the stroma. The arrangement of the thylakoid membrane system creates a single huge compartment inside the chloroplast, the thylakoid lumen. In addition to creating a single internal space this structure builds a membrane surface that is much larger than a simple invagination of the inner envelope would generate.

The dominant protein complexes of the thylakoids are Photosystems I (Chitnis 2001, Xu, Tang et al. 2001) and II (Hankamer, Barber et al. 1997, Hankamer, Nield et al. 1997, Morris, Hankamer et al. 1997) and their associated light harvesting antenna, the cytochrome b_6f complex (Berry, Guergova-Kuras et al. 2000) and the proton-translocating ATP synthase (Groth and Schirwitz 1999). These complexes comprise not only many peripheral and integral proteins but also a variety of pigments and co-factors (Wollman, Minai et al. 1999). Their assembly is, therefore, a complex process and requires a larger number of auxiliary and regulatory factors (Wollman, Minai et al. 1999, Choquet and Vallon 2000). These factors are involved in the membrane integration, modification and later degradation of the proteinaceous components and are also required for the addition of the pigments

and co-factors. To complicate matters, certain components, like the two photosystems, are unevenly distributed in the thylakoid membrane network. While photosystem I is most abundant in the non-stacked stroma lamellae, photosystem II is the dominating component of the grana stacks (Albertsson 1995). Thus thylakoid biogenesis and maintenance have to assure not only the arrangement of a functional but at the same time asymmetric architecture of both the lipid and the protein components of this membrane. Despite the importance that the thylakoid membrane system has for photosynthesis and the energy metabolism of plants and cyanobacteria, the molecular processes connected to the origin, synthesis, maintenance and adaptation of these membranes remain elusive.

C. Discussion of Internal PSI/e^- transport

The primary photochemical event in Photosystem I (PSI) is started by the absorption of light by antenna chlorophyll molecules with subsequent energy travelling to the specialized reaction center P_{700}. Charge separation takes place within 10 ps between the primary donor P_{700}, a chlorophyll dimer, and the primary acceptor A_0, a chlorophyll monomer (Kirilovsky, Boussac et al. 1992, Hastings, Hoshina et al. 1995, Hastings, Reed et al. 1995) (Figure 1-3). This step is followed by subsequent stages of charge stabilization on a series of electron carriers, including A_l (a phylloquinone) and three [4Fe-4S] clusters, F_x, F_A, and F_B. Whereas P_{700}, A_0, A_1, and F_X are bound to the PsaA/PsaB reaction center heterodimer, the

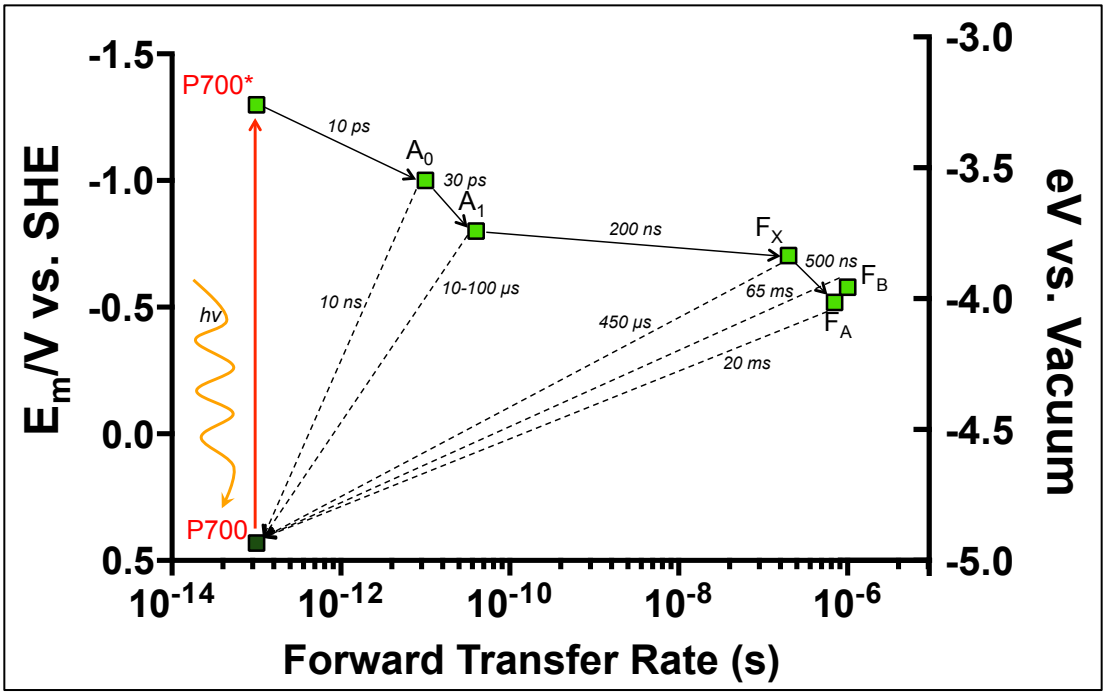

Figure 1-3. Kinetics of e^- transfer in Photosystem I (PSI).

After light excitation of P_{700} to P_{700}*, electrons travel downstream in energy to cofactors A_0, A_1, F_X, F_A, F_B. Forward e^- transfer lifetimes are shown (solid black arrows) on a log scale against the midpoint potential (mV) of the cofactors. Backward e^- transfer (charge recombination) lifetimes are shown (dashed arrow) from cofactors back to P_{700}. (Nguyen and Bruce 2014)

terminal clusters F_A and F_B are located on the tightly bound PsaC subunit (Xu and Chitnis 1995, Xu, Hoppe et al. 1995).

Many initial studies in PSI were carried out by analysis of the kinetics of photo-induced optical absorbance changes of the electron-transport components, especially that of the primary donor, P_{700}. Photo-oxidation of P_{700} is characterized by a difference spectrum with large negative absorption changes (photo-bleaching) around 430 and 700 nm and smaller positive absorption changes around 450 and 820 nm (Hiyama and Ke 1972). In spite of the about 8-10 times lower extinction coefficient compared with 700 nm, the spectral region around 820 nm provides advantages for monitoring the changes in redox state of P_{700} because neither charge separation nor chlorophyll fluorescence are induced by light in this spectral region, and absorbance changes may be monitored at relatively high chlorophyll concentrations in the sample. In the absence of soluble electron donors and acceptors, charge separation in isolated PSI preparations is followed by charge recombination with one or more of the bound electron acceptors, and can be measured by the decay of the photo-induced absorbance change of P_{700}. In isolated PSI complexes that contain the F_A and F_B clusters as the terminal acceptors, charge recombination takes place with a half-time of about 20 - 65 ms (Hiyama and Ke 1972). The kinetics of the back-reactions of earlier electron acceptors are observed either upon chemical pre-reduction of the F_A and F_B clusters (Sauer, Mathis et al. 1978) or in PSI-core preparations (Brettel and Golbeck 1995). The half-time for the F_x back-reaction at room temperature was found to be 250 μs in a PSI complex with F_A and F_B reduced with dithionite (Sauer, Mathis et al. 1978) and 1-2 ms in a F_A-F_B-

less, P_{700}-Fx core (Warden and Golbeck 1986). The A_l back-reactions were reported to be 3 μs (Sauer, Mathis et al. 1979), 250 μs (Polm and Brettel 1998), or 10 μs (Warren, Golbeck et al. 1993) depending on the type of preparation and the reduction protocol. Another study made on a F_x-less, P_{700}-A_l core shows that the A_l back-reaction follows multi-exponential kinetics, where the majority of the charge recombination occurs with half-times of 10 μs and 150 μs at room temperature, and with kinetics only slightly slower at liquid helium temperatures (Brettel and Golbeck 1995). It is not clear, however, whether A_1 can transfer electrons back to P_{700} when only the terminal clusters (F_A and F_B) are removed.

D. Discussion of External PSI/e^- transport

Cytochrome (cyt) c_6 is known to transfer electrons in the thylakoid lumen between Cyt b_6-f complex and photosystem I (PSI) of many varieties of cyanobacteria and green algae (Hervas, Navarro et al. 2003, Molina-Heredia, Wastl et al. 2003). In some photosynthetic organisms, the iron containing cyt c_6, can be substituted for plastocyanin (PC) under copper limiting conditions as the electron donor to PSI.

Intensive work has been carried out on PC and cyt c_6 to understand their function and how it depends on their structure/composition (De la Rosa, Navarro et al. 2002). The surface of the interaction regions of cyt c_6 and PC are similar, despite they are structurally unrelated proteins, within any given organism (Ullmann, Hauswald et al. 1997). It has been generally thought that PC completely displaced

cyt c_6 in plants along evolution (Kerfeld and Krogmann 1998). However, a modified cyt c_6, called cyt c_{6A}, is found in plants and green algae and it is evolutionary related to cyanobacteria cyt c_6 but is unable to serve as electron donor in the photosynthetic electron transfer chain due to differences in midpoint potentials (Molina-Heredia, Wastl et al. 2003, Weigel, Pesaresi et al. 2003)

Vigorous structural and functional investigations by the De la Rosa group have provided strong evidence that the docking site for the electron donors to PSI underwent rapid and large changes during evolution (Hervas, De la Rosa et al. 1992, Diaz, Navarro et al. 1994, Frazao, Soares et al. 1995, De la Cerda, Diaz-Quintana et al. 1999, De la Rosa, Navarro et al. 2002, Molina-Heredia, Balme et al. 2002, Schlarb-Ridley, Bendall et al. 2002). The authors hypothesized that cyt c_6 may be the older evolutionary electron donor, which was later replaced by the copper-containing plastocyanin, due to iron limitations in the environment (De la Rosa, Navarro et al. 2002). While green plants use PC as the only electron donor to the PSI, some cyanobacteria can use both PC and cyt c_6 as electron donors. Furthermore, the electron donation complex formation varies significantly among different organisms. In plants and green algae the PSI subunit, PsaF, contains an insertion of around 25 amino acids in its luminal domain, which is responsible for formation of a tight electrostatic interaction and complex between PC and PSI (Hippler, Reichert et al. 1996, Hippler, Drepper et al. 1998). Most cyanobacteria do not form the tight complex and the interaction is purely diffusion-based. Despite the variability in the docking site of PC/cyt c_6 by PSI, the interaction site, where the electron transfer occurs, is strongly conserved among different organisms.

PC and cyt c_6 bind to PSI at an indentation at the luminal side to re-reduce the primary electron donor $P700^+$ which is caused by photo-oxidation. The major interaction site is formed by two helices, located at the luminal indentation close to $P700^+$. They provide a hydrophobic docking site for PC and cyt c_6. Potential docking sites for PC and cyt c_6 have been predicted and shown via dynamic models (Fromme, Melkozernov et al. 2003). Both PC and cyt c_6 have hydrophobic faces that match the hydrophobic docking site of PSI (Frazao, Soares et al. 1995). Surface mutations that disturb this site can affect the binding and electron transfer (Molina-Heredia, Diaz-Quintana et al. 1999). A larger increase in affinity can be provided by positively charged patches of both PC and cyt c_6 that may electrostatically drive their attractive movement toward PSI (Molina-Heredia, Diaz-Quintana et al. 1999). Two tryptophan residues partially exposed to the aqueous phase are also distinguished features of the docking site. They may form an important part of the recognition site for the soluble electron donors and may even be involved in the electron transfer from PC/cyt c_6 to P700. Experimental evidence for this hypothesis was provided by mutagenesis studies on one of these tryptophan residues (Sommer, Drepper et al. 2002).

E. PSI-Based Bioenergy Applications

Photosynthetic Proteins and Bioenergy Applications

There are many excellent reviews that cover the kinetics and thermodynamics of electron transfer of PSI (Ke 1973, Karapetyan, Holzwarth et al.

1999, Setif 2001, Karapetyan 2004, Semenov, Chamorovsky et al. 2004, Santabarbara, Heathcote et al. 2005, Medina 2009). In order to exploit the robust and highly efficient nature of PSI, considerable interest has recently been directed to the utilization of its charge separation with applied goals in solar energy applications such as hydrogen production (Iwuchukwu, Vaughn et al. 2010, Iwuchukwu, Iwuchukwu et al. 2011) and generation of photocurrent in photovoltaic devices (Mukherjee, Vaughn et al. 2011, Mershin, Matsumoto et al. 2012), exploiting the robust and highly efficient nature of PSI (Amunts and Nelson 2009).

Versatility and power of PSI reaction centers

PSI is an example of a Type I reaction center which has a different acceptor system than Type II reactions centers (Mazor, Greenberg et al. 2012). For example, Type I reaction centers, in contrast to the dual quinone acceptors, Q_A and Q_B, in the Type II reaction centers of purple bacteria and Photosystem II, have an FeS center that functions as the first stable acceptor (shown as F_X in Figure 1-3).

This is similar to the reaction centers found in the green sulfur bacteria (Hauska, Schoedl et al. 2001) and the heliobacteria (Liebl, Mockensturmwilson et al. 1993). Another feature of the Type I reaction center is that the special pair, P_{700} produces a much stronger electron donor when excited, P_{700}* has a midpoint potential of -1.3 V where as P_{870}* and P_{680}* found in the purple bacteria and PSII only have a midpoint potential of -600 mV (Rutherford and Evans 1980) and -650 mV (Nugent 1996), respectively. This more negative potential is a result of the chemical nature of the special pair but is also a consequence of the protein environment that coordinates these pigments and acceptors. The strong reductant produced by P_{700}* allows this

reaction center to directly drive the reduction of protons into H_2 via a hydrogenase (Lubner, Grimme et al. 2010, Lubner, Knorzer et al. 2010) or nanocatalyst (Millsaps, Bruce et al. 2001, Evans, O'Neill et al. 2004, Iwuchukwu, Vaughn et al. 2010).

These properties make PSI the source of the most powerful reductant in biological electron transfer (Amunts and Nelson 2009, Nelson 2009, Nelson 2011, Nelson 2013). It is this strikingly large negative midpoint potential that has attracted our lab and others to investigate the use of PSI as the preferred electron donor for applied photosynthetic purposes such as photosynthetic hydrogen production and photovoltaics (Millsaps, Bruce et al. 2001, Evans, O'Neill et al. 2004, Kiley, Zhao et al. 2005, Matsumoto, Vaughn et al. 2009, Mukherjee, May et al. 2010, Mukherjee, Vaughn et al. 2011, Baker, Manocchi et al. 2012, Manocchi, Baker et al. 2012, Mershin, Matsumoto et al. 2012, Pendley, Hurley et al. 2012, Manocchi, Baker et al. 2013, Patel, Bigler et al. 2013). Another interesting feature of PSI is the observation that the redox potential of the primary electron donor P_{700} special pair can vary considerably between organisms (Nakamura, Suzawa et al. 2011). Using comparative biochemical analysis their work has demonstrated that P_{700} can have a potential that varies by over 70 mV. This work also suggests that the molecular environment of P_{700} may be quite responsive to bioengineering such that the energy levels of the primary charge separation may be "tuned" to the energy levels of either the electron donor or the electron acceptor. This ability to adjust the energy levels may be used to both enhance the kinetics of electron transfer as well as reduce the loss of free energy due to large over potentials. This potential versatility in

electrochemistry will enable new, non-biological materials to be incorporated into future device design.

Finally, another attractive feature of PSI is the recent demonstration that the absorption properties of this reaction center can be varied based on the chlorophyll composition and the organism from which it is isolated. For example, it was shown in *Acaryochloris marina,* which contains predominately chl *d*, the reaction center special pair P_{740} (most likely a dimer of Chl d, (Tomo, Kato et al. 2008)) is shifted ~40 nm to the red (Schenderlein, Cetin et al. 2008). This finding would suggest that the discovery of more photosynthetic organisms would enable the optical properties of PSI to be further tuned. This is the precise design that has been invoked by a recent review by Blankenship *et al.* (Blankenship, Tiede et al. 2011) where they propose that a two photosystem solar cell could be constructed to allow both the extraction of electrons from water via a PSII-like or biomimetic system and hydrogen production using a second, PSI-type reaction center. By shifting the absorption properties of PSI into the red region, these two photosystems will not compete for the same spectral region and will thus be able to harvest more of the solar spectrum, enabling a higher external quantum yield. It appears that PSI provides considerable variability in both its optical properties and redox potentials that may help facilitate future device design and optimization.

PSI structural advantages for bio-hybrid devices

Availability of high-resolution structural data

Although the photosynthetic reaction center was the first membrane protein to have its structure determined in 1984 (Deisenhofer, Epp et al. 1984, Deisenhofer,

Epp et al. 1985), it was nearly 20 years before the structure of PSI was determined at 2.5 Å (Jordan, Fromme et al. 2001) and several more years before the first PSII structure was determined (Ferreira, Iverson et al. 2004). Both photosystem structures were determined initially from thermophilic cyanobacteria, *Thermosynechococcus elonga*tus or closely related organism *Thermosynechococcus vulcanus*. *T. elongatus* for example, has many advantages such as a fully sequenced genome, amenability to genetic transformation, and ability to undergo homologous recombination.

In most cyanobacteria the PSI complex is a trimer. As a trimer, the MW of PSI is nearly a megadalton, and each monomer contains 12 subunits (PsaA-F, PsaI-M, PsaX) and many cofactors, including 22 carotenoids, 96 chlorophylls, 2 phylloquinones, 3 Fe_4S_4 clusters, 4 lipids, and ~200 water molecules. More recent work has indicated that the trimer may contain over 330 chlorophyll molecules (El-Mohsnawy, Kopczak et al. 2010). In addition to the high-resolution X-ray structure of PSI, there are many TEM single particle structures (Bottcher, Graber et al. 1992, Kruip, Chitnis et al. 1997) and even some high-resolution AFM structures of the PSI complex in native membranes (Fotiadis, Muller et al. 1998, Kaftan, Brumfeld et al. 2002).

Recently, time resolved crystallography has been performed using femtosecond X-ray protein nanocrystallography. This method uses very bright femtosecond pulses from a hard-X-ray free-electron laser to generate a large number of single-crystal X-ray diffraction patterns that each provide a "snapshot" of the protein as a function of time (Chapman, Fromme et al. 2011), which would allow

the capture of millions of diffraction patterns from individual PSI nanocrystals. This technique also has the potential to avoid the significant problem of radiation damage characteristic of normal X-ray crystallography since the laser pulses are too short to generate degradation. This advantage is particular attractive to photosynthetic complexes since they are particular sensitive to radiation damage.

In addition to the cyanobacteria PSI complex, there have also been several structures determined from higher plants. The first structure from *Pisum sativum* var. Alaska was resolved to 4.4 Å resolution (Ben-Shem, Frolow et al. 2003). A higher resolution was later achieved using a PSI complex from Spinach to a resolution of 3.4 Å (Amunts, Drory et al. 2007). Both of these structures were part of a supercomplex that contained both the PSI reaction centers as well as four of the light harvesting complexes, LHCPa-d. Collectively, this complex contained 17 protein subunits, 168 chlorophylls, 2 phylloquinones, 3 Fe_4S_4 clusters and 5 carotenoids. Unlike trimers found in cyanobacteria, higher plant PSI complexes exist in nature as a monomer.

Finally, there are many structures of the individual subunits made available by NMR or X-ray analysis, which provide insight into the structural determinants of redox potentials and/or the individual protein dynamics. These reports include the primary donor cytochrome c_6 (Beissinger, Sticht et al. 1998), the soluble electron acceptors ferredoxin (Hatanaka, Tanimura et al. 1997) and flavodoxin (Hoover, Drennan et al. 1999) and finally the individual stromal domain subunits PsaC (Antonkine, Liu et al. 2002), PsaD (Xia, Broadhurst et al. 1998), and PsaE (Falzone, Kao et al. 1994),

As a result of this abundance of X-ray, NMR, TEM, and AFM data, the opportunity to make highly tailored site-directed mutations and gene fusions is unsurpassed. This high level of structural insight combined with the ever expanding molecular genetic tools for gene editing (Marton, Zuker et al. 2010, Tzfira, Weinthal et al. 2012, Liu, Yuan et al. 2013) and the emerging tools for synthetic biology (Caruana and Howorka 2010, Ansari and Husain 2012, You and Zhang 2013), provide researchers with a tremendously powerful toolkit for manipulating PSI for applied photosynthesis.

Surface access to electron acceptors

Regardless of the oligomeric nature of PSI, a common feature is the presence of an extramembraneous domain known as the "stromal hump". This domain protrudes out from the membrane and is composed of three subunits, PsaC, PsaD, and PsaE. These subunits are composed of loosely packed beta strands and some short alpha helices, yet none of the subunits contain a membrane spanning element This domain is found to be quite similar in both cyanobacteria and higher plants.

Unlike the Type II reaction centers in purple bacteria and PSII, the organization of the cofactors associated with electron transfer (specifically F_X, F_A and F_B) are quite close to the surface of PSI permitting rapid electron transfer to the soluble electron transfer components ferredoxin and flavodoxin (Golbeck 1999). These iron sulfur centers are in close proximity to the surface of PSI. In fact the FeS centers from both F_A and F_B are within 5-11 Å from the surface throughout the stromal hump. This close distance will allow relatively rapid electron transfer to a host of acceptors including the native electron acceptor, ferredoxin/flavodoxin

(Golbeck 1999) but also non-native electron acceptors such as MV (Izawa 1980) organic semiconductors such as C_{60} (Das, Kiley et al. 2004)and inorganic semiconductors such as TiO_2 and ZnO (Mershin, Matsumoto et al. 2012). Some of these electron acceptors are schematically shown in Figure 1-4.

An additional advantage of the non-membrane spanning nature of the stromal hump is the relatively straightforward means to replace these subunits *in vitro*. This design feature of PSI provides many opportunities for further bioengineering since these subunits can be both easily removed and replaced using *E. coli* expressed proteins *in vitro* (PsaC, PsaD and PsaE) (Zhao, Warren et al. 1990, Minai, Cohen et al. 1996, Minai, Fish et al. 2001, Lushy, Verchovsky et al. 2002). This may allow the powerful tools of synthetic biology in *E. coli* to be applied to PSI without having to develop an entirely new synthetic biology toolkit for a photosynthetic organism. In addition, certain mutations or subunit modifications that may disrupt the photosynthetic process *in vivo* may still be obtained via this *in vitro* re-assembly process, as was recently demonstrated with the introduction of ZnO and TiO_2 binding domains to PsaD and PsaE of *T. elongatus* (Mershin, Matsumoto et al. 2012). However, it may still be preferred to have an *in vivo* method of making these changes since the process of re-assembly may never be complete and could lead to heterogeneity in the PSI complex, lowering the efficiency of a device.

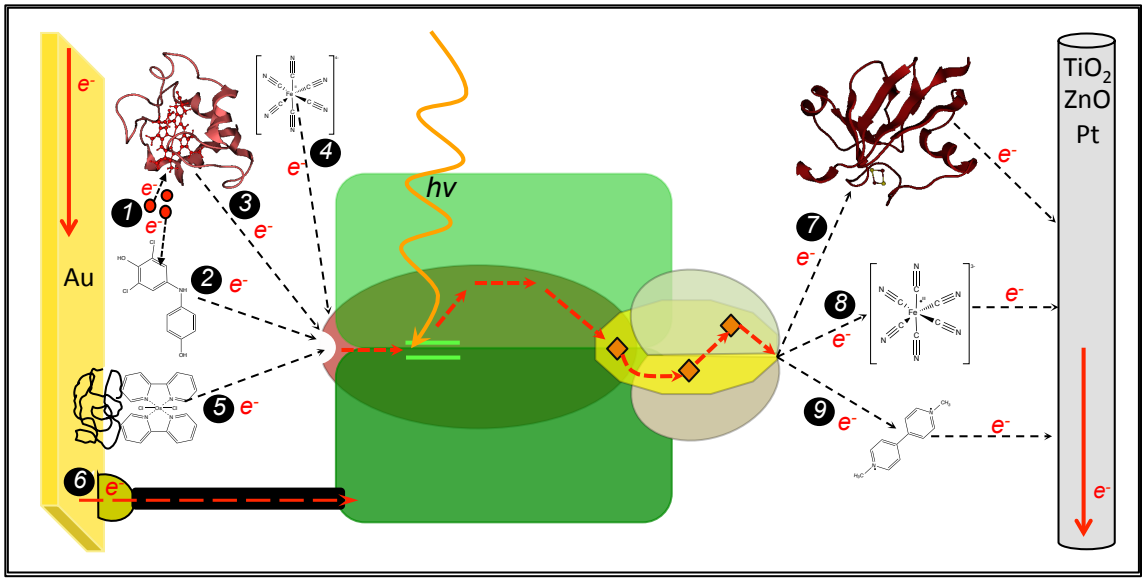

Figure 1-4. Bio-hybrid schemes integrating PSI with various e^- transfer mediators.

Soluble mediators (2) DCPIP, (3) cytochrome c_6, (4) $[Fe(CN)_6]^{4-}$, or (5) $Os(bpy)_2Cl_2$ can be reduced by Au electrode or (1) sodium ascorbate, allowing the electron transfer to (6) immobilized PSI. PSI can also be directly reduced by immobilization wire (6) (NTA-Ni-His_6-PSI). Soluble acceptors (7) ferredoxin, (8) $[Fe(CN)_6]^{3-}$, or methyl viologen can be used to transfer electrons from the F_B Fe-S center of PSI to TiO_2, ZnO, or Pt electrode. (Nguyen and Bruce 2014)

Interaction with Diverse Electron Donors

Although both PSI and PSII accept electrons from their lumenal surface, PSI is distinct in that it is quite promiscuous in terms of a viable electron donor. P_{680} in PSII, upon photo-oxidation, receives its electrons from the oxygen-evolving complex that is attached peripherally to the lumenal surface. Although this enables water to function as the electron donor to PSII, it is also a relatively labile system, which is easily photodamaged with a high turnover rate and must be repaired frequently (Barber and Andersson 1992, Aro, Virgin et al. 1993). PSI on the other hand is much more robust and can also accept electrons from a wide range of proteins including the native electron donors, cytochrome c_6 and plastocyanin (Hervas, De la Rosa et al. 1992), organic redox compounds such as dichlorophenol indophenol (DCPIP) (Ort and Izawa 1974), synthetic redox-active organometallic complexes such as $Os(bpy)_2Cl_2$ (Badura, Guschin et al. 2011), Au surfaces (Ko, Babcock et al. 2004), self assembled alkanethiols attached to Au (Kincaid, Niedringhaus et al. 2006), and graphene (Gunther, LeBlanc et al. 2013).

This ability to accept electrons from a diverse set of donors is shown schematically in Figure 1-4, and we demonstrate the re-reduction of P_{700} using some of these various donors after photobleaching via flash photolysis (Figure 1-5). However, in many cases these systems need to be in a high molar excess to keep up with the rapid electron transfer reactions with PSI. Future works will fine-tune both the electrochemistry and the interactivity of these systems to facilitate the highest PSI turnover with the least energy loss due to an over potential.

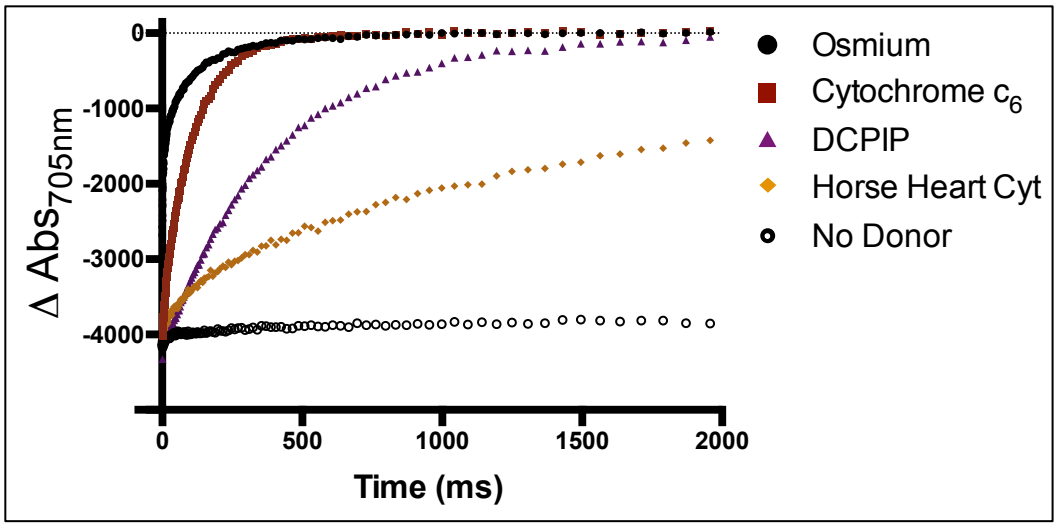

Figure 1-5. PSI-P_{700} reduction by various e^- donors.

T. elongatus PSI (30 nM) e^- transfer rates were measured with a LED pump-probe spectrometer (Joliot Type Spectrometer, JTS-10), detecting at 705 nm. Donors individually tested include $Os(bpy)_2Cl_2$ (2 nM), recombinant *T. elongatus* cytochrome c_6 (300 nM), DCPIP (1.2 μM), and horse heart cytochrome (1 mM). Reaction mix also included 2 mM sodium ascorbate and 1 mM methyl viologen, and 0.03% n-Dodecyl-β-D-maltoside in MES buffer (pH 6.4). (Nguyen and Bruce 2014)

Availability of Multiple Oligomeric Forms

Interestingly, unlike the non-oxygenic, monomeric bacterial reaction centers, photosynthetic reaction centers in oxygenic organisms are found as monomers (plant PSI), dimers (all PSII), trimers (most cyanobacterial PSI), and tetramers (few cyanobacterial PSI). Cyanobacterial PSI trimers have been reported in many published works (Ford and Holzenburg 1988, Almog, Shoham et al. 1991, Kruip, Boekema et al. 1993, Kruip, Bald et al. 1994, Tsiotis, Haase et al. 1995, Kruip, Chitnis et al. 1997, Garczarek, van der Staay et al. 1998, Tucker and Sherman 2000, Boekema, Hifney et al. 2001, Mangels, Kruip et al. 2002, Bibby, Mary et al. 2003, Brecht, Hussels et al. 2012) and the only existing crystal structure of a cyanobacterial PSI, from *Thermosynechococcus elongatus* BP-1 (*T. elongatus*) (Jordan, Fromme et al. 2001), suggests that cyanobacteria PSI preferentially form a trimer. Supporting this idea is the observation that cyanobacteria PSI trimers have been reported in almost every subclass of cyanobacteria. The most well characterized PSI trimers are from *Synechocystis*, *Synechococcus*, and *Thermosynechococcus*, where PsaL is needed for PSI trimerization in these cyanobacteria (Chitnis and Chitnis 1993, Chitnis, Xu et al. 1993, Schluchter, Shen et al. 1996, Aspinwall, Sarcina et al. 2004). In contrast, plant PSI is monomeric in the presence of PsaL, possibly due to interaction with the PsaH subunit that is not found in cyanobacteria (Ben-Shem, Frolow et al. 2004, Nelson and Ben-Shem 2005, Amunts and Nelson 2008). The fact that PSI can come in two oligomeric states (monomer and trimer) provides an advantage for increasing the density of PSI in a device. The trimer yields a very high local concentration, yet due to its high

molecular weight, high coverage or penetration will be difficult. By using both the trimer and monomer forms of PSI, it may be possible to get increased coverage as demonstrated in Figure 1-6. This configuration shows a random deposition of PSI trimers on a gold surface that is then further treated with a second deposition of PSI monomer, increasing the coverage by 35%. We also demonstrate the re-reduction of monomer vs. trimer PSI using cyt c_6 after photobleaching via flash photolysis (Figure 1-7).

Thermotolerance and Extended Stability

One of the advantages of PSI is the availability of well-characterized and easily cultivated thermophilic strains of cyanobacteria such as *Thermosynechococcus elongatus* (Nakamura, Kaneko et al. 2002). This organism is capable of growth at temperatures up to 60°C and was the source of the first crystal structure for PSI (Jordan, Fromme et al. 2001). In addition, this protein complex has been shown to have a thermotolerance of up to 70°C based on the protein structure as reflected by circular dichroism spectrometry (Iwuchukwu, Vaughn et al. 2010). This extreme thermal tolerance may be an attractive trait when PSI is integrated into various solid-state devices or solar cells that may be subject to high temperatures during illumination. Moreover, it has been shown that PSI isolated from both cyanobacteria and plants remains photochemically active in a solid state for over 21 days (Kiley, Zhao et al. 2005), in an aqueous hydrogen producing bioreactor for over 85 days (Iwuchukwu, Vaughn et al. 2010), and in a wet electrochemical cell for over 280 days (Ciesielski, Hijazi et al. 2010), respectively. It should be noted that in both

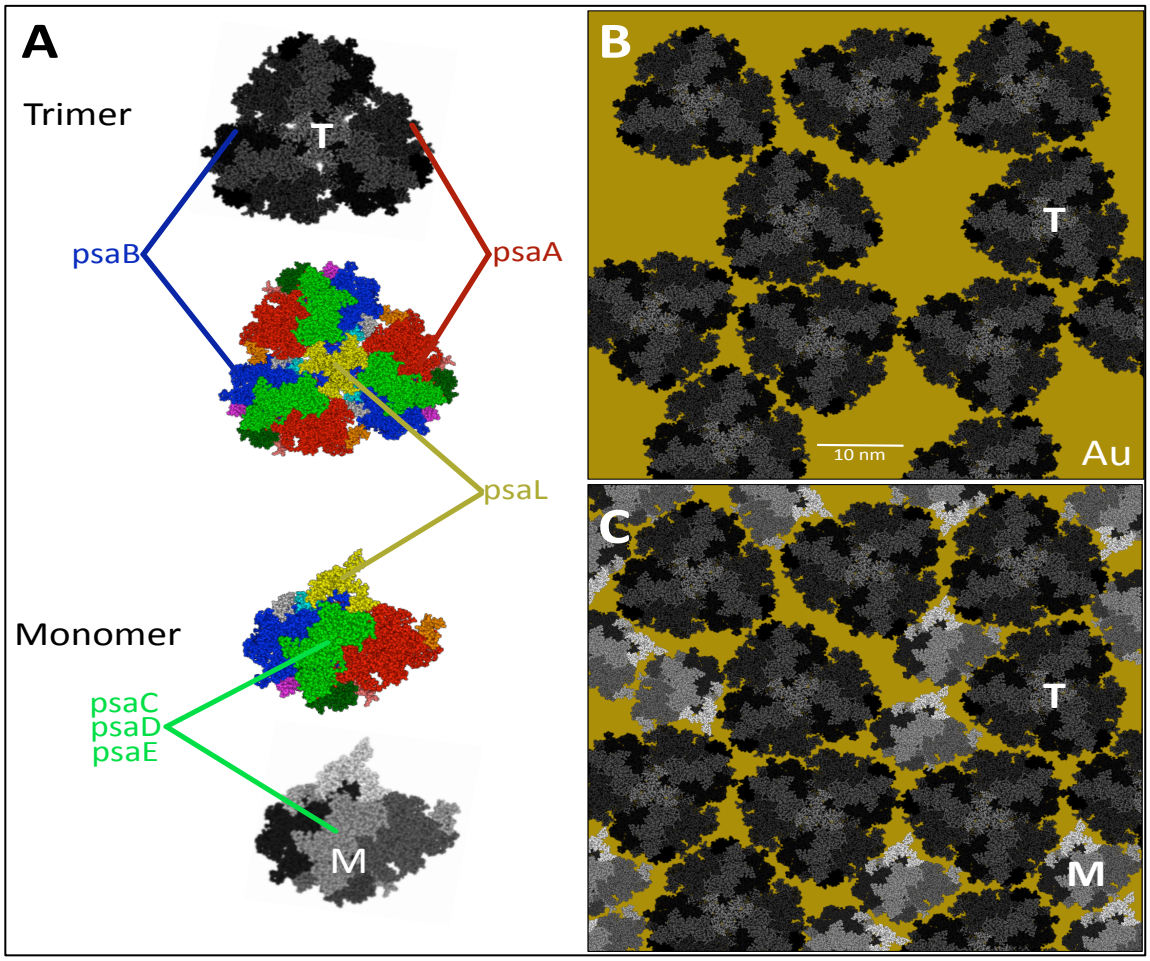

Figure 1-6. Proposed improved surface coverage using electro-deposited PSI trimers and monomers.

(A) Labeling of PSI subunits: Core subunits PsaA (red), PsaB (blue); stromal subunits PsaC, PsaD, PsaE (green); and PsaL (yellow).(B) An example of a random and arbitrary deposition of PSI trimers on an AU SAM is shown with 60.2% coverage. (C) The pattern in B was further treated to a random deposition of the PSI monomers yielding an increase in coverage to 84.0 %. Pixel calculations were done with ImageJ and PDB *T. elongatus* PSI crystal structure (1JB0) was constructed with MOE software. (Nguyen and Bruce 2014)

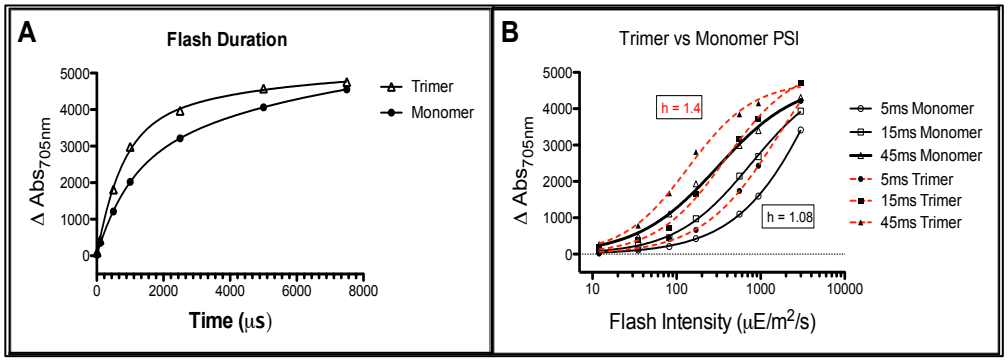

Figure 1-7. Reduction of *T. elongatus* PSI (trimer vs monomer) by recombinant *T. elongatus* cyt c_6.

A) Amount of P_{700} photo-bleaching is compared between trimer and monomer PSI at 7 given actinic flash durations. B) Comparing cooperativity of light saturation of trimer versus monomer PSI at three flash durations (5, 15, and 45 ms) with increasing flash intensities.

of these studies the activity of the PSI complex was nearly unchanged after months of continuous testing. This robust stability makes it very difficult to estimate the true functional longevity and stability of PSI, however it is expected that it will be affected by various conditions including spectral variations, light intensity, and temperature (Iwuchukwu, Iwuchukwu et al. 2011).

Established Ability to Genetically Engineer PSI in Cyanobacteria

Oxygenic photosynthesis is the primary energy source on Earth, capturing solar energy via absorption by chl. *a*/*b*, with water photolysis as the electron donor providing reducing equivalents for the fixation of atmospheric levels of CO_2 into hydrocarbons. Cyanobacteria, commonly called blue/green algae, containing only chla, are the only prokaryotes capable of using solar energy to support oxygenic photosynthesis. As prokaryotes, most of the well-established genetic tools of bacterial genetics are applicable to cyanobacteria, making it considerably easier to genetically engineer than eukaryotic photosynthetic organisms such as green algae and plants. With this advantage, considerable progress has been made over the past thirty years to engineer many strains of cyanobacteria including but not restricted to the model organism *Synechocystis* PCC #6803 (Vermaas 1994, Chitnis, Xu et al. 1995, Pakrasi 1995). More recently, however, the powerful tools of molecular and synthetic biology have been directed to bioengineering cyanobacteria for a host of new bioenergy and environmental applications, including biohydrogen production (Heidorn, Camsund et al. 2011, Srirangan, Pyne et al. 2011, Masukawa, Kitashima et al. 2012, Tiwari and Pandey 2012, Oliver, Machado et al. 2013, Ortiz-Marquez, Do

Nascimento et al. 2013), advanced CO_2 sequestration (Chen, Liu et al. 2012), production of next generation biofuels (Lindberg, Park et al. 2010, Radakovits, Jinkerson et al. 2010, Parmar, Singh et al. 2011, Li and Liao 2013), and various bioactive/value-added compounds (Pulz and Gross 2004, Singh, Kate et al. 2005, Wang, Pugh et al. 2013).

Not surprisingly, one of the first areas to attract the application of molecular biology and genetic engineering of cyanobacteria was the ability to perform gene knockouts, gene replacement and site-directed mutagenesis (Tsinoremas, Kutach et al. 1994, Muhlenhoff and Chauvat 1996, Vermaas 1996). These techniques were broadly applied to the analysis of the photosystems and in particular photosystem I which demonstrated the robust ability to be manipulated. For example, nearly all of the PSI subunits have been either deleted or genetically altered in some form including PsaA/B (Sommer, Drepper et al. 2002, Xu, Wang et al. 2011), PsaC (Takahashi, Goldschmidtclermont et al. 1991, Yu, Smart et al. 1995, Mannan, He et al. 1996), PsaD, PsaE (Rousseau, Setif et al. 1993, Zhao, Snyder et al. 1993), PsaF (Chitnis, Purvis et al. 1991, Kubota, Sakurai et al. 2010), PsaI (Nakamoto 1995), PsaJ (Xu, Odom et al. 1994, Xu, Yu et al. 1994), PsaK (Naithani, Hou et al. 2000), PsaL (Muhlenhoff and Chauvat 1996) and PsaM (Naithani, Hou et al. 2000). In addition, there has been considerable effort to optimize both the interactions with the primary donors cytochrome c_6 and plastocyanin (Duran, Hervas et al. 2006) and the terminal acceptor ferredoxin(Setif, Fischer et al. 2002). Future work on integrating PSI into photovoltaic devices will require progress in bioengineering to facilitate

specific attachment of the reaction centers to different types of surfaces, including semiconductors and catalysts (LeBlanc, Chen et al. 2012, LeBlanc, Chen et al. 2012).

PSI Surface Immobilization

The integration of redox proteins such as PSI into photo-electrochemical devices require immobilization strategies that ideally would allow direct electron transfer between the electrode and protein's active site(s) (e.g. PSI's P_{700}/F_B). Due to the dipole nature of PSI, proper orientation on and proximity to the electrode surface appears to be an essential factor in attachment design. The conductive and semi-conductive substrate surfaces used for PSI depositions have evolved from the widely used Au to other materials including, TiO_2, ITO, glass, ZnO, alumina, and graphene.

The most commonly utilized strategies often involve the usage of organothiol-based self-assembled monolayers (SAMs). For attachment of PSI, SAMs can be terminated or functionalized with mercaptoacetic acid/2-mercaptoethanol (Lee, Lee et al. 1997), nitrilotriacetic acid (NTA) (Das, Kiley et al. 2004), alkanethiols (Ko, Babcock et al. 2004, Kincaid, Niedringhaus et al. 2006, Ciobanu, Kincaid et al. 2007, Manocchi, Baker et al. 2013), terephthaldialdahyde (TPDA) (Ciesielski, Scott et al. 2008, Faulkner, Lees et al. 2008, Ciesielski, Cliffel et al. 2011), 3-mercapto-1-propanesulfonic acid (Terasaki, Yamamoto et al. 2009, Terasaki, Yamamoto et al. 2009), aminoethanethiol (Ciesielski, Faulkner et al. 2010, Ciesielski, Cliffel et al. 2011), and pyrroloquinoline quinone (Efrati, Yehezkeli et al. 2012). Because of the highly variable design and attachment chemistries, we briefly summarize the studies utilizing these variations below:

PSI on (Au)-based SAMs

Lee et al. 1997 (Lee, Lee et al. 1997): Tested -OH, -COOH, - SH terminated SAMs to immobilize and control the orientation of 2D spatial arrays of PSI on Au surfaces. They found that -OH terminated SAMs gave the most desired, perpendicular orientation of PSI.

Das et al. 2004 (Das, Kiley et al. 2004): To achieve oriented PSI assembly, recombinant PsaD-His_6 was immobilized on Ni^{2+}-NTA functionalized Au surface. This then was exposed to native PSI complexes where the intrinsic PsaD subunit naturally exchanged with an excess of the recombinant PsaD-His_6, resulting in immobilization of PSI with P_{700} facing away from the ITO/Au substrate. Peptide surfactants were also used to increase PSI stability during and after assembly.

Ko et al. 2004 (Ko, Babcock et al. 2004): Examined the PSI to *ω-functionalized* and *n-alkanethiols* gold surface adsorption based on surface composition. They concluded that the PSI-solubilizing agent, Triton X-100, adsorbs to low-energy surfaces (hydrophobic SAM), and the PEG groups of the Triton layer is very resistant to protein adsorption. This inhibiting effect can be prevented by the addition of a more active surfactant (e.g. dodecanol).

Frolov et al. 2005 (Frolov, Rosenwaks et al. 2005): Various cystein mutations were made to residues on the lumen exposed face of PSI to allow for direct thiol coupling to the Au surface. Even with the mutations being placed in an increasing distance from the P700 site, PSI attachment was achieved with all mutants, suggesting that a specific location is not required as long as the cystein is on an extramembranal loop of PSI's lumenal surface.

Kincaid et al. 2006 (Kincaid, Niedringhaus et al. 2006): In an attempt to mimic the natural thylakoid membrane that surrounds PSI, this group immobilized PSI using HOC_6S/Au SAMs followed by a backfilling step to adsorb longer-chained methyl-terminated alkanethiols in the interprotein domains to displace the shorter, more unorganized HOC_6S monolayer.

Ciobanu et al. 2007 (Ciobanu, Kincaid et al. 2007): PSI adsorbed on hydroxyl-terminated hexanethiol (HSC_6OH) modified gold substrate showed an enhanced reduction current for P_{700}^+ in the presence of light and methyl viologen. They also saw that HSC_8OH terminated SAMs formed a more ordered monolayer than the HSC_6OH monolayer. They were able to analyze PSI functionality after adsorption by cyclic voltammetry, looking at signals of F_A, F_B, and P_{700}.

Faulkner et al. 2008 (Faulkner, Lees et al. 2008): To address the issue of the labor intensive and time consuming procedures required in previous studies to adsorb PSI to SAMs, this group demonstrated that a vacuum-assisted method can produce dense, oriented monolayers of PSI about 80 times faster than the traditional solution adsorption techniques. This vacuum-assisted method also to enabled PSI assembly on other surfaces that were resistant to protein adsorption.

Ciesielski et al. 2008 (Ciesielski, Scott et al. 2008): PSI was immobilized on the surface of nanoporous gold leaf (NPGL) electrodes via covalent bonds between the aldehydic groups of the TPDA-functionalized NPGL SAM and the exposed lysines on PSI. The resulting photocurrent from the electrodes was shown to be dependent on irradiating light intensity and dealloying times of the electrode production.

Terasaki et al. 2009b (Terasaki, Yamamoto et al. 2009): PSI was bound on an

Au/3-mercapto-1-propane-sulfonic acid-SAM by electrostatic interactions. They were able to show the ability of the PSI-Au electrode to act as a gate film in FET sensoring for imaging devices.

Mukherjee et al. 2010 (Mukherjee, May et al. 2010): The deposition of PSI onto hydroxyl-terminated alkanethiolate SAM/Au substrates were investigated with the goal of having better control of the assembly morphology. They showed that a lower PSI concentration via electric-field deposition, minimizes PSI aggregation while providing a more uniform coverage onto the surface as compared to gravity-driven deposition methods.

Ciesielski et al. 2011 (Ciesielski, Cliffel et al. 2011): Dense monolayers of PSI were immobilized to aminoethanethiol terminated SAMs functionalized with TPDA (similar to that of Ciesielski *et al.* (Ciesielski, Scott et al. 2008)). A mechanistic model was developed for PSI immobilized SAMs, in which kinetic and electrochemical parameters were used to predict photocurrent densities. Discrepancies between simulated and experimental current densities were discussed, along with a predicted conclusion that unless at least 80% of the PSI was oriented the same way, the majority of the photocurrent is nullified.

Mukherjee et al. 2011(Mukherjee, Vaughn et al. 2011): Various immobilization conditions of PSI onto SAM/Au substrates was tested. Conditions tested included adsorption temperature, monomeric/trimeric forms of PSI, and type of detergent used. A comparision was also made on the immobilization charateristics when applying a gravity driven versus an electric field assisted assembly technique. This study provided one of the few direct demonstrations of the uniform orientation of

PSI by using an immunofluorescent detection strategy. This analysis can provide both a method to quantitate the attachment density and confirm the predicted orientation based on the strong PSI dipole.

Efrati et al. 2012 (Efrati, Yehezkeli et al. 2012): CdS quantum dots (QDs) and PSI, immobilized onto a pyrroloquinoline quinone (PQQ) monolayer linked to Au electrodes were compared based on their anodic/cathodic switchability of the photocurrents in the presence of different photoelectrochemical configurations. They concluded that upon irradiation under O_2, the two systems gave rise to a potential-induced control of anodic and cathodic directions in photocurrent.

Manocchi et al. 2013 (Manocchi, Baker et al. 2013): By using an electrophoretic deposition procedure, PSI assembly on alkanthiol SAMs was enhanced, and the immobilized PSI density was easily controlled. SAM surface charge composition, specifically MHO and MHA, greatly increased the amount of bound PSI. This work demonstrated that there is some interaction between the terminating group of the SAM and some surface property of PSI. The stability of the PSI/SAM electrode was shown to be maintained for a minimum of 3 hours with illumination.

Other Metal/Conductive Surface-SAMs

While gold has been the main conductive surface used in the above studies, other materials like gallium (III) arsenide (GaAs) (Frolov, Rosenwaks et al. 2008), titanium oxide (TiO_2) (Nikandrov, Borisova et al. 2012), silicon (Si) (LeBlanc, Chen et al. 2012), and graphene (Gunther, LeBlanc et al. 2013) have also emerged as a suitable and attractive material for PSI devices.

Frolov et al. 2008b (Frolov, Rosenwaks et al. 2008): Cysteine mutant PSI was chemisorbed to malemide-functionalized GaAs SAMs. The dry-oriented junction allowed for a non-aqueous system, and was still functional after one year.

Nikandrov 2012 (Nikandrov, Borisova et al. 2012): PSI was immobilized in a mesoporous TiO_2 semiconductor matrix. The larger pore diameter of the TiO_2 matrix allowed for a high concentration of PSI to be immobilized, thus allowing the complex to absorb high light.

LeBlanc et al. 2012 (LeBlanc, Chen et al. 2012): Conducted a systematic study on how both n- and p-doped silicon can increase the photocurrent density of PSI films. By comparing silicon doping types and densities, they concluded that heavily p-doped silicon provided the best surface for PSI attachment and photocurrent generation.

Gunther et al. 2013 (Gunther, LeBlanc et al. 2013): First group to exploit the transparent and highly conductive properties of graphene in PSI attachment. Graphene's transparency is noted to be very attractive for the usage of high concentrations of opaque mediators.

Carbon Nanotubes / NanoParticles

While the previous studies looked at PSI functionality as a monolayer on a planar substrate surface, other works have investigated the potential enhancement in photocurrent by utilizing (3D) nanostructured electrodes that provide an increased surface area, consequently allowing for a greater deposition of PSI particles. These nanostructured substrates such as nanoparticles (NP) (Terasaki, Yamamoto et al. 2006), nanowires (Mershin, Matsumoto et al. 2012), and nanotubes

(Carmeli, Frolov et al. 2007, Kaniber, Brandstetter et al. 2010) have been used for PSI attachment and increased photocurrent in the following studies:

Terasaki 2006 (Terasaki, Yamamoto et al. 2006): Constructed PSI–gold nanoparticle hybrid electrodes, by depositing gold NPs onto a planar gold substrate followed by SAM formation by MPS. PSI was then electrostatically adsorbed to the MPS modified electrodes.

Carmeli et al. 2007 (Carmeli, Frolov et al. 2007): Used cysteine mutants of PSI to bind maleimide modified carbon nanotubes (CNTs) through a chemical process on a gold electrode. Variations of this process also allowed for the construction of cross-junctions between two CNTs by a PSI connection.

Kaniber 2010 (Kaniber, Brandstetter et al. 2010): Three different strategies for on-chip functionalization of CNT-PSI hybrids were demonstrated. The covalent attachment utilized cysteine mutant PSIs bonding to maleimide functionalized CNTs. The second method proposed a hydrogen bond formation between the amino groups of the ethylenediamine functionalized CNT and cysteine mutant PSI treated with dithiothreitol. The final method exploited the electrostatic forces between the positively charged regions on PSI and the CNTs negatively charged terminal groups.

Mershin 2012 (Mershin, Matsumoto et al. 2012): PSI was attached to two semiconducting substrates (TiO_2 and ZnO). PSI was physisorbed to TiO_2 on FTO coated glass and self assembled on ZnO nanowires with a PsaE-ZnO replacement strategy.

Other PSI Assemblies (Multilayers, Sol-Gels, and Redox Polymers)

Aside from deposition of PSI monolayers directly onto surfaces, the following

works have demonstrated improved functionality, stability, and photocurrent generation with the incorporation of PSI multilayers, sol-gels, and redox polymers into their device fabrication schemes:

O'Neill and Greenbaum 2005 (O'neill and Greenbaum 2005): PSI was immobilized onto a clear organosilicate glass reacted with a colloidal sol solution (sol-gel). This sol-gel matrix, while enabling the entrapment of PSI, also offered a stabilizing environment for other biomolecules such as redox mediators, allowing their chemical reactivities to be retained. In addition, the transparent nature of the matrix is an obvious advantage in applications requiring full optical functionality of the photoactive biomolecules.

Frolov et al. 2008a (Frolov, Rosenwaks et al. 2005): Serially-oriented multilayers of PSI were assembled on an Au electrode. This assembly was created with a mutant PSI containing a lumen-exposed cysteine, which formed a sulfide bond with Au to form the first layer. Platinum was then deposited to the stromal face of PSI, allowing for the sequential layer of mutant PSI to form a sulfide bond with the platinum patches. The highest photovoltage was achieved with the multilayer of Au-PSI-Pt-PSI-Pt-PSI.

Ciesielski et al. 2010 (Ciesielski, Hijazi et al. 2010): Developed a photoelectrochemical cell with multilayer assembly of PSI. A PSI suspension and liquid electrolyte was injected into a reservoir held between a gold cathode and a Cu-modified ITO anode.

Ciesielski et al. 2010b (Ciesielski, Faulkner et al. 2010): By mimicking stacked thylakoid structures, multilayers of PSI were formed through sequential deposition

of a liquid PSI suspension onto gold and glass substrates via a vacuum-assisted assembly. PSI deposition of up to 7 layers was shown to have a matching increase in absorption intensity and photocurrent generation.

Kopnov et al. 2011 (Kopnov, Cohen-Ofri et al. 2011): Tested the combinations of coupling PSII and PSI in order to enable electron flow from water splitting at PSII to reducing P_{700} of PSI. The variations included one protein in solution and the other sol-gel encapsulated, both in solution, or both sol-gel encapsulated. These implementations offered a simple solution the challenging task of utilizing both photosystems in the same device, allowing the usage of water as the sacrificial electron source.

Toporik 2012 (Toporik, Carmeli et al. 2012): PEG-treated PSI crystals were immobilized onto ITO coated glass slides. Although photocurrent densities were not reported, large photovoltages (~50V) were seen, which would be the largest reported for any inorganic material device. This anomalous value was proposed to be a result of "electron trapping in deep centers in the vicinity of the FB acceptor", due to the packing and alignment of PSI's dipole in the crystallized state.

Yehezkeli 2013 (Yehezkeli, Tel-Vered et al. 2013): The redox polymer, poly-benzyl viologen (PBV2+) was employed as an "interprotein glue" in the layered assembly of PSI on a transparent ITO electrode. Increasing photocurrent was seen with the sequential addition of PSI-PBV layers up to a maximum of 3 layers.

PSI Stabilization/Enhancement

While enhancements have been made to increase photocurrent via surface modifications, variable redox mediators, and increased PSI packing densities, it is

also crucial to retain PSI's optical functionality for an extended period of time in order for the device to be practical. The following approaches tried to address the main issue of PSI's hydrophobic domains being unnaturally exposed on the surface, causing rapid protein degradation. In this regard, Kiley *et al*. (Kiley, Zhao et al. 2005) studied the effects of various peptide detergents on PSI stability and function. They saw that the designed peptide detergent, acetyl-AAAAAAK (A6K), stabilized PSI for at least 3 weeks in the dry form. This discovery followed some intial studies with peptide surfactants done by Das *et al.* (Das, Kiley et al. 2004). Along this line , Matsumoto *et al*. (Matsumoto, Vaughn et al. 2009) studied a new class of designer peptide surfactants (ac-I6K2-CONH2, ac-A6K-CONH2, ac-V6K2-CONH2, and ac-V6R2-CONH2). They concluded by offering a guide to designing future peptide surfactants for optimal stabilization of active PS-I. The four main factors included: 1) an acetylated N-terminus 2) a short hydrophobic tail consisting of 6 consecutive hydrophobic residues 3) 1-2 C-terminal positively charged polar residues and 4) an amidated C-terminus (Matsumoto, Vaughn et al. 2009). Another approach taken by Kincaid *et al.* (Kincaid, Niedringhaus et al. 2006) attempted to mimic the natural thylakoid membrane that surrounds PSI. After the immobilization of PSI using HOC_6S/Au SAMs, they added a backfilling step to adsorb longer-chained methyl-terminated alkanethiols in the interprotein domains to displace the shorter, more unorganized HOC_6S monolayer.

The previous studies have analyzed PSI stability with techniques probing for its optical properties, such as steady-state emission spectra (Kiley, Zhao et al. 2005), fluorescence spectra (Das, Kiley et al. 2004), and reflectance absorption infrared

spectroscopy (Kincaid, Niedringhaus et al. 2006); however Gerster *et al.* (Gerster, Reichert et al. 2012) were able to look at the photocurrent generated by a single PSI molecule immobilized on an Au surface. The immobilization of PSI between the substrate and the metallized scanning near-field optical microscopy (SNOM) tip was achieved with PSI cysteine mutations and the ability to control SNOM tip to substrate distance by a high-resolution piezoelectric element.

Along with stabilizing and maintaining PSI's native optical properties, increasing the range of its absorption spectra has also been of interest. Although having a quantum efficiency nearing unity, PSI is still limited to absorbing about 1% of natural sunlight. Carmeli *et al*. (Carmeli, Lieberman et al. 2010) were able to enhance PSI's light absorption capability with the attachment of colloidal metal (gold and silver) nanoparticles, which acted as optical antennas to functionalize more of the spectrum to photons for P_{700} activation. They also described a new method that enables a higher yield of PSI attachment to NPs.

Diffusable Redox Mediators / Molecular Wires

While the native donors to PSI are metalloproteins (plastocyanin or cytochrome c_{553}), the majority of these works employ the combination of sodium ascorbate (NaAs) and 2,6-dichlorophenolindophenol (DCPIP) to transfer the electron from substrate surface to PSI where NaAs acts to keep a reduced pool of DCPIP for P_{700} reduction (Terasaki, Yamamoto et al. 2006, Terasaki, Yamamoto et al. 2007, Ciesielski, Scott et al. 2008, Faulkner, Lees et al. 2008, Frolov, Wilner et al. 2008, Terasaki, Yamamoto et al. 2009, Ciesielski, Hijazi et al. 2010, Yehezkeli, Wilner et al. 2010). The following complexes have also been used for electron donation to

PSI: reduced ferricyanide $K_4Fe(CN)_6$ (Ciesielski, Faulkner et al. 2010), osmium complexes ($Os(bpy)_2Cl_2$) (Badura, Guschin et al. 2011, Manocchi, Baker et al. 2013), Z813 Co(II)/Co(III) electrolyte (Mershin, Matsumoto et al. 2012), and ruthenium hexamine trichloride (RuHex) (Gunther, LeBlanc et al. 2013).

In many studies an electron acceptor has also been used to prevent the charge recombination reaction of electron flow from F_B back to P_{700} and transferring electrons to the opposing electrode. With a midpoint potential of (-0.446 V vs SHE), methyl viologen (MV) has been widely used to accept electrons from PSI F_B (-0.58 V vs SHE) (Ciobanu, Kincaid et al. 2007, Terasaki, Yamamoto et al. 2009, Badura, Guschin et al. 2011, LeBlanc, Chen et al. 2012, Manocchi, Baker et al. 2013). Other notable acceptors used include a naphthoquinone-derivative (NQC15) (Terasaki, Yamamoto et al. 2007, Terasaki, Yamamoto et al. 2009), oxidized $K_3Fe(CN)_6$ (Ciesielski, Faulkner et al. 2010), and methylene blue (Gunther, LeBlanc et al. 2013). Ciesielski *et al.* (Ciesielski, Faulkner et al. 2010) showed that $Fe(CN)_6$ was able be used as both donor and acceptor, minimizing ET components by oxidizing $[Fe(CN)_6]^{4-}$ to $[Fe(CN)_6]^{3-}$ at the lumenal P_{700} interface and reducing $[Fe(CN)_6]^{3-}$ to $[Fe(CN)_6]^{4-}$ at the stromal F_B site.

After P_{700} photo-excitation, electron transfer follows the scheme of $P_{700} \rightarrow A_0 \rightarrow A_1 \rightarrow F_X \rightarrow F_A \rightarrow F_B$, with these active cofactor sites buried deep within PSI. The wiring of PSI to a substrate via an electron transfer cofactor was attempted by Terasaki *et al.* (Terasaki, Yamamoto et al. 2007), where the A_1-phylloquinone was extracted and reconstituted with a naphthoquinone-derivate (NQC_{15}) attached to Au NP. The NQC_{15} molecular wire has a very similar length as the native A_1, allowing

the Au NP to be attached near the PSI surface. This NQC_{15}S-Au(NP)-PSI was then immobilized with an Au-S bond via a SAM of 1,4-benzenedimethanethiol. By wiring the A_1 cofactor of PSI's electron transfer chain to the substrate surface, the direct electron transfer was achieved to the electrode from A_1 while bypassing the FeS clusters (F_X, F_A, F_B) in the stromal hump of PSI. DCPIP and NaAs were also used for electron donation to P_{700}. This group further improved on this method with an A_1 replacement using a naphthoquinone-viologen linked compound ($NQC_{15}EV$), where the viologen had the appropriate redox potential (-0.446 V vs SHE) to mediate electron transfer through the wire from A_1 (-1.05 V vs SHE) (Terasaki, Yamamoto et al. 2009). The use of methyl viologen at the end of the NQC_{15} instead of an Au NP, increased the photocurrent by about 25 times as shown in Table I. With these two studies, Terasaki *et al.* was able to demonstrate that electron transfer to an electrode is possible via a direct connection from a PSI cofactor (A_1), utilizing either a conductive metal NP (Au) (Terasaki, Yamamoto et al. 2007), or an electron mediator (MV) (Terasaki, Yamamoto et al. 2009).

Miyachi *et al.* followed up on this A_1-phylloquinone replacement method with a study that demonstrated how the addition of two surfactants enhanced the sensitivity of the NQC_{15}S-Au(NP)-PSI system by enabling electron storage in the AuNPs (Miyachi, Yamanoi et al. 2009). This group also implemented a terpyridine-terminated naphthoquinone, allowing for a connection to Co(II) ions to form the complex of PSI_tpy-C_{15}NQ_ITO (Miyachi, Yamanoi et al. 2010). The development of these new strategies has contributed to the immobilization of PSI on surfaces for applications in both photovoltaic cells and photosensing devices.

Photocurrent Production

As seen in Figure 1-8, much progress has been achieved in enhancing PSI-photocurrent density since the early 2000's. In less than a decade, over 30 papers have been published reporting various activities of PSI. From these papers, the reported photocurrent density, when normalized to excitation intensity, has jumped up almost 4 orders of magnitude from 0.48 (Terasaki, Yamamoto et al. 2006) to 4,469 (Mershin, Matsumoto et al. 2012) ($\mu A\ cm^{-2}\ mW^{-1}$). Although it might be impossible to pinpoint all the subtle changes made in fabricating PSI-biohybrid devices during this time, along with their individual levels of contribution toward increasing photocurrent yield, some significant factors are evident. The combination of NaAs/DCPIP has been the most widely used electron source and donor for these systems. Aside from two studies (Frolov, Wilner et al. 2008, Ciesielski, Hijazi et al. 2010), all others utilizing NaAs/DCPIP achieved less than 2 $\mu A\ cm^{-2}$ in photocurrent generation. The two exceptions from Frolov *et al*. (Frolov, Wilner et al. 2008) and Ciesielski *et al*. (Ciesielski, Hijazi et al. 2010) both assembled a multilayer of PSI, while the others had just a monolayer deposited. Even with a photocurrent of 2 $\mu A\ cm^{-2}$, Ciesielski *et al*. had used twice as much DCPIP (5 mM) as any other study (Ciesielski, Hijazi et al. 2010). Although probably one of the most cost effective PSI donors, DCPIP proves to be a limiting factor in photocurrent production as it is considered a much poorer electron donor to PSI compared to native metalloproteins or other artificial complexes.

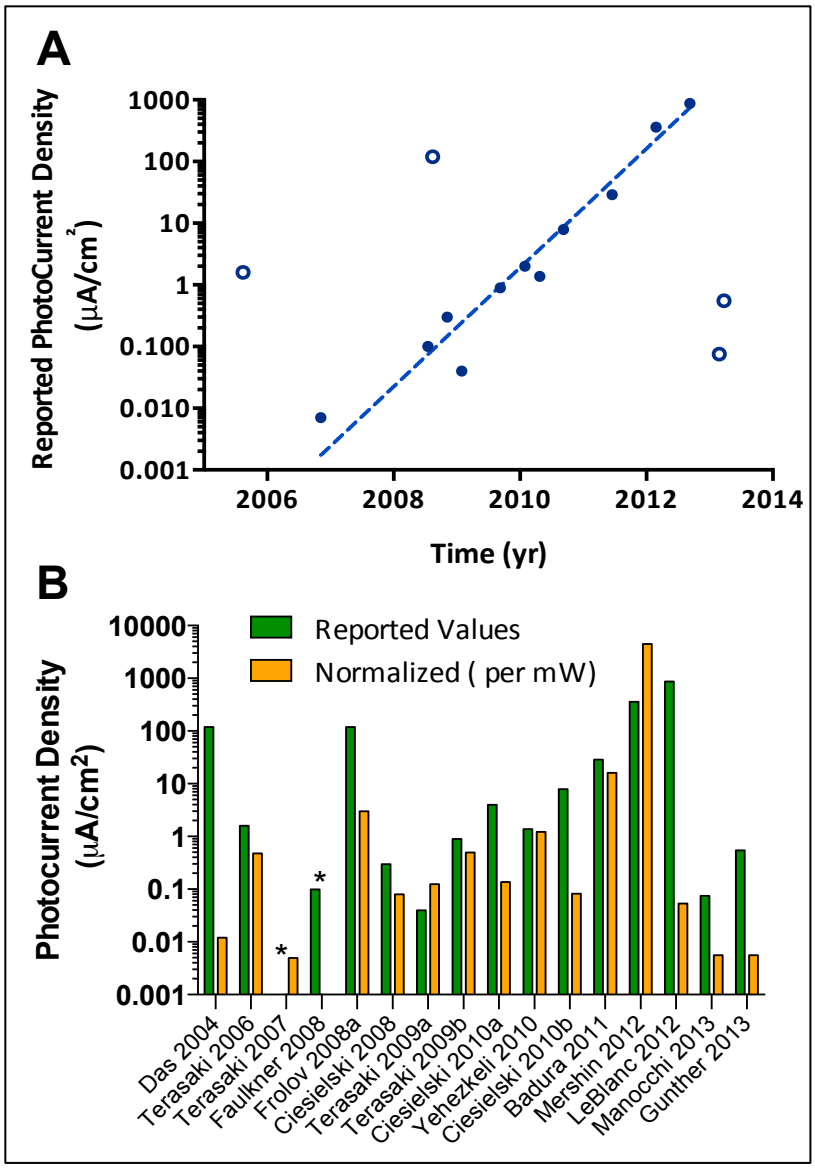

Figure 1-8. Progress of PSI-generated photocurrent .

A) Photocurrent density extracted from PSI studies from 2005-2013. About a 10 fold increase in rate ($\mu A/cm^2$) is seen per year with the fitted trend line (open points excluded). B) A comparison between the reported maximal current density and when normalized to $1mW/cm^2$ of applied excitation intensity. *Unable to extrapolate both values due to lack of reported data. (Nguyen and Bruce 2014)

Potassium ferricyanide was implemented as both electron donor to P_{700} and electron acceptor from F_B with a continuous redox cycle from $[Fe(CN)_6]^{4-}$ to $[Fe(CN)_6]^{3-}$ at P_{700} and $[Fe(CN)_6]^{3-}$ to $[Fe(CN)_6]^{4-}$ at F_B to produce an enhanced photocurrent of 7.9 μA cm^{-2} (Ciesielski, Faulkner et al. 2010). This can prove to be a fairly attractive feature for large-scale implementations, as it would minimize the input to drive the reaction. The metal osmium (Os), a dense and stable element (Arblaster 1989), has also been used recently as both an immobilization matrix and electron donor in the form of an "Os-complex modified polymer" (Badura, Guschin et al. 2011) and also as an ET mediator, $Os(bpy)_2Cl_2$, sitting atop alkanthiol-SAMs (Manocchi, Baker et al. 2013). While the Os-complex polymer gave an enhanced photocurrent of 29 μA cm^{-2} (Badura, Guschin et al. 2011), osmium is also the least abundant of the stable elements (Wedepohl 1995) and therefore not practical for large-scale applications. Though synthesized and tested originally for dye-synthesized solar cells (Nusbaumer, Zakeeruddin et al. 2003), the Co(II)/Co(III) ion-containing electrolyte Z813 was used with PSI to generate one of the highest (highest if normalized to excitation intensity) photocurrents of 362 (4,469-normalized to mW^{-1}) μA cm^{-2} (Mershin, Matsumoto et al. 2012). This significant increase in photocurrent, if attributed to Z813, shows a tremendous potential for the usage of synthesized redox mediators instead of relatively expensive rare metals.

While the majority of electrode surfaces and immobilization schemes used with PSI involve SAMs on an Au surface, we will discuss the variation in strategies implemented by the top performers. A noticeable trend in enhanced photocurrent

generation with values of 2 (Ciesielski, Hijazi et al. 2010), 7.9 (Ciesielski, Faulkner et al. 2010), and 120 (Frolov, Wilner et al. 2008) μA cm^{-2} are seen in the assembly procedures that utilize a multilayer of PSI instead of a single immobilized monolayer. Amongst these works, there appears to be a noticeable trade-off between PSI orientation within the multilayer and the generated photocurrent. With the two lower values achieved by the Ciesielski group, PSI multilayer depositions were made without bias to PSI's dipole orientation in relation to the surface electrode. On the other hand, the device that generated a 10-fold higher photocurrent by the Frolov group was constructed with cysteine mutant PSIs that allowed for subsequent attachment of Pt patches between each PSI layer. Whether or not the cost of the added steps in generating mutant PSIs and the application of expensive platinum salts is worth the 10-fold increase in photocurrent is debatable.

In looking at the two recent reports that generated the highest photocurrents ever produced by a PSI-based device, (LeBlanc, Chen et al. 2012, Mershin, Matsumoto et al. 2012) we notice the unique surfaces used for PSI immobilization. Heavily p-doped silicon (Hp-Silicon) was found to generate a significant increase in photocurrent at 875 μA cm^{-2}, as directly compared to only 0.35 μA cm^{-2} of the same conditions on gold electrodes (LeBlanc, Chen et al. 2012). This result by LeBlanc *et al*. was attributed to the favorable valance band alignment of silicon to the P_{700} site, allowing for a unidirectional flow of electrons from silicon to P_{700}, with methyl viologen accepting electrons at F_B (LeBlanc, Chen et al. 2012). Coupling its relative affordability and abundance to other metals, this work has shown silicon to be a highly attractive material for use in PSI-biohybrid devices. The next strategy by

Mershin *et al.* (Mershin, Matsumoto et al. 2012) takes advantage of an increased electrode area for PSI deposition (estimated to be about 50 times per μm of film thickness) offered by the added dimension of the nanocrystalline TiO_2 and ZnO nanowires. Along with the nanostructured electrode surface, designer peptide surfactants (similar to that of Kiley *et al*.(Kiley, Zhao et al. 2005)) were utilized for PSI stabilization to prevent protein denaturation and retain functionality after the drying process. These methods were used in conjunction with the novel Z813 electrolyte to achieve a photocurrent of 362 μA cm^{-2}, the second highest reported value and highest value by over 3 orders of magnitude if normalized to excitation intensity (4469 μA cm^{-2} mW^{-1}).

In our systematic breakdown of the PSI-generated photocurrents (Table 1-1), we have identified some key characteristics that have contributed in increasing this value over 4 orders of magnitude since the initial studies done a decade ago. The works done on PSI-biohybrids also extends to literature (Table 1-2) that primarily focuses on the characterization and analysis of PSI immobilization strategies that do not include a value for photocurrent. By providing insight into PSI functionality and detailed characterization after immobilization, these studies should be looked at in conjunction with photocurrent studies to maximize the potential of PSI on nanostructured biohybrid devices for the generation of *green* electricity.

Table 1-1. Component breakdown of biohybrid devices with PSI-generated photocurrent.

Photocurrent Analysis									
PSI Source	Electrode Surface/ Immobilization	Redox Mediators			Photocurrent[a] ($\mu A\ cm^{-2}$)	Ex. Intensity ($mW\ cm^{-2}$)	Wave-length (nm)	Current Density[b] ($\mu A\ cm^{-2}\ mW^{-1}$)	Reference
		Donor	Acceptor	Concentrations					
T.e.	Au nanoparticles/(SAM)/MPS/PSI	NaAs / DCIP	-	250mM / 2.5mM	1.6	3.3	680	0.48	Terasaki 2006
T.e.	NQC15S-Au NP on gold	NaAs / DCPIP	*NQC_{15}**	250mM / 2.5mM	-	3.3	680	0.007	Terasaki 2007
Spinach	TPDA-SAM on nanoporous gold	NaAs / DCIP	-	5mM / 0.25mM	0.3	3.7	(red filter)	0.08	Ciesielski 2008
Spinach	Bare gold	NaAs / DCPIP	-	5mM / 0.25mM	-	-	-	0.1	Faulkner 2008
6803	Au-PSI-Pt-PSI-Pt-PSI	NaAs / DCIP	-	20mM / 0.05mM	120	40	670	3	Frolov 2008a
T.e.	NQC15EV on gold	NaAs / DCIP	*$NQC_{15}EV$**	250mM / 0.25mM	0.04	0.32	680	0.125	Terasaki 2009a
T.e.	MPS-SAM	DCPIP	MV	250mM / 0.25mM	0.9	1.8	680	0.5	Terasaki 2009b
Spinach	PS I – Based biohybrid cells	NaAs / DCIP	-	100mM / 5mM	2	29	-	0.138	Ciesielski 2010a
Spinach	Cysteamine-SA /PSI multilayer	$K_4Fe(CN)_6$	$K_3Fe(CN)_6$	0.1mM / 0.1mM	7.9	95	(white light)	0.083	Ciesielski 2010b
M.l.	Bis-aniline-NP-Pt-Fd-NP/PSI composite	NaAs / DCPIP	*Bis-aniline-NP; Fd**	40mM / 0.056mM	1.38	1.13	420	1.22	Yehezkeli 2010
T.e.	Osmium complex modified polymer	*Os complexes**	MV	2mM	29	1.8	680	16.1	Badura 2011
Spinach	PSI films/p-doped silicon	-	MV	0.2mM	875	190	633	4.6	LeBlanc 2012
T.e.	Nanocrystalline TiO2/ZnO-psaD/E-PSI	*Z813 Co(II)/ Co(III)**	-	-	362	0.081	(full sun)	4469.1	Mershin 2012
Spinach	PSI-graphene	(RuHex)	Methylene Blue	0.2mM / 20mM	0.55	98	633	0.0056	Gunther 2013
T.e.	Alkanethiol-SAMs (MHO,MHA)	$Os(bpy)_2Cl_2$	MV	0.0135mM / 0.25mM	0.075	1.4	676	0.054	Manocchi 2013

PSI source came from either plant (green) or cyanobacteria (orange). Electron donors were sodium ascorbate (NaAs), 2,6-dichlorophenolindophenol (DCIP/DCPIP), reduced ferricyanide [$K_4Fe(CN)_6$], osmium[$Os(bpy)_2Cl_2$]/Os-polymer, Z813 electrolytes, and rutheniumhexamine (RuHex). Electron Acceptors included naphthoquinone derivative molecular wire (NQC_{15}/$NQC_{15}EV$), methyl viologen (MV), oxidized ferricyanide [$K_3Fe(CN)_6$], composite Bis-aniline nanoparticle-ferredoxin (Bis-aniline-NP; Fd), and methylene blue. Mediator concentrations are also reported when possible, with * indicating that the concentration was not reported or composite mixture was used. Reported photocurrents (a) are shown in ($\mu A\ cm^{-2}$) with increasing values from a gradient of bright red (lowest—0.04) to bright green (highest—875). Excitation wavelength (nm) and intensity ($mW\ cm^{-2}$) are shown, with the latter going from dark gray (lowest—0.081) to yellow (highest—190). Photocurrent values normalized (b) to 1 $mW\ cm^{-2}$ of excitation intensity are then shown from bright red (lowest—0.0056) ($\mu A\ cm^{-2} * mW$) to bright green (highest—4469.1). Unavailable data is indicated by (–). (Nguyen and Bruce 2014)

Table 1-2. Various studies on strategies for PSI immobilization, characterization, and enhancement.

Characterization and Analysis of Immobilization Strategy			
PSI Source	**Electrode Surface/ Immobilization**	**Methods**	**Reference**
Spinach	Au/alkanethiol-SAMs	Triton X-100, adsorbs to low-energy surfaces (hydrophobic SAM), and its PEG groups prevents protein adsorption.	Ko 2004
6803	Au/SAM	PSI attachment by lumenal cysteins. Specific location not essential as long as on extramembranal loop.	Frolov 2005
Spinach	Au-coated-Ni-NTA glass	Designed peptide detergents, acetyl-AAAAAAK (A_6K), preserves PSI's native spectral properties/stabilizes PSI in the dry form for >3 wk.	Kiley 2005
Spinach	Hybrid Organosilicate Glass (Sol-gel)	Enables entrapment of PSI/offers a stabilizing environment for other biomolecules e.g. redox mediators. Matrix transparency is an advantage.	O'neill 2005
Spinach	PSI/HOC_6S/Au backfilled with $C_{22}SH$ or $C_{18}OC_{19}SH$	PSI on HOC6S/Au SAMs, followed by a backfilling of longer-chained methyl-terminated alkanethiols in the interprotein domains," mimics thylakoid".	Kincaid 2006
6803	NP-PS I-NP	Showed that colloidal metal NPs (gold and silver) bound to PSI, acting as optical antennas, enable enhanced broad-band light absorption.	Carmeli 2010
T.e.	hydroxyl-terminated alkanethiolate SAM/Au	Improved on PSI monolayer uniformity via an electric-field assisted deposition. Prevented PSI aggregates that normally formed with the more widely used gravity-driven deposition.	Mukherjee 2010
6803	PSI-CNT hybrids.	Three different strategies for on-chip functionalization of CNT-PSI hybrids were demonstrated (covalent bond, hydrogen bond, and electrostatic forces).	Kaniber 2010
Spinach	PSI/aminoethanethiol-terephthaldialdehyde SAM	Developed mechanistic-kinetic model to investigate the various contributions to the photocurrent production / effects of adsorbed PSI orientation.	Ciesielski 2011
T.e.	PSI-PSII/Sol-Gel Glasses	Combinations of mediated coupling of PSII and/or PSI in solution or sol-gel encapsulated. Enables e^- flow from water photooxidized by PSII to PSI F_B.	Kopnov 2011
T.e.	(Monomer/Trimer)PS I/ alkanethiolate SAM/Au	Showed how temp., mono-/trimeric forms of PSI, and detergent used affects PSI adsorption, along with gravity driven versus an electric field assisted assembly.	Mukherjee 2011
M.l.	PQQ/PSI/(DNaAs/DCPIP)	Anodic/cathodic switchability of photocurrent via PQQ/CdS QDs/(TEOA) or PQQ/PSI/(DNaAs/DCPIP) under various photoelectrochemical configurations.	Efrati 2012
6803	PSI/Au	Photocurrent of an individual PSI via SNOM shows the preservation of its native biomolecular properties after being integrated into nanodevices.	Gerster 2012
6803	PSI/Mesoporous TiO2 Films	TiO_2 matrix's larger pore diameter allowed for a high concentration of PSI to be immobilized, allowing the complex to absorb higher light levels.	Nikandrov 2012
N/A	N/A	Computational model for dipole calculations, luminal surface hydropathicity and polarity characterization were used to predict improvements in surface-assembled monolayer design.	Pendley 2013

PSI source, plant (green) and cyanobacteria (orange), electrode immobilization strategy, and PSI characterization/enhancement methods are described. (Nguyen and Bruce 2014)

Chapter 2

Materials and Methods

A. Genomic Analysis

The crystal structures and genomic sequences of *T. elongatus* PSI and Cyt c_6 were acquired from PDB (1JB0 and 1MZ4 respectively). Genomic DNA/protein sequences were gathered from Uniprot and listed will be listed in proceeding tables (Tables 3-3, 4-1, 4-2, 4-3, 4-4, 5-1, 5-2). *T. elongatus* genomic DNA was previously extracted by Wu et al. 2000(Wu, Zarka et al. 2000). Primers were designed to allow cloning of PetJ into the cloning vector pGEM-T Easy for further subcloning with a 6x-Histadine tag in front of the N-terminus. Using the restriction sites of XhoI and NdeI, the 6x-His-PetJ sequence was subcloned into the expression vector pet30B.

B. Protein Isolation and Purification

Growth of T. elongatus

The thermophilic cyanobacterium *T. elongatus* BP-1 (originally isolated from a hot-springs in Beppu, Japan) was grown in 2-liter airlift fermenters (Bethesda Research Labs) in BG-11 media. The growth temperature was held between 45 - 55°C with continuous illumination by fluorescent lights. The light level was increased as the cultures got denser to a maximum of 50 $\mu E/m^2/s$. Cells were collected by centrifugation for 10 min at 7,000g during late log phase and washed

once in wash buffer (20 mM 2-(N-morpholino) ethanesulphonic acid (MES) pH 6.5, 5 mM $MgCl_2$ and 5 mM $CaCl_2$) before storage at -20°C until use for PSI preparation.

Isolation of PSI

Frozen *T. elongatus* cells were thawed at room temperature and resuspended in wash buffer and 500 mM sorbitol. The resuspended cells were adjusted to a chlorophyll a content of 1 mg/ml and homogenized using a Dounce homogenizer. Lysozyme was added to 0.2% (w/v) and the mixture was incubated for 2 hrs at 37°C with shaking. The resulting mixture was centrifuged for 10 min at 7,000g and the light blue supernatant was discarded. The pellet was resuspended in the wash buffer. The volume was adjusted again so that the chlorophyll a concentration was 1 mg/ml; the mixture was then passed twice through French Press (Amino) at a cell pressure of 20,000 psi. The blue, highly fluorescent lysate (containing phycocyanin) was centrifuged at 50,000g for 20 min, and the supernatant was discarded. The crude membrane fragments collected in the pellet were washed in wash buffer supplemented with 3 M NaBr and then twice in the initial wash buffer. The final washed membrane fragments were adjusted to a chlorophyll a concentration of 1 mg/ml and n-Dodecyl-β-D-maltoside (DDM) (Glycon Biochemicals, Germany) was added to a final concentration of 0.6% (w/v) and the mixture incubated for 20 min at 20°C in darkness with gentle stirring. The insoluble material was removed from the solubilized membrane mixture by centrifugation at 50,000g for 30 min. The supernatant was separated immediately from the pellet and then loaded onto 10–30% sucrose gradients with 60% cushion; all solutions in the gradient also contained 20 mM MES pH 6.5 and 0.03% DDM. Density gradient centrifugation was

performed at 80,000g at 10°C for 16 hrs. The lowest green band contained the trimeric PSI complex; these bands were collected and pooled using a large syringe. Pooled PSI samples were slowly diluted five-fold by addition of 20 mM MES pH 6.5 with 0.03% DDM (w/v), and then loaded onto a POROS 20HQ (Applied Biosystems) anion exchange column and eluted with a linear 0 to 400 mM $MgSO_4$ gradient. The $MgSO_4$ was removed by dialysing against 20 mM MES pH 6.5, 5 mM $CaCl_2$, 5 mM $MgCl_2$ and 0.03% DM, and aliquots were stored at -80°C for future use.

C. Recombinant Cytochrome Expression/Purification

This expression and purification protocol was originally created and optimized by Natalie Myers as a part of her Master's Thesis.

Mature form of the *T. elongatus* cytochrome c_6 was expressed in *E. coli* using the System I or CCM maturation system from Feissner, Richard-Fogal et al. (2006). Competent E. coli (BL21 DE3) cells were double transformed with a pet30B plasmid that contained petJ from *T. elongatus* with a 6x-His Tag, along with a plasmid that contained System I-CCM haem maturation cassette. Cells were plated on LB media supplemented with both Kan and Amp antibiotics for selection of colonies that picked up both plasmids. Resistant colonies that appeared overnight were re-streaked on a new LB/Kan/Amp plate and 5 mL of LB liquid broth containing Kan and Amp. Once reaching about 0.6 O.D., the 1 mL of the 5 mL liquid culture was then added to 1 L of SV media supplemented with Kan and Amp. The cells were left to shake for 12-16 hrs at 37°C at 225 rpm. Once an O.D. of about 0.4-0.5 was reached, cultures were induced with 1 mL of 1 mg/mL IPTG and ALA and allowed to shake at 20°C for at least 16 hrs or until cells turned pink. The one-liter cultures were then

centrifuged and pelleted into 50 mL Falcon tubes. Tubes were then stored in the -80°C for future usage.

Periplasmic Shock

For immediate purification, the cells then were resuspended in 5-10 mLs of (Column Wash Buffer - 10 mM Hepes) and flash frozen in liquid Nitrogen. Periplasmic shock was then performed by submerging the frozen tubes in 65°C water bath. After thawed, tubes were centrifuged and the cytochrome containing supernatant was collected. This procedure was repeated 3-4 times until most, if not all the reddish pink color was gone from the pellets. A high-speed spin was then performed on the collected supernatant so that no cell residues would be loaded onto the Nickel column for purification.

IMAC Purification

Nickel columns were equilibrated with at least 20 column volumes of wash buffer. Cytochrome containing supernatant was then loaded, making sure that the reddish color sticks to the blue resin. Flow-thru were then collected. Once loaded, columns were washed with 20 columns of wash buffer containing 0.5 -1.0 mM imidazole. After sufficient washing of the columns, the bound cyt c_6-6xHis was eluted with 20 mM imidazole. Following elution, purified cyt c_6 was dialyzed against (HEPES buffer) for 8 hours at 4°C to remove the majority of imidazole. The remaining product was then lyophilized and stored at -80°C until needed.

D. LED Flash Photolysis of PSI

Sample Setup for JTS-10

Samples are comprised of purified *T. elongatus* PSI at 3 μg chlorophyll/ml or ~35 nM (assuming 96 chl a/PSI), with a 10-fold molar excess of recombinantly expressed *T. elongatus* cytochrome c_6 as described previously (Iwuchukwu, Vaughn et al. 2010). Both PSI and cyt c_6 were purified using the methods described previously.

The sample mix also includes 2 mM sodium ascorbate, 0.1 mM methyl viologen, 5 mM $MgCl_2$, 5 mM $MgSO_4$, brought up to 1 mL of 20 mM MES buffer (pH 6.4) with 0.03% n-Dodecyl-β-D-maltoside (Glycon Biochemicals, Germany). The buffer composition was only changed if noted, where the salts, reductant, and electron acceptor was a variable.

JTS-10 Configuration and Data collection

Basic configurations of JTS utilize an "Orange Ring" array of LEDs (630 nm peak emission) for the actinic source at 3000 μE/m^2/s intensity (unless otherwise noted), with the probe LEDs either at 705 nm or 810 nm (including interference filters at the respective wavelengths). Data collection consists of 15 discrete points (500 ms apart) to establish a pre-actinic flash baseline, followed by 200 points of post-actinic flash, exponentially increasing from 60 μs to 10 s. The first 15 points (pre-actinic flash) and the last 10 points are used for a linear regression of each sample trace (Figure 2-1). Data shown are an average of three individual traces with a subtraction of a non-actinic trace, accounting for any actinic activity given off by

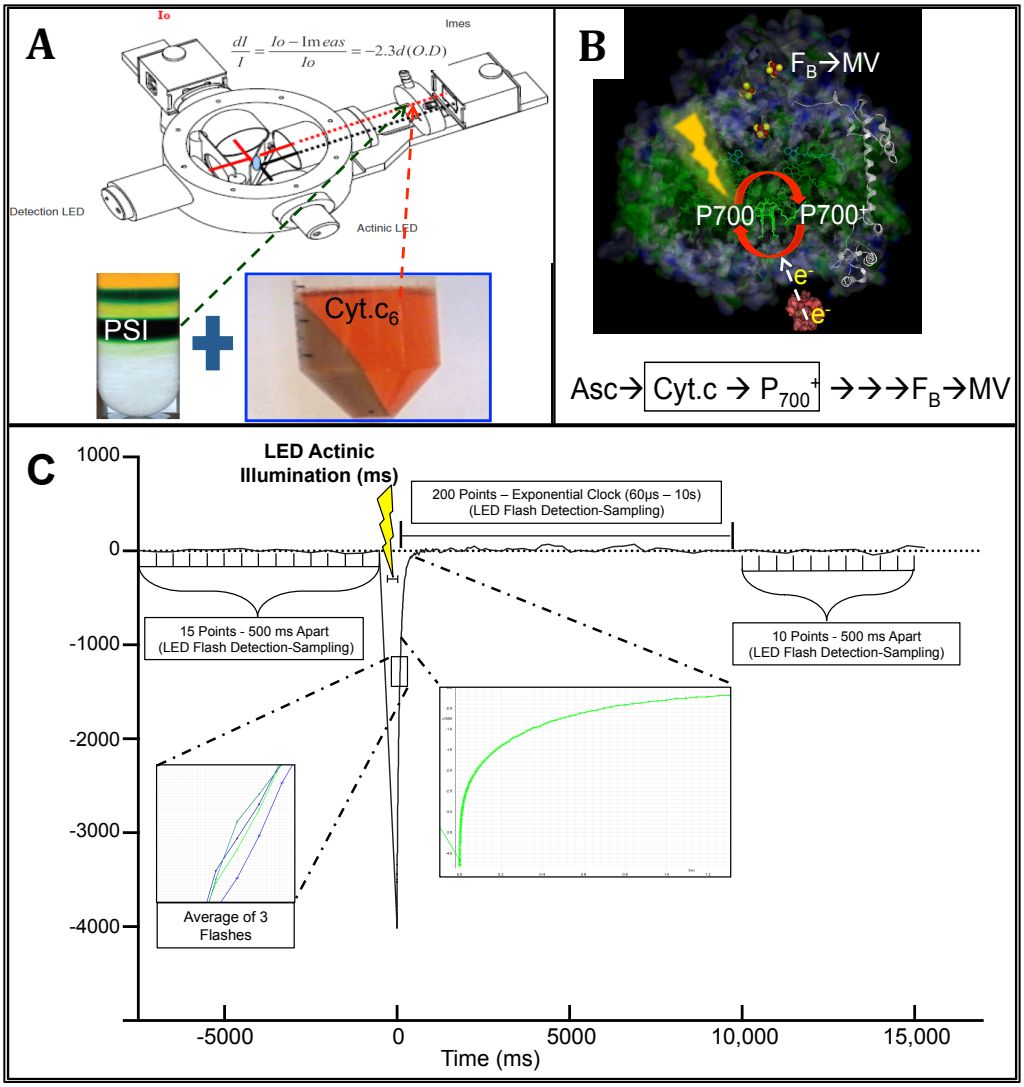

Figure 2-1. JTS-10 Flash Photolysis of PSI

A) Schematic of JTS-10 spectrophotometer B) Depiction of e^- transport pathway in flash-photolysis reactions with the included reagents: sodium ascorbate, recombinant cyt c_6, purified PSI, methyl viologen, and buffer. C) Schematic of JTS-10 sample acquisition. Detection points (15) were taken 500 ms apart before LED actinic flash. After the LED actinic illumination was triggered, 200 points are collected using an exponential clock from 60 µs to 10 s. Detection points (10) were then collected 500 ms apart after exponential clock. Each sample run consisted of an average of 3 repeated flashes.

the probe LEDs. Data analysis and curve fitting were performed using GraphPad Prism ® software.

E. Cloning of Mutant/Poly/Variable Cytochromes

Electrostatic Mutant Cytochromes

Cyt c_6 primers were constructed to be utilized with site-directed mutagenesis, where single point mutations would be introduced after multiple rounds of PCR amplification. Residues that were changed individually were at position G63D, D67E, and Q69E. After individual mutants were made and confirmed by DNA sequencing, double mutants were made, utilizing the single mutants as the DNA template for PCR. Detailed methods will be further discussed in Chapter 3, section D.

Poly-Cytochrome

To make these constructs, we made a cloning scheme that would allow successive rounds of mutagenesis, adding one more wild type cytochrome each time. Using the XhoI restriction site at the C-terminus of the "Triple" mutant cytochrome, we inserted WT cytochrome using SalI and XhoI (SalI_WT_XhoI), abolishing the XhoI site on the C-terminus of the "Triple" mutant, leaving only one XhoI site at the C-terminus of the WT cytochrome (Triple-WT_XhoI). This allowed us to successively clone in WT cytochromes with the same strategy. Detailed strategies and schematic will be shown in Chapter 4, section A.

Variable Cytochrome

As part of the electron transfer chain in photosynthesis, a soluble carrier (either cytochrome c or plastocyanin) accepts an electron from the Cytb6f complex and shuttles it to Photosystem I, allowing for the reduction of the special pair chlorophyll P_{700}. The interaction between cytochrome c_6 and PSI is known to occur near or at the psaF subunit of PSI. This protein pair has been investigated in previous literature to show that an electrostatic interaction (acidic on cytochrome and basic on psaF) has emerged from cyanobacteria (very little or none) to algae and plants (prominent interaction), which affects their electron transfer rate. In order to investigate this transition, we aim to focus on the interacting interface between the cytochrome and psaF, and their charge content. Ten cytochromes were chosen from a selected group of about 100, with the criteria of covering a wide range of surface charge properties. These include protein pI, psaF-interface net charge, number of psaF-interface acidic residues and total protein net charge. This will be later shown in Chapter 4, section B in more detail. From the coding sequences, the cytochromes were synthesized, subcloned into the pet30B expression vector behind a His-tag, and transformed into E. coli expression strain along with a CCM heme maturase vector. All these cytochromes followed the same purification scheme as discussed earlier in Chapter 2, section C.

F. Western Blots for *in vivo* PSI/Cyt c_6 Content

The psaD and cyt c_6 gene was cloned from *T. elongatus* genomic DNA. A synthetic codon-optimized DNA fragment encoding the psaF gene from *T. elongatus*

was purchased (Epoch Life Science, Inc., Missouri City, TX). Both psaD and psaF sequences were cloned into pTYB2 vector, and the gene product was expressed and purified from *E. coli* using the IMPACT system (New England Biolabs, Ipswich, MA). Polyclonal antibodies were produced in rabbits (Pocono Rabbit Farm, Canadensis, PA) following immunization and boosting with the recombinant cytochrome c_6, PsaD, and PsaF.

Western blot analysis was performed on *T. elongatus* intact whole cells along with recombinant proteins were separated using the same 15% SDS PAGE gel and transferred onto Immobilon-P Transfer Membrane (Millipore) using a graphite electroblotter (Idea Scientific, Minneapolis, MN). Immobilon-P was blocked for 3 hrs in TBS buffer with 0.1% Tween-20, 2% BSA, and 2% NFM. After blocking, incubation with primary antibodies (α-PsaD 1:50,000, α-PsaF 1:10,000, α-cyt. c_6 1:5,000) was done in the same buffer overnight at 4°C. Three washes with TBS-Tween (2% NFM) were performed before a 1 hr incubation with a goat anti-rabbit IgG HRP secondary antibody (1:50,000). Final visualization was achieved with SuperSignal West Dura Extended Duration Substrate (Thermo Scientific).

For each antigen a standard curve of 4 concentrations were used and a range of cell numbers were tested on a single blot. This permitted a standard curve to be generated and 3-4 independent concentrations determined. All measurements were repeated three times to provide a final N-value of 12-15 for each antigen. This can be better visualized in the next Chapter, with Figure 3-1, section A.

Chapter 3

Electrostatic Mutants of Cytochrome - PSI Pair

A. Introduction

The bio-hybrid devices listed in Chapter 1, either with the goal of evolving molecular hydrogen or generating a photocurrent, utilize PSI's ability to energize electrons via light input so that they can flow freely through the reaction center, allowing them to be fed to acceptors on the stromal side. The energetics and rate of which these electrons travel through the internal cofactors of PSI have been thoroughly discussed and worked on by various groups in the last decade, (Ali, Santabarbara et al. 2006, Byrdin, Santabarbara et al. 2006, Ihara, Nakamoto et al. 2006, Li, van der Est et al. 2006, Santabarbara, Kuprov et al. 2006, Santabarbara, Chen et al. 2007, Agalarov, Byrdin et al. 2008, Bender and Barry 2008, Goni, Serrano et al. 2008, Santabarbara, Jasaitis et al. 2008, Chen, Bender et al. 2009, Giera, Gibasiewicz et al. 2009, Matsumoto, Zhang et al. 2010, Muller, Slavov et al. 2010, Santabarbara, Galuppini et al. 2010, Santabarbara, Kuprov et al. 2010, Santabarbara, Reifschneider et al. 2010, Berthold, von Gromoff et al. 2012, Moal and Lagoutte 2012, Mula, Savitsky et al. 2012, Semenov, Shelaev et al. 2012, Renaud, Powell et al. 2013, Makita and Hastings 2015, McConnell, Sun et al. 2015, Santabarbara, Bullock et al. 2015, Semenov, Petrova et al. 2015) with the potential to increase this rate for applied photosynthesis. The majority of our work here however, focuses on the preceding steps of how the electrons can even be donated to PSI, allowing it to be processed through the complex.

In working with this project, we started with a well characterized, model cyanobacterium, *Thermosynechococcus elongatus BP-1*. This thermophilic cyanobacterium, with a fully sequenced genome (Nakamura, Kaneko et al. 2002), and available PSI crystal structure (PDB ID- 1JB0)(Byrdin, Jordan et al. 2002), gave us a thermo-tolerant platform in which we were able to manipulate in various aspects, toward the goal of increasing electron transfer. Previous literature have reported fast electron transfer rates in plant and algae systems, which were attributed to the increased electrostatic interactions between the electron donor and the lumen exposed, N-terminal portion of the PsaF subunit of PSI (Hippler, Drepper et al. 1998, Sommer, Drepper et al. 2006). These protein surface interactions have been shown to be due to increased positively charged residues on PsaF and negatively charged residues on the electron donors, cyt c_6 or PC (Hippler, Drepper et al. 1998, Sommer, Drepper et al. 2006). This gave us an idea to where we thought it would be very advantageous to be able to increase the rate of electron transfer to P_{700}, but also easily manipulate other features of PSI by working with a basic cyanobacteria PSI background. Before starting to think about increasing the electron transport rate, we first had to be sure that we had the ability to well characterize our WT electron donor/PSI system with our own instrumentation.

We start with the recombinant expression of cyt c_6 from *T. elongatus* and the schematic of this process is shown in Figure 3-1. The purification of PSI from cyanobacteria have been developed in previous studies, where a sucrose density gradient was used to separate out the solubilized membrane proteins before further

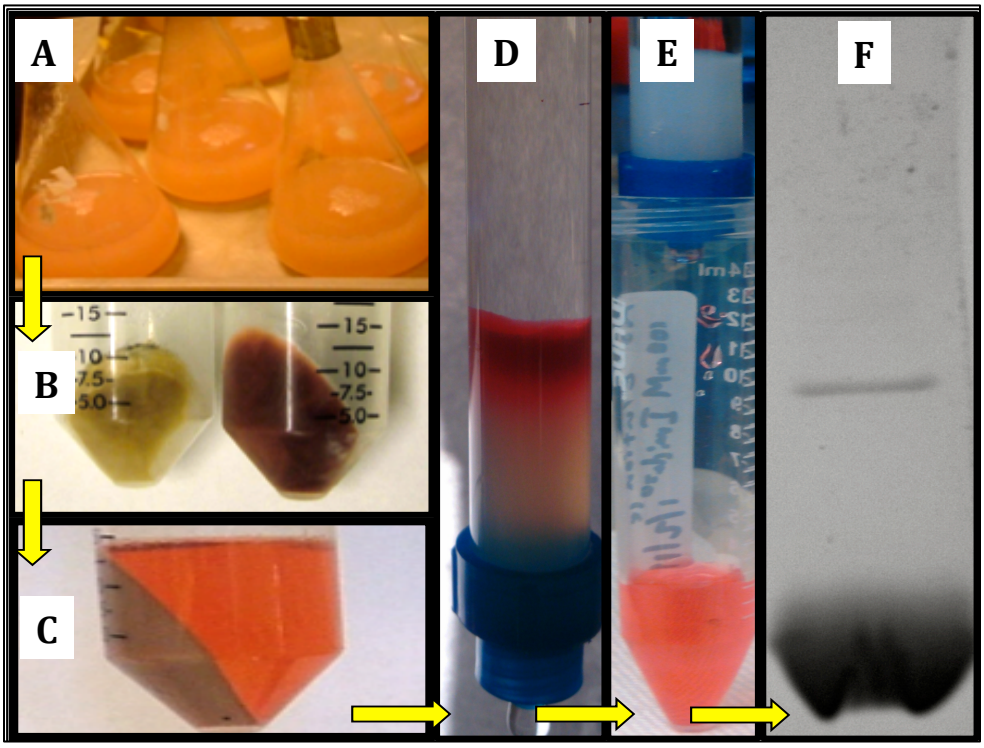

Figure 3-1. Recombinant cytochrome c_6 (cyt c_6) production/purification

A) 2L Flasks of transformed *E. coli* grown and induced in SV media. B) Uninduced (left) compared to induced (right) cells pelleted. C) Supernatant after periplasmic shock and subsequent spin. D) Supernatant containing 6xHis-tagged cyt c_6 loaded and bound onto Nickle-NTA column. E) Elution of cyt c_6 with immidazole. F) SDS-PAGE of purified recombinant cyt c_6

purification. This has been published by our lab in a previous work (Iwuchukwu, Vaughn et al. 2010).

The purity of both proteins was determined by SDS-PAGE (Figure 3-2a) and BN-PAGE (Figure 3-2b). The BN-PAGE indicates that yield and homogeneity of PSI was primarily in the trimeric form at ~1068 kDa with very little PSI monomer (~400 kDa) and a very small amount of PSII monomers or dimers (Li, Semchonok et al. 2014). The lack of PSII was also confirmed from the low temperature fluorescence at 77K, which had a single prominent peak at 728 nm (Figure 3-2c) and lacked the characteristic fluorescent peak at 695 nm (Schlodder, Hussels et al. 2011). The reduced minus oxidized difference spectra of cyt c_6 (also c_{553}) showed a characteristic peak at 553 nm as expected (Figure 3-2d).

B. Characterization of Cytochromes in Cyanobacteria (*T. elongatus*)

Western Blot Quantification of Intracellular Cyt c_6 and PSI Ratio

In order determine the relevant range of the intracellular cytochrome c_6 to PSI ratio, we conducted a quantitative Western blot analysis using known amounts of purified recombinant cyt c_6 and PSI subunits (PsaD and PsaF) that were used to standardized the signal from intact *T. elongatus* cells probed with polyclonal antibodies (α-PsaD, α-PsaF, α-cyt. c_6) (Figure 3-3 & 3-4).

In order to quantify and compare the intracellular concentration of PSI and cytochrome c_6, we can not directly look at the western blots of the intact cells alone since many variables like primary antibody specificity, slight variations in SDS gel

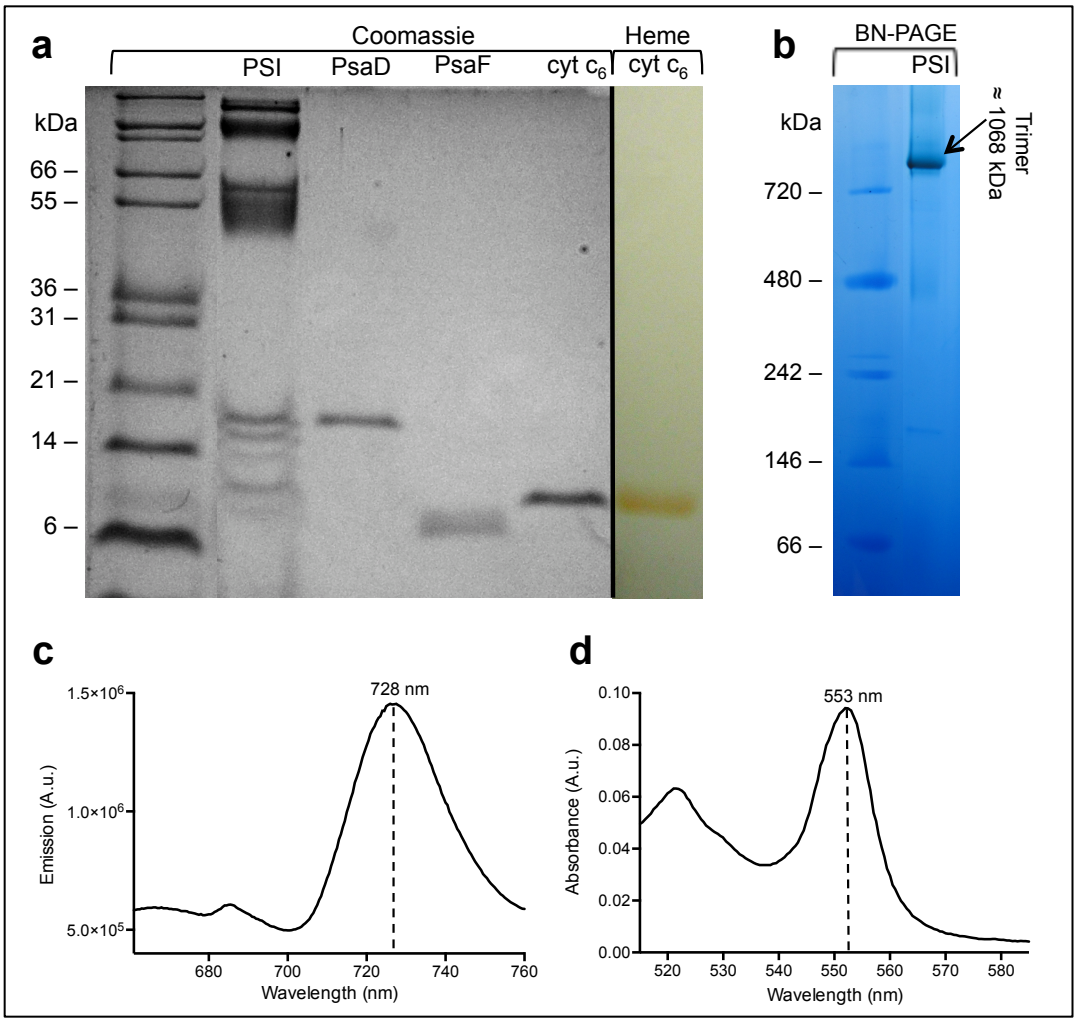

Figure 3-2. Purified cytochrome c_6 and PSI confirmation.

(a) SDS-PAGE of purified PSI, recombinantly expressed *T. elongatus* PsaD, PsaF (N-term) and cyt c_6 (left: coomassie stained and right: heme stain). (b) Blue Native PAGE of purified *T. elongatus* PSI, showing a high molecular weight band above the 720 kDa band, with *T. elongatus* PSI trimer estimated to be about 1068 kDa (Li, M et al. 2014). (c) Low temperature (77K) fluorescence scan of PSI, showing a characteristic emission peak at 728 nm. (d) Reduced minus oxidized difference spectra of cytochrome c_6, with a characteristic peak at 553 nm.

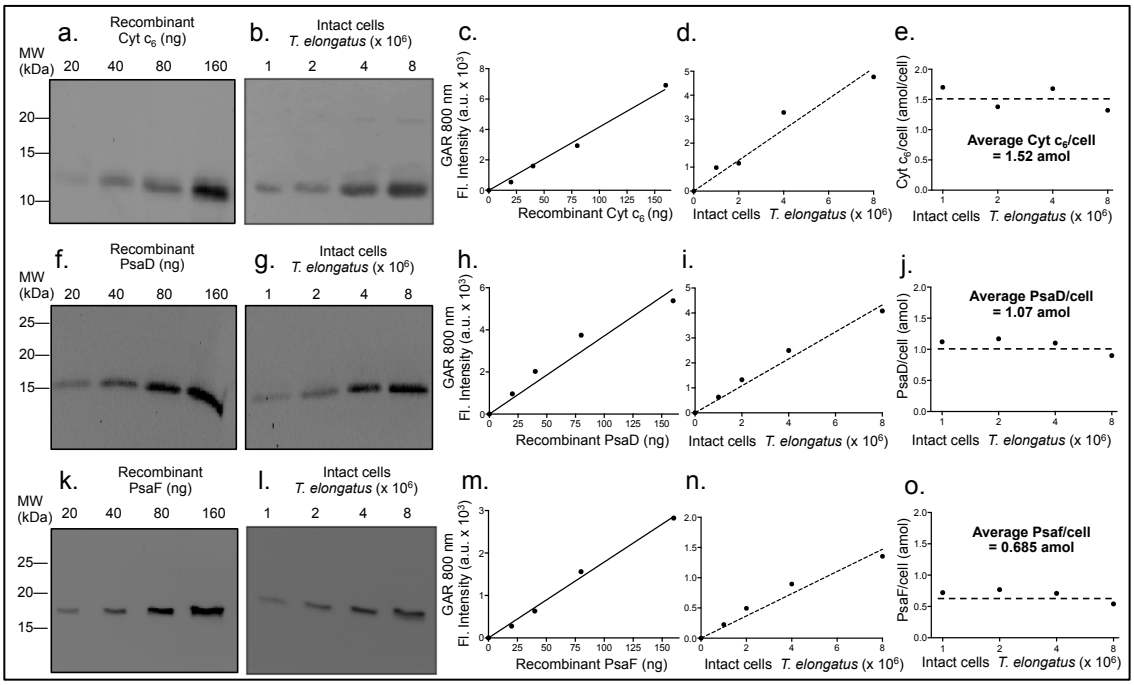

Figure 3-3. Western blot quantification of cyt c_6 (a-e), PsaD (f-j), and PsaF (k-o).

Western blot detection of recombinant cyt c_6 (20-160 ng) (a) and intact *T. elongatus* cells (1-8 x10^6) (b) using α-cyt c_6. Quantification of a (c) and b (d) resulting in calculation of amount of cyt c_6 per *T. elongatus* cell (e). The same technique was used for PsaD (f-j) and PsaF (k-o).

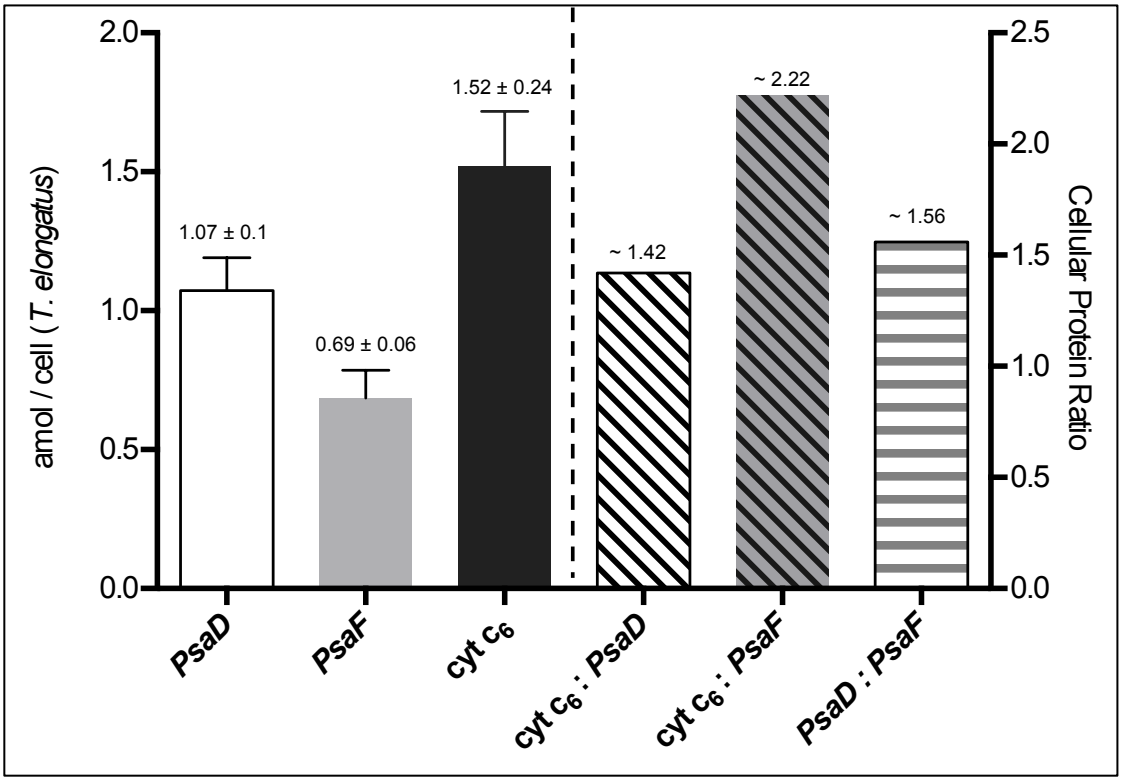

Figure 3-4. Quantification of western blot analysis for cellular content of PSI (PsaD/PsaF) and cytochrome c_6 in *T. elongatus*.

On the left y-axis, PsaD (solid white bar) was estimated to populate a *T. elongatus* cell at a concentration of 1.07 ± 0.1 amol, PsaF (solid gray bar) at 0.69 ± 0.06 amol, and cyt c_6 (solid black bar) at 1.52 ± 0.24 amol. The resulting cellular ratio (right y-axis) of cyt c_6 to PsaD (white with black stripes bar) is estimated to be 1.4, cyt c_6 to PsaF (gray with black stripes bar) at 2.2, and PsaD to PsaF (white with gray stripes bar) at 1.56.

running, and blot exposure time will affect the signal intensities of the bands. Instead, known amounts of the respective recombinant proteins are ran on the same gel as the intact cells, allowing a direct comparison to standards going through the exact blotting conditions.

To generate these standard curves, recombinant cyt c_6 *(20-160 ng)* was ran on the same SDS PAGE as *T. elongatus* cells *(1-8 x10^6)*, which was then blotted using α-cyt c_6 (Figure 3-3a-b) and quantified using NIH ImageJ (Figure 3-3c-d). From here, 4 independent concentrations of cyt c_6 per *T. elongatus* cell were calculated giving an average value of 1.52 ± 0.24 amol/cell of cyt c_6 (Figure 3-3e). The same technique was repeated for PsaD (α-PsaD) (Figure 3-3f-j) and PsaF (α-PsaF) (Figure 3-3k - o), yielding 1.07 ± 0.1 and 0.69 ± 0.06 amol/cell respectively (Figure 3-3j & o). The resulting values are shown in Figure 3-4 (left y-axis), along with the cellular protein ratio (right y-axis). The cyt c_6 to PsaD and to PsaF ratios (Figure 3-4) were calculated to *1.42* (white bar with black stripes), 2.22 (gray bar with black stripes) respectively. The PsaD to PsaF was calculated to be 1.56 for PSI. We suspect that PsaD, being on the stromal hump of PSI, has the potential to be in greater quantity than the thylakoid bound PsaF, which would have a slower turnover time while in the membrane.

The only intracellular concentration of PSI that we found was calculated for *Synechocystis 6803* via chlorophyll extrapolation, which resulted in about 96,000 units per cell (Keren, Aurora et al. 2004). Considering the values we calculated for PsaD (15.24 kDa) and PsaF (17.7 kDa) (1.07 amol and 0.69 amol respectively), along with an estimated cell volume of 1.5 x 10^{-14} L, the resulting average of PSI units per

cell was about 530,000. Using the same cellular volume and 1.52 amol, cyt c_6 (11.8 kDa) came to about 915,000 units per cell. With *Synechosystis 6803* being a mesophile and our *T. elongatus* a thermophile, many factors, including growth conditions, chlorophyll approximation, and cell volume estimation could have contributed to the 5x difference in intracellular PSI content. This discrepancy however should not affect our resulting relative ratio of the two proteins.

By directly measuring the relative amounts of both PSI (PsaD and PsaF) and the cytochrome c_6 in intact cells using this method, we are able to conclude that the relative ratio of cyt c_6 to PSI is close to the same relative concentrations. Although there are many caveats to making an absolute measurement considering such factors as membrane excluded space, sub-cellular localization, cellular organization, and possibly macromolecular crowding, to our knowledge, this is the first such reported ratio in a cyanobacteria and is most probably the lowest limit of the ratio due to the caveats described above. Thus we conclude the ratios of cyt c_6 to PSI used in our experiments should be close to the *in vivo* ratio, within instrument detection limits, of about 1.7:1 of cyt c_6 to PSI per *T. elongatus* cell.

C. PSI Characterization Parameters via JTS-10

Illumination - Flash Intensity and Duration

The ability of the JTS-10 spectrometer to completely photo-oxidize P_{700} using its LED-based actinic light source was investigated. The amplitude of absorbance change at 705 nm was monitored by varying the length of the LED illumination from 10 μs to 7.5 ms. Fully photo-oxidized samples containing 35 nM PSI (3 μg

chlorophyll/ml) displayed a plateau in the intensity of the photo-bleaching after 2.5 ms (Figure 3-5A). The actinic LED intensity was also varied from 12 to 3000 $\mu E/m^2/s$ with three different exposure times (5, 15, and 45 ms). The sigmoidal shape of this light intensity effect on photo-bleaching reached the same saturating value yet took considerable higher light levels when the illumination intensity was reduced from 45 ms to 15 and 5 ms. The complete conversion of P_{700} to P_{700}^+ required a flash duration longer than 5 ms at intensities below 3000 $\mu E/m^2/s$ as indicated by maximum ΔAbs_{705nm} (Figure 3-5B). Considering the required actinic flash duration to reach complete P_{700}^+ formation for this LED based system is 2-3 ms and previously reported rates of charge separation (approximately 1 μs) to form the (P_{700}^+, F_B^-) pair (Brettel and Leibl 2001), suggests that multiple turnover events of P_{700}^+ reduction by cyt c_6 may be occurring when actinic flash durations in the millisecond range is used. We also tested the effect of the cyt c_6:PSI ratio on the signal intensity. Measurements were performed in triplicate at four concentrations of cyt c_6, ranging between 10 and 60-fold molar excess to PSI, each of which gave similar absorbance amplitudes at each flash duration (Figure 3-5A).

The sensitivity of the photodiodes used by the JTS-10 allowed P_{700} activity to be measured with very dilute samples. We tested the signal-to-noise of the ΔAbs_{705nm} measurement as a function of P_{700} concentration (Figure 3-6). Using an initial PSI concentration of 544 nM, we diluted the sample twofold in eight steps to a final concentration of 2.13 nM, taking measurements at each dilution. The reduction curves were then multiplied by the dilution factor to get normalized curves, which were then fitted to a model that is the sum of two exponentials, 34 nM to 2 nM are

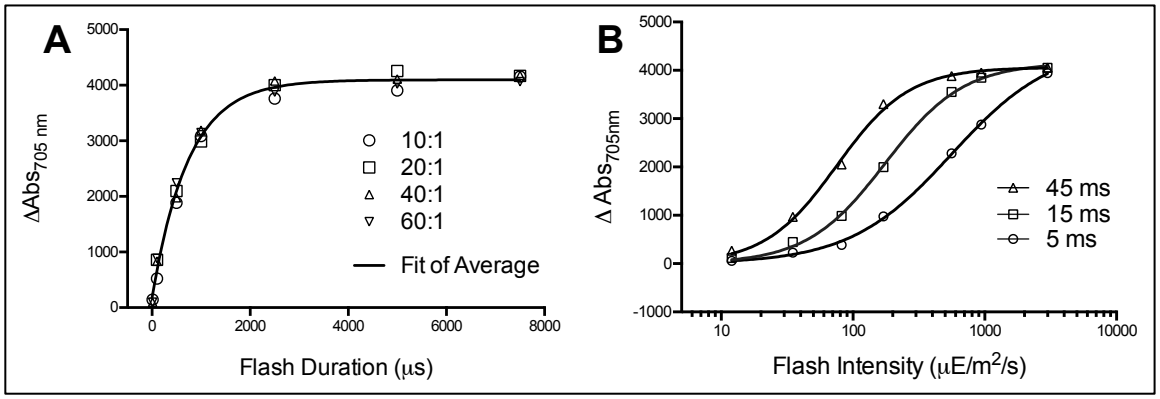

Figure 3-5. Total P_{700} photo-oxidation displayed as a function of (A) flash duration and (B) flash intensity.

A) 35 nM of PSI was used with 10, 20, 40, and 60-fold molar excess of cyt c_6. Absorbance change was shown from 0 to 7500 μs. B) 35 nM of PSI was used with a 10-fold molar excess of cyt c_6 and flash intensity ranged from 12 to 3000 $\mu E/m^2/s$, shown with 3 different flash durations.

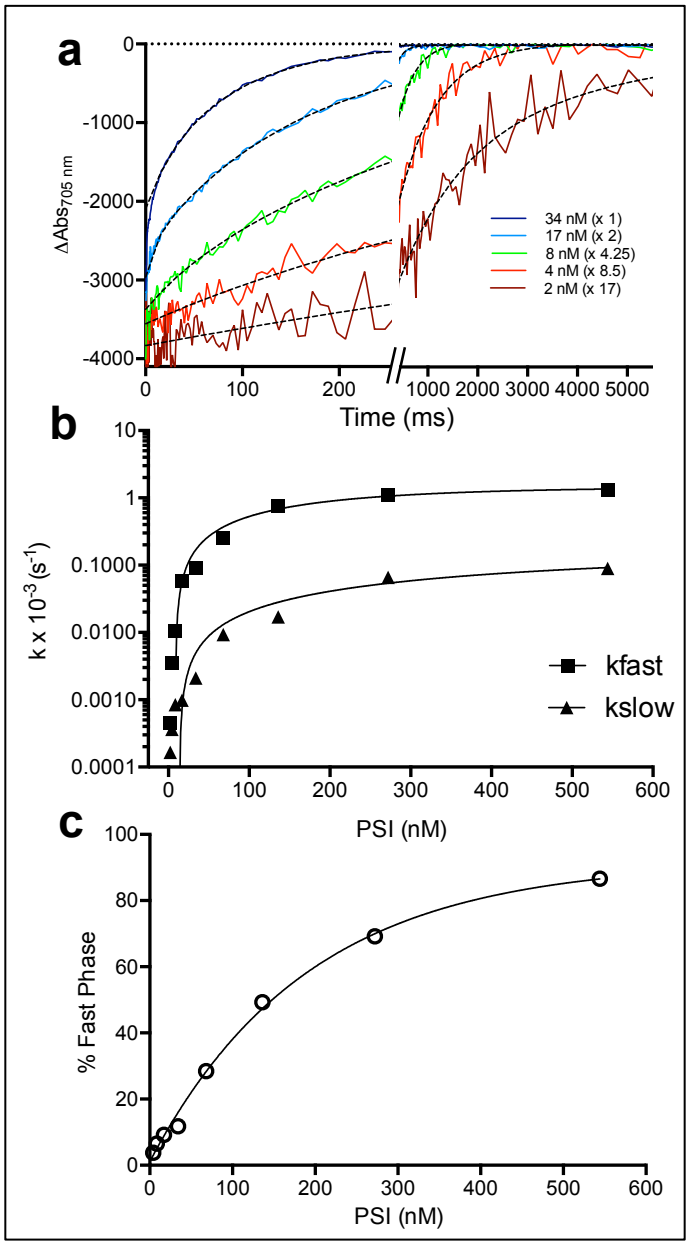

Figure 3-6. P_{700} reduction measured by LED (JTS) is dependent on total protein concentration.

a) Raw P_{700} reduction curves, normalized to the dilution factor (cyt:PSI, 10:1) of 34 nM PSI. b) Rates from two phase kinetic fits of 2-fold dilutions from 544 nM PSI (cyt:PSI, 10:1). c) Percentage of the fast phase from two phase kinetic fits of 2-fold dilutions from 544 nM PSI (cyt:PSI, 10:1).

shown in Figure 3-6A (y-axis normalized to 34 nM amplitude). The two-phase rate constants were reported for each normalized dilution (Figure 3-6B), along with the percentage of the fast phase (Figure 3-6C). At a 10:1 molar ratio of cyt c_6 to PSI, we see kinetics sequentially slow down with each dilution along with the percent of the fast phase. We observed P_{700} photo-bleaching and with high quality data fits of the reduction kinetics all the way down to 0.3 µg chlorophyll/ml, as the R^2 for 4 nM PSI was still at 0.985 (Table 3-1). This is significantly lower concentration of PSI than was used in similar reports in literature range from 10 µg chlorophyll/ml (Hatanaka, Sonoike et al. 1993) (10 x more sensitive) to 0.75 mg chlorophyll/ml (Hervas, Navarro et al. 1995) (750 x more sensitive), which indicates the sensitivity of the optical design and photodiodes used in the JTS-10.

Fast phase dependence on methyl viologen concentration was analyzed to ensure that we had provided an adequate amount of electron acceptors (MV) to PSI, allowing for continuous electron flow through the internal PSI cofactors (P_{700} -> A_0 -> A_1 -> F_X -> F_A -> F_B). Without enough MV to take electrons from the FB iron-sulfur cluster, electrons may travel backwards from F_B to P_{700} (charge recombination). These charge recombination events occur on the tens of milliseconds, depending on where we visualize this re-reduction of P_{700}, where it is reported in literature in various cyanobacteria to be about 20 ms from F_A or 65 ms from F_B (Shinkarev, Zybailov et al. 2002, Santabarbara, Heathcote et al. 2005). We performed a detailed MV titration to confirm this (Figure 3-7). With PSI kept constant at 35 nm and cytochrome was in 10-fold excess, we see that without methyl viologen there is a distinct fast phase occurring in the tens of milliseconds (Figure 3-7A). The absolute

Table 3-1. Values from two-phase kinetic fits as shown in Figure 3-6. The R^2 values are also shown.

PSI (nM)	$\%k_{fast}$	k_{fast}	k_{slow}	R^2
2.13	ND	4.57×10^{-4}	1.65×10^{-4}	0.976
4.25	3.80	3.50×10^{-3}	3.65×10^{-4}	0.985
8.5	6.53	1.06×10^{-2}	8.47×10^{-4}	0.997
17	9.21	5.79×10^{-2}	9.86×10^{-4}	0.998
34	11.78	9.03×10^{-2}	2.10×10^{-3}	0.997
68	28.44	2.57×10^{-1}	9.34×10^{-3}	0.998
136	49.32	7.64×10^{-1}	1.71×10^{-2}	0.998
272	69.24	1.10×10^{-1}	6.60×10^{-2}	0.998
544	86.59	1.33×10^{-1}	8.94×10^{-2}	0.999

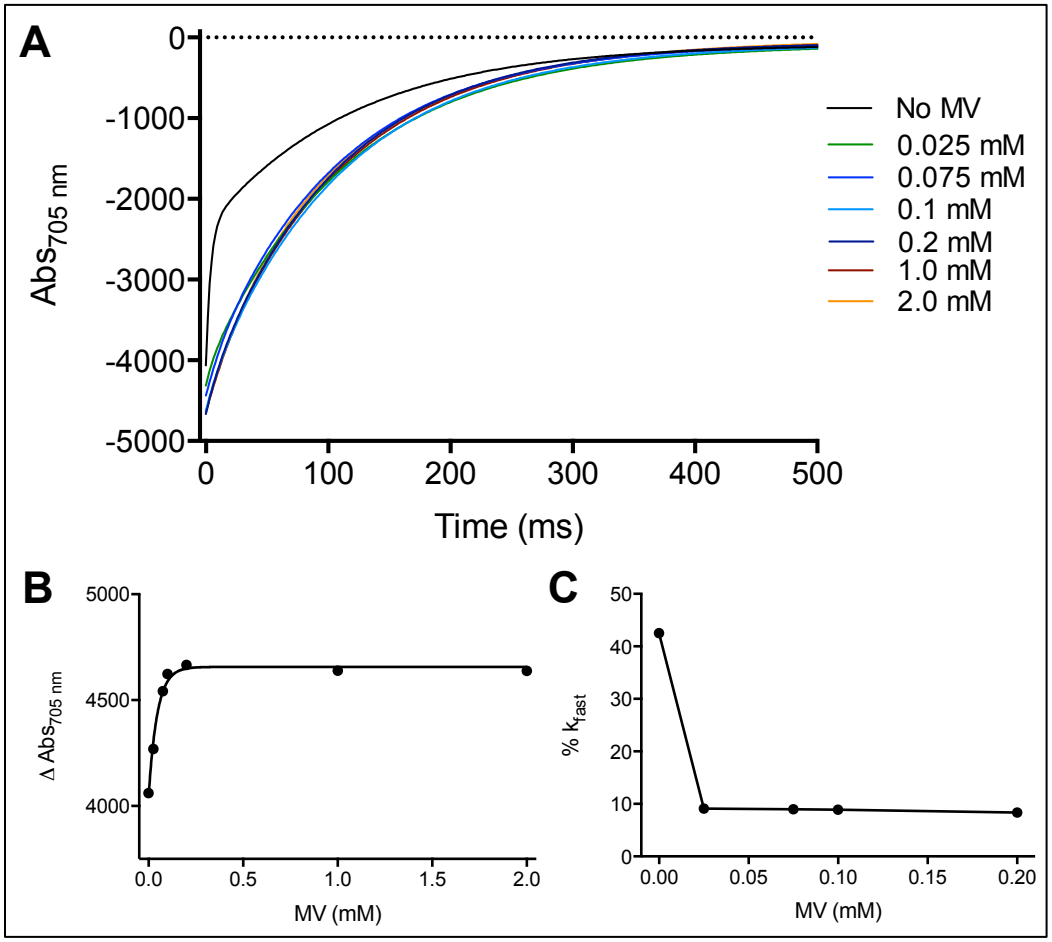

Figure 3-7. Effect of methyl viologen on P_{700} reduction in JTS-10.

A) Recovery curve of 35 nM PSI by 0.35 μM cyt c_6, with varying amounts of methyl viologen (MV). B) The absolute change in absorbance at 705 nm with increasing MV concentration, plateauing around 0.1 mM. C) The percentage of the fast phase of the two-phase fits for PSI recovery curves from A).

change in absorbance of P_{700}, also was greatly affected, with a plateau around 0.1 mM MV (Figure 3-7B). The percentage of the fast phase without any MV is approximately 43%, with a steep decrease to about 10% when even 0.025 mM MV was added, reaching a plateau with additional MV (Figure 3-7C). We conclude that the recombination reactions that occur with no final electron acceptor (MV) can be completely alleviated by the addition of as little 0.1 mM MV, as shown by a plateau of P_{700} absorbance and percent fast phase at MV nears 0.1 mM (Figure 3-7B, C). Therefore all of our work that was done using 0.1mM was free from this back reaction.

D. JTS-10 flash photolysis

In order to accurately evaluate any mutant cytochromes/e- donor and PSI, we must test the wild type PSI under various conditions to set a standard electron transfer profile. The re-reduction curves of P_{700+} were analyzed with both single and double exponential fits, with the double exponential yielding a cleaner residual plot (Figure 3-8A), suggesting a bi-phasic nature in the re-reduction rate of P_{700+} by cyt c_6. Re-reduction did not occur within our measurement sequence when no cytochrome was added to the sample mix. When broken down to two phases, the slow phase (k_{slow}) closely resembled the single exponential rate (k_{obs}), increasing linearly with increasing cytochrome concentration, while the fast phase (k_{fast}) increases in a single exponential manner (Figure 3-8B). The contribution of the k_{fast} is minimal as it is only around 10% of the overall recovery rate.

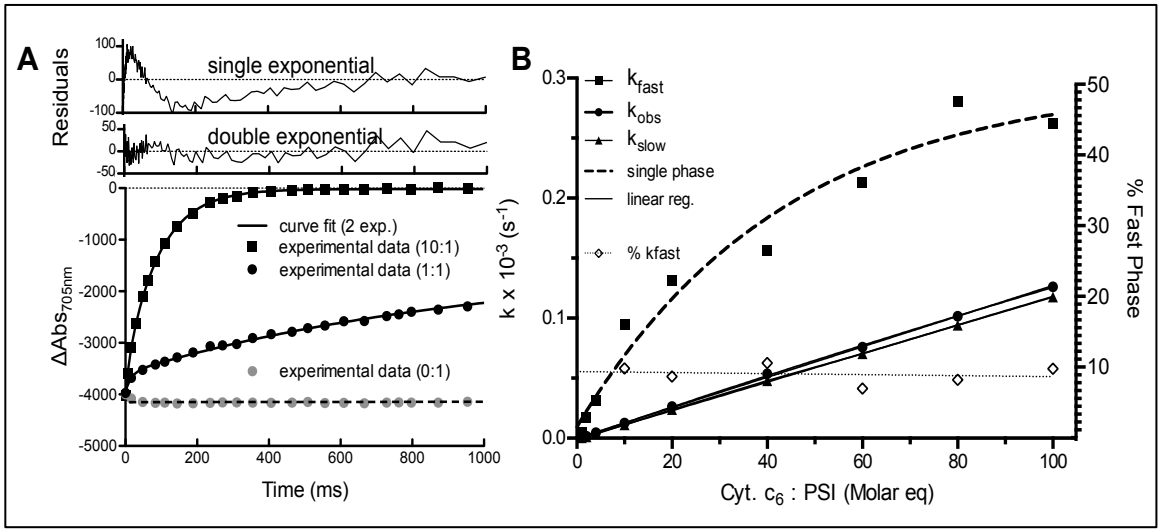

Figure 3-8. Total P_{700} re-reduction as a function of cytochrome c_6 concentration.

A) 35 nM of PSI was used with 0,1, and 10-fold molar excess of cyt c_6. Residuals of P_{700} re-reduction shows better fit to two phases as compared to one. B) 35 nM of PSI was used with excess molar ratios of cytochrome ranging from 0 to 100. Rates of two phases (k_{fast} & k_{slow}) compared to single phase rate (k_{obs}). K_{fast} fits to a single exponential while k_{slow} and k_{obs} follows a linear fit. The % k_{fast} shows all ratios have about 10% fast phase

Reported rate constants for proteins from *T. elongatus* ranges from 1.7 x 10^6 (M^{-1} s^{-1}) (Hatanaka, Sonoike et al. (1993) to 5.9 x 10^6 (M^{-1} s^{-1}) (Proux-Delrouyre, Demaille et al. 2003), in which the variability can be attributed to variations in sample set-up and measurement conditions. We report a value of 1.27 x 10^6 (M^{-1} s^{-1}) for the observed rate constant with cytochrome concentration ranging from 34 nM to 3.4 μM (1 to 100 molar excess to P_{700}). The linear increase in the k_{slow} and k_{obs} indicates that we may still be using fairly low, sub-saturating concentrations of cyt c_6.

We previously tested the electron acceptor, methyl viologen, (Figure 3-7) to ensure that our concentrations did not create any back-reactions to P_{700}, which held true. We also then wanted to make sure there was a sufficient amount of the electron source, sodium ascorbate to reduce the 34 nM to 3.4 μM cytochrome concentrations. Using an excess 8 μM of cytochrome, we saw that 2 mM of sodium ascorbate would completely reduce it within 30s, which was well within the time between actinic flashes. This is shown in Figure 3-9.

With previous reports suggesting that cyanobacteria PSI lacking specificity for its electron donor (Hervas, Diaz-Quintana et al. 2005), we are surprised to see the bi-phasic nature of the re-reduction kinetics since the interaction seems to be mainly collisional. This suggested an instrument/light source specific artifact that we will investigate further.

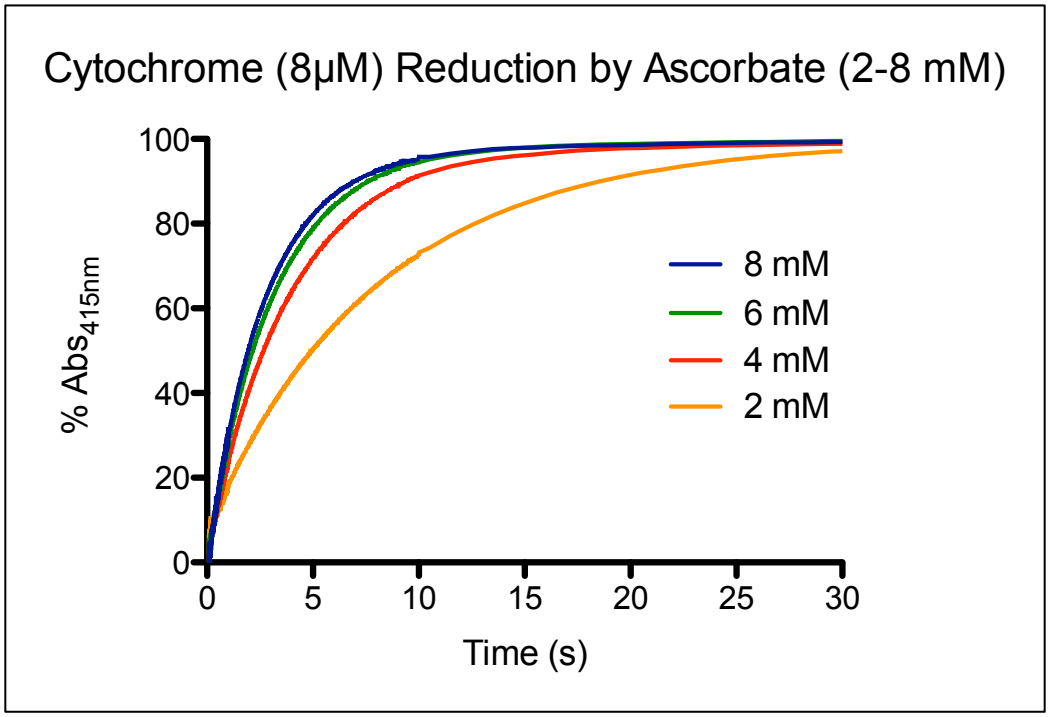

Figure 3-9. Reduction of cytochrome c_6 by sodium ascorbate.

Measured at 415 nM, the reduction of 8μM cyt c_6 is shown with 2, 4, 6, and 8 mM concentrations of sodium ascorbate. Within 15 seconds, the 8μM cyt c_6 is fully reduced by 4, 6, and 8 mM ascorbate, while 2 mM ascorbate takes about 30 seconds.

E. Analysis of Kinetics of Interaction

Temperature

Measurement temperature was also analyzed, ranging from 5°C to 60°C, showing a similar trend in a linear increase in k_{slow} and a single exponential increase in k_{fast} with increasing temperature (Figure 3-10A). The temperature dependence of the k_{slow} is shown at three different protein ratios (Figure 3-10B), all of which display similar, linear rate increases. Samples measured at 5°C and 60°C showed similar absorbance amplitudes, indicating both proteins were still active and stable, while higher temperatures of 65°C and 70°C gave much lower amplitudes that continued to decrease with time (not shown), indicating possible protein degradation or irreversible folding. The temperature effect was also plotted onto an Arrhenius plot which we then calculated the activation energy to be (28.25, 23.10, and 21.69 kJ/mol) for 2.5, 10, and 40 molar excess of Cyt c_6: PSI respectively (Figure 3-10C). An inflection point can be seen at about 40-45°C, which is similar to proteins tested from other thermophilic cyanobacteria (Balme, Hervas et al. 2001).

Effects of pH

The P_{700}^+ reduction rate increased with decreasing pH (8.2 to 5.5) (Figure 3-11A), which agrees with previous reports utilizing similar donor proteins with pI's around that of *T. elongatus* cyt c_6 (5.5) (Takabe, Ishikawa et al. 1983, Hervas, De la Rosa et al. 1992, Medina, Diaz et al. 1993). In addition to varying pH, changing the

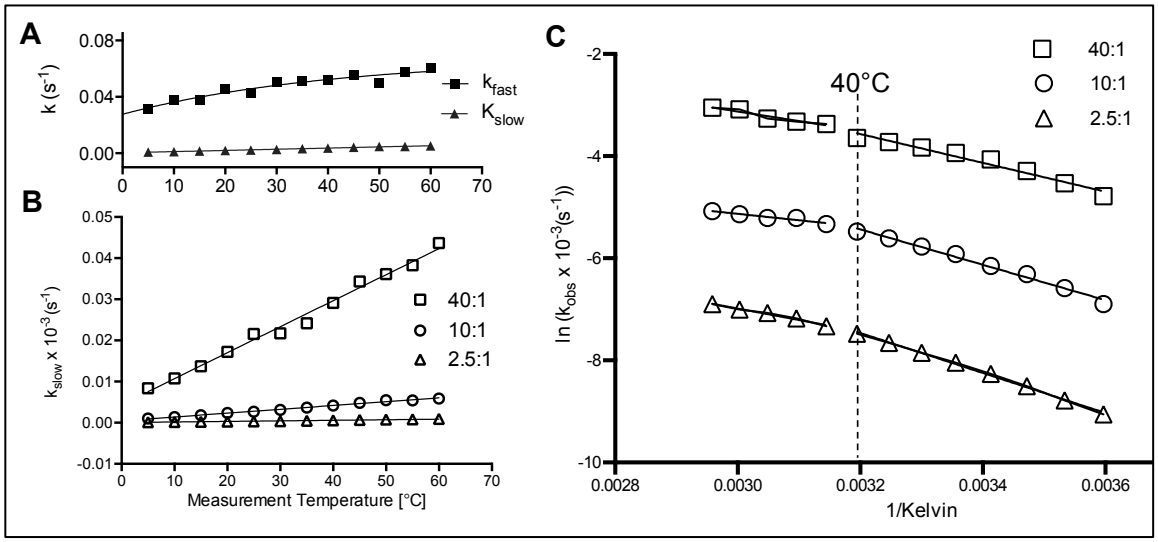

Figure 3-10. Temperature dependence of the observed rate constant at three different ratios of cyt c_6 to PSI.

A) As temperature goes from 5 to 60°C, there is a linear increase in k_{slow} and single exponential increase in k_{fast}, with $\%k_{fast}$ ~10% (not shown). B) Increased P_{700} reduction rate (k_{slow}) as the measurement temperature is raised from 5 to 60°C for 2.5, 10, and 40-fold molar excess of cytochrome to PSI. C) Arrhenius plot shows possible inflection point between 40 and 45°C.

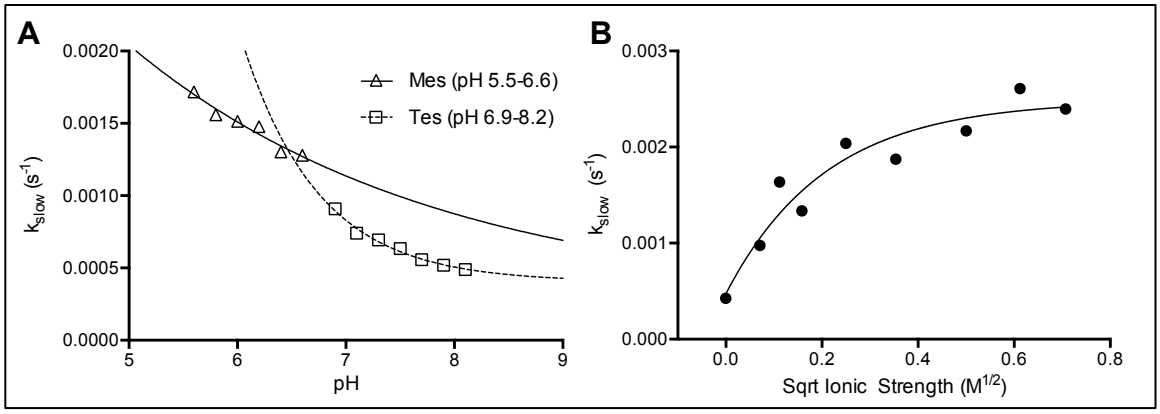

Figure 3-11. Effect of pH and ionic strength on P_{700} reduction rates.

Starting with 35 nM PSI at a 10:1 Cyt:P_{700}, A) Rate decreases as pH increases (5.5-8.2). Data with MES and TES buffer fit to two different exponential fits. B) Rate increases and plateaus with increasing ionic strength (0-50 mM $MgCl_2$).

buffer composition between MES and TES also appears to have an added effect as seen in Figure 3-11A, where two separate fits are used for the two buffers between pH's of 6.6 and 6.9.

Ionic Strength

Effects of ionic strength also agreed with previous reports (Balme, Hervas et al. 2001) with a rise in P_{700}^+ reduction rate with increasing ionic strength by increasing $MgCl_2$ concentration which reaches a plateau of about 30 mM (Figure 3-11B). This has been interpreted as the weakening of any repulsive electrostatic forces between cyt c_6 and PsaF subunit of PSI that might be repulsive (Balme, Hervas et al. 2001).

JTS-10 LED vs. Laser Flash Photolysis

Laser flash photolysis was performed on the same sample measured in the JTS-10 with the LED actinic source. Although the probe beam of the YAG laser-based system was 830 nm, we demonstrate that 705 nm and 810 nm detection on the JTS yield virtually identical P_{700}^+ reduction kinetics (Figure 3-12). The measured change in absorbance at 705 nm and 810 nm correlated well with difference spectra of *T. elongatus* P_{700} from previous reports, showing the absorption change to be about 8 times more intense at 705 nm and in the negative direction (Nakamura, Suzawa et al. 2011). The bleaching at 705 nm is the disappearance of P_{700} while the concomitant appearance of the broad 800-840 nm peak is the direct observation of

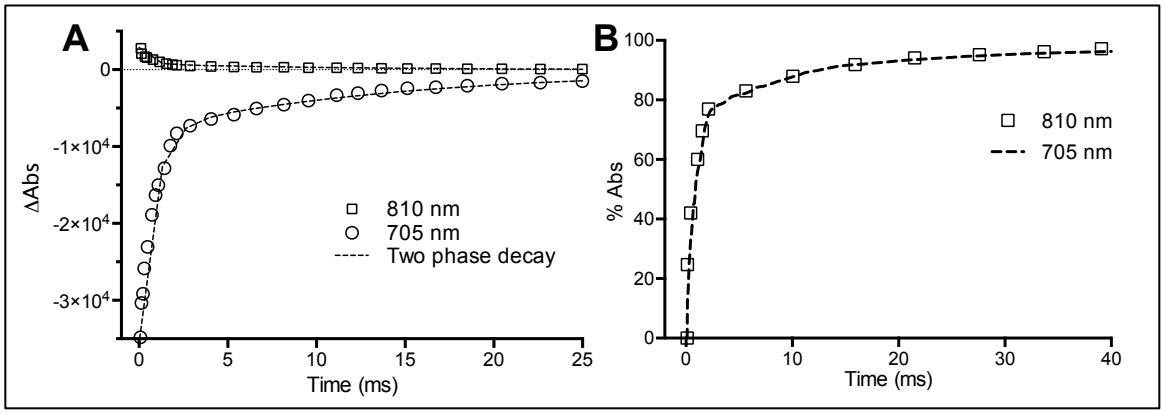

Figure 3-12. Comparison of P_{700} reduction rate as a function of measurement wavelength.

Starting with 35 nM PSI at a 10:1 Cyt:P_{700}, A) 705 nm shows about 8 times the change in amplitude of absorbance in the negative direction as 810 nm. B) Superimposition of normalized re-recovery curves.

P_{700}^{+}. Results for each cyt c_6: PSI ratio showed similar total P_{700}^{+} recovery times for both actinic light sources, with the main difference being in the curve fit of the laser data showing a single phase in re-reduction as compared with the JTS-10's two phases (Figure 3-13, Table 3-2). At each cyt c_6: PSI ratio, the curves shown in Figure 3-13 were normalized, with 100 percent being the maximal absorbance change, since the exact same sample was used for both the laser and LED (JTS) systems.

In order to detect a measurable signal with our laser system, the chlorophyll content had to be increased more than 10-fold to 544 nM (48 ug chlorophyll ml^{-1}) and with that caveat, the same sample was then analyzed using the LED based JTS-10 yielding an unexpected increase in the percent k_{fast} of our bi-phasic results (Figure 3-6). This led to the analysis of the contribution of the fast phase of the P_{700}^{+} reduction rate as with increased total PSI concentration from 20 nM to 544 nM, keeping cyt c_6: PSI ratio constant, resulting in the rise of $\%K_{fast}$ from less than 10% to nearly 90%. As shown by Figure 3-6, both the fast and slow components of PSI recovery are shown to increase with increasing total protein concentration (PSI and cyt c_6) even with the ratio of cyt c_6: PSI (10:1) is kept constant. We wanted to distinguish the effect of increased total protein concentration, which increases the P700 reduction rates from the true "molecular crowding", with the addition of a foreign crowding agent, which affects the P_{700} reduction rates by altering the cyt c_6 to PSI interaction. We found one crowding agent (PEG10k) that could potentially mimic our increased rates (Figure 3-14). This is further shown in Figure 3-15, as we plot the fast and slow phase with increasing crowding agent (PEG10k) compared to

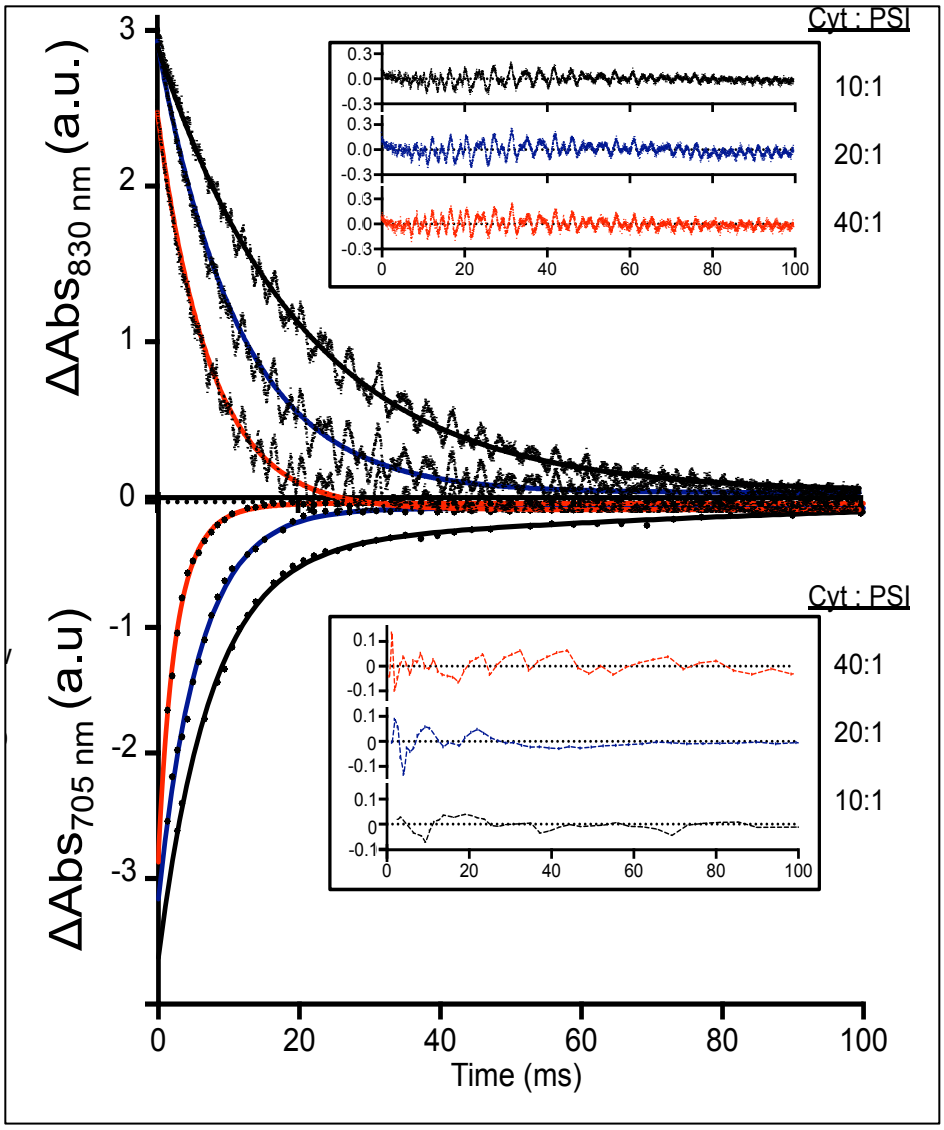

Figure 3-13. P_{700} reduction measured by LED (JTS) vs Laser actinic source

Recovery curve comparison between actinic sources (top-Laser @830 nm vs bottom-LED @705 nm) at 544 nM PSI with three cyt:PSI ratios shown (10:1, 20:1, and 40:1). The y-axis shows both curves normalized to 100% of the maximal absorbance change. JTS illuminations were kept at a maximal 3000 $\mu E/m^2/s$ with a duration of 5 ms. The top laser traces were fitted to a 1-phase exponential, while the bottom JTS traces fitted to a 2-exponential. Residuals of each fit are shown in the in-set boxes.

Table 3-2. Values from the comparison of single-phase fit laser data versus the double exponential fits from the JTS. The R^2 values are also shown.

544 nM PSI	JTS-10 (Two exponential fit)				Laser (Single exponential fit)	
Cyt:PSI	$\%k_{fast}$	k_{fast}	k_{slow}	R^2	k_{obs}	R^2
10:1	86.63	1.34	9.23×10^{-2}	0.999	4.84×10^{-1}	0.994
20:1	88.34	1.69	1.39×10^{-1}	0.994	8.66×10^{-1}	0.983
40:1	85.04	1.85	3.44×10^{-1}	0.991	1.34	0.981

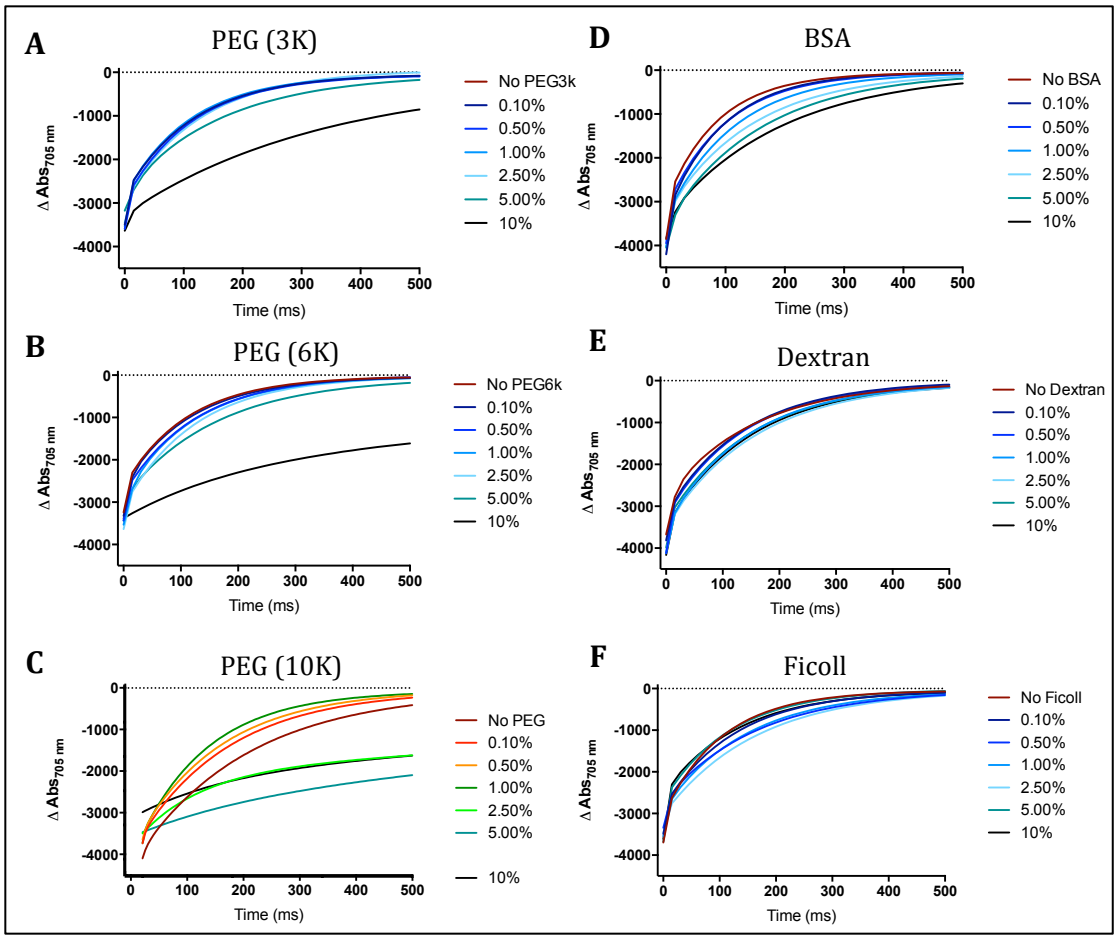

Figure 3-14. Reduction of *T. elongatus* PSI by recombinant *T. elongatus* cyt c_6 with added crowding agents

Each crowding agent was added to the final (w/v) % concentrations listed before each flash-photolysis assay. PEG 3K (A), PEG 6K (B), Dextran (E), and Ficoll (F) did not seem to affect electron transfer to PSI at concentrations below 10%. Both PEG 10K (C) and BSA (D) affected electron transfer as the concentrations were increased, but only PEG 10K seemed to increase the reduction rate of PSI by cyt c_6.

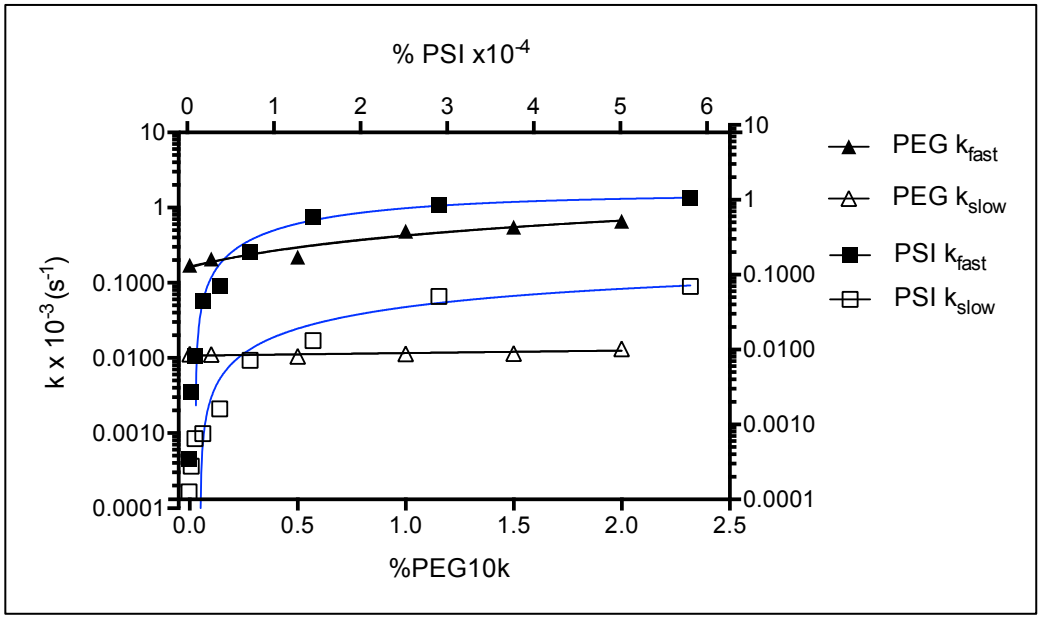

Figure 3-15. Two-phase kinetics of PSI reduction with and without PEG 10K

The rates from the two-phase recovery curves of PSI with and without crowding agents are plotted. The top x-axis plots the rates as PSI concentration is increased (solid and open squares) where cyt c_6 to PSI ratio is kept constant. The bottom x-axis plots the rates as the crowding agent (PEG10k) is increased (solid and open triangles) where the cyt $c_6$to PSI concentration and ratio is kept constant at 60 nM PSI and 0.6 µM cyt c_6.

that of an increase of the two proteins involved in oxidation and reduction (PSI and cyt c_6) for this assay. The slow phase of the flash-photolysis with PEG as a crowding agent shows very little change as we increase the %PEG (open triangles), but there is a exponential increase of the slow phase when the %PSI (open squares) is increased. There is a slight linear increase in the fast phase of the PEG (closed triangle) as compared to exponential increase seen with the increase in %PSI (closed square). With this assay, we wanted to make a clear distinction between adding a foreign crowding agent (PEG10k) that does not contribute to the oxidation or reduction of PSI versus raising both the %PSI (and cyt c_6) within the sample solution, with the ratio of cyt: PSI kept constant.

Molecular crowding or total protein density can impact kinetic rates via two contributions. One, large macromolecules will occupy more volume, creating an increased effective concentration, thereby increasing reaction rates. The other opposing effect is that the higher viscosity results in decreased protein diffusion (Ellis and Minton 2006, Kirchhoff 2008). Many kinetic models have been described for the donor/PSI interaction, with variability being attributed to the different source organisms (Hervas, Ortega et al. 1994, Hervas, Navarro et al. 1995, Hervas, Diaz-Quintana et al. 2005). In eukaryotes, the electron donor to PSI is predominantly acidic, interacting with a well conserved positively charged docking site on the N-terminus of PSI's PsaF subunit via electrostatic interactions (Ben-Shem, Frolow et al. 2003, Hervas, Navarro et al. 2003). This has been suggested by previous studies to result in a biphasic kinetic rate where the electron transfer of the preformed donor/PSI complex gives rise to the initial fast phase and the

following slow phase is attributed to donor/PSI complex formation (Hervas, Navarro et al. 1995, Fromme, Melkozernov et al. 2003, Hervas, Navarro et al. 2003). This is not the case for cyanobacteria systems however, where a simpler diffusion based collisional mechanism is thought to exist for electron transfer from donor to PSI, suggesting the kinetic rates would be better fitted to monophasic model in single-turnover experiments that utilizes an actinic laser (Hervas and Navarro 2011).

In further analyzing the longer flash duration used in the JTS-10, we see that the light history, along with total protein concentration plays a role in determining the kinetic behavior of the system. As both protein concentrations are increased, keeping the cyt: PSI ratio constant, we see an added effect of increased rates. To compare our results with multiple turnovers, we performed flash photolysis with a laser system with an actinic flash duration of only 6-9 ns, allowing only a single turnover of P_{700}. In this analysis, even with a similar rate of P_{700} recovery, we are able to see only one phase, which would represent a simple collision rate of cyt c_6 to P_{700} as dominated by the second order rate constant of complex formation. We attribute this kinetic difference to the relatively long actinic light source duration where the system will undergo multiple P_{700} turnovers of oxidation/reduction.

During prolonged illumination, P_{700} is photo-oxidized very rapidly, and the majority of the P_{700} population accumulates in the oxidized state regardless of cyt c_6 concentration. In this regime, the oxidized P_{700}^{+} may have a different affinity for cyt^{2+} and in any case as its concentration is increased and the equilibrium is shifted toward complex formation. The cycle of ($cyt^{2+} + P_{700}^{+} \rightarrow cyt^{3+} + P_{700}$) can have

various contributing rates (Figure 3-16). If $k_{-2} < k_3 < k_1$, the complex will arrive at a nonzero concentration dependent steady state and k_3 will become directly observable. As the total protein concentration increases, the complex formation between cyt^{2+} and P_{700}^{+} is also favored, further increasing the pool of [cyt: P_{700}], leading to a higher percentage of the fast k_3 phase being observed versus the slower complex formation of k_2. Within one 5ms P_{700} oxidation/reduction cycle, it is suspected that the conversion of cyt^{2+} to cyt^{3+} is much less than 10% of the total [cyt c_6], where ascorbate is in excess, leading to cyt^{2+} depletion to be insignificant. The inverse also holds true when we decrease the protein concentration to more dilute conditions and the percent of the fast phase lowered with each dilution where the cyt: P_{700} pool is lessened (Figure 3-16 & Table 3-1). While these observations differ from single-turnover laser-based observations, the sensitivity is much greater, requiring much less sample, and more importantly, the direct observation of the first-order decay of the electron transfer is possible. This situation is precluded by the single-turnover experiment, which requires a sequential formation of each population, of which the first is a relatively low probability event, and eliminates the observation of the second faster step.

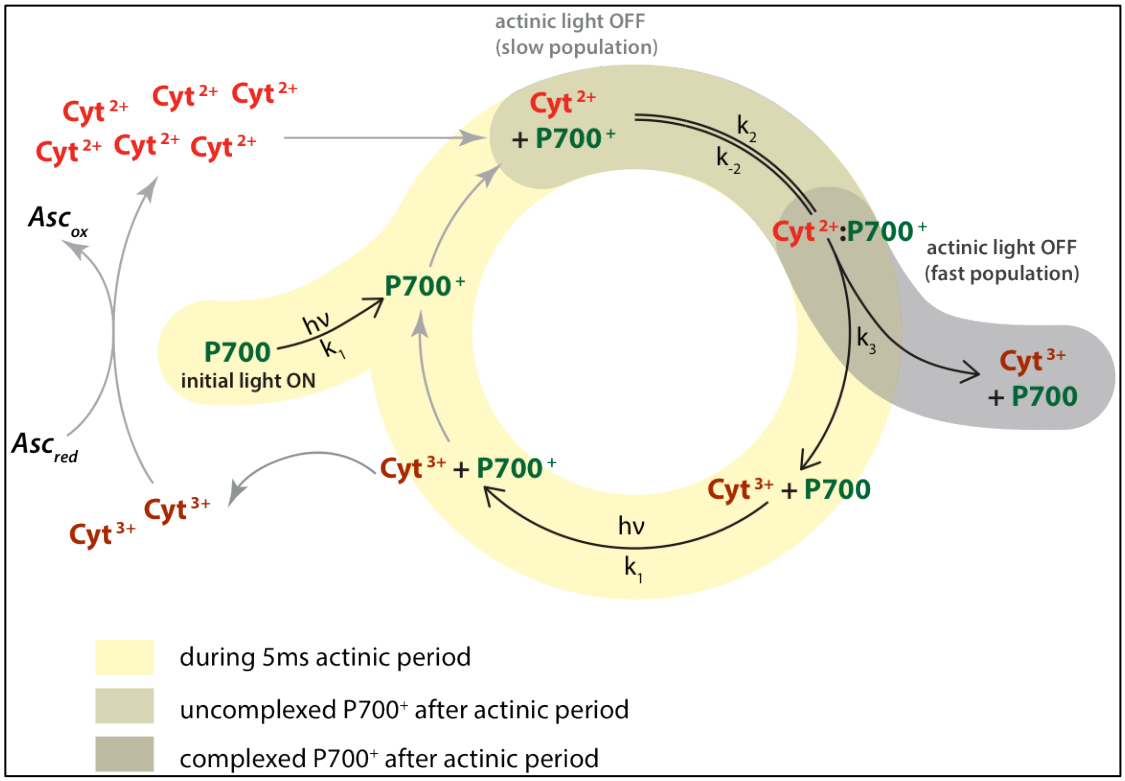

Figure 3-16. Schematic of proposed kinetic model for PSI (P_{700}) reduction by cyt c_6 via JTS-10 LED flash-photolysis

Measurement of P_{700}^{+} reduction after 5 ms actinic period is shown in gray with k_2 and k_3, while multiple P_{700} oxidation/reduction turnovers are depicted in yellow during actinic light on, such that P_{700}^{+} pool is fully oxidized. As actinic light (*hv*) oxidizes P_{700} to P_{700}^{+}, a pre-complex population of [cyt^{2+} + P_{700}^{+}] is available, leading to [cyt^{2+}:P_{700}^{+}] complex formation represented as k_2 rate constant. The electron transfer event from [cyt^{2+}:P_{700}^{+}] to [cyt^{3+} +P_{700}] is shown as k_3. Thank you to Dr. Michael Vaughn for assistance with this graphic.

F. PsaF - Cytochrome Alignment

Prokaryotes vs. Eukaryotes

Previous literature has shown that although the basic PSI structure is highly similar in higher plants, algae, and cyanobacteria (Saenger, Jordan et al. 2002), the psaF subunit plays an essential role in the reduction rate of P_{700}^{+} only in plants and algae, but not in the prokaryotic cyanobacteria (Hippler, Drepper et al. 1997, Hippler, Drepper et al. 1998). This was further investigated to reveal that there exists a positively charged N-terminal domain of psaF that is conserved in higher plants and algae, responsible for precise binding of the mobile electron donor (plastocyanin or cytochrome c), but is missing in the primordial cyanobacteria (Hippler, Drepper et al. 1998, Sommer, Drepper et al. 2006). Keeping in mind the endosymbiotic theory and how certain organelles of eukaryotic cells might have originated from bacteria, it had been noted from previous research that since chloroplasts found in higher plants and algae came from cyanobacteria, the PSI/cyt c_6 interface had also evolved to where tighter binding was necessary in chloroplasts due to the rearrangement and stacking of the thylakoid membranes into what is known as grana (Mustardy, Buttle et al. 2008).

We further investigated this electrostatic interaction with the protein alignment of each component from a variety of organisms (Table 3-3). We aligned the N-terminal peptide sequence of the psaF subunit of PSI that is thought to be responsible for this interaction from various plant and algal species and compared it

Table 3-3. The Uniprot entry IDs for psaF/petJ sequences used for "PetJ vs psaF charge analysis"

Organism	Uniprot Entry ID	
	psaF	Cyt c6/PetJ
1 – *Synechocystis sp. PCC 6803*	P29256	P46445
2 – *Synechococcus sp. (strain WH8102)*	Q7U572	Q7U642
3 – *Prochlorococcus marinus MIT 9303*	A2C7G1	A2CAJ0
4 – *Chroococcidiopsis thermalis PCC 7203*	K9TZX8	K9U169
5 – *Thermosynechococcus elongatus BP-1*	P0A401	P0A3X9
6 – *Nostoc punctiforme*	B2J589	B2IVD6
7 – *Anabaena variabilis PCC 7937*	P31091	Q3MDW2
8 – *Cyanophora paradoxa*	P48115	Q9LEN1
9 – *Nannochloropsis salina*	T1RJE2	T1RJI9
10 – *Nannochloropsis oculata*	T1RHN9	T1RJE1
11 – *Nannochloropsis gaditana*	K9ZV47	K9ZXM5
12 – *Nannochloropsis oceanica*	T1RJ05	T1RJX4
13 – *Nannochloropsis granulata*	T1RIP4	T1RIK8
14 – *Fucus vesiculosus*	D1GJK8	D1GJF8
15 – *Pyropia yezoensis*	Q1XDU4	Q8WKJ8
16 – *Porphyra purpurea*	P51193	P51200
17 – *Porphyra umbilicalis*	J7F637	J7F7H0
18 – *Gracilaria tenuistipitata*	Q6B948	Q6B941
19 – *Chondrus crispus*	M5DEQ3	M5DDA6
20 – *Galdiera sulpuraria*	E3UIU5	A0A075W1M7
21 – *Cyanidium caldarium*	Q9TLW6	Q9TLW1
22 – *Cyanidioschyzon merolae*	Q85FS9	Q85FS2
23 – *Chlamydomonas reinhardtii*	P12356	P08197
24 – *Zea Maize*	P13193	B6TIZ9
25 – *Arabidopsis thaliana*	Q9SHE8	Q93VA3

with our cyanobacteria (Figure 3-17B). Two regions (A and B) were identified from the PDB crystal structure of *T. elongatus* (1JB0) as potential lumen exposed, cytochrome-interacting regions. We noticed that there is a basic (lysine-rich) patch of residues present in plants and algae, but missing in cyanobacteria. Region "A" has an average net charge of +0.6 (cyanobacteria), +5.4 (algae), and +7 (plants). Region "B" has an average net charge of +2.3 (cyanobacteria), +6.1 (algae), +5.5 (plants). This confirms that indeed, from the selected organisms, plant and algae have a much more positively charged psaF than cyanobacteria. We then proceed to look at the electron donor side of the same set of organisms (Figure 3-17A). From alignment, we see that the algae group was the most negatively charged, while cyanobacteria and plants were close to neutral. Some plants, like Zea mays and Arabidopsis thaliana have copies of cytochrome c_6-like sequences (potentially cyt c_{6A}) although the copper protein, plastocyanin is the main electron donor to PSI. From Figure 3-17C, we can assume that these added charges on cyt c_6 and psaF, evolved together, as three distinct charge groups can be seen, matching up with cyanobacteria, algae, and plants.

G. PsaF Mutagenesis

Cloning of algal psaF to cyanobacteria

Working with this premise, we attempted to optimize the interactions between PSI and its electron donor, cytochrome c_6, hoping to achieve faster and

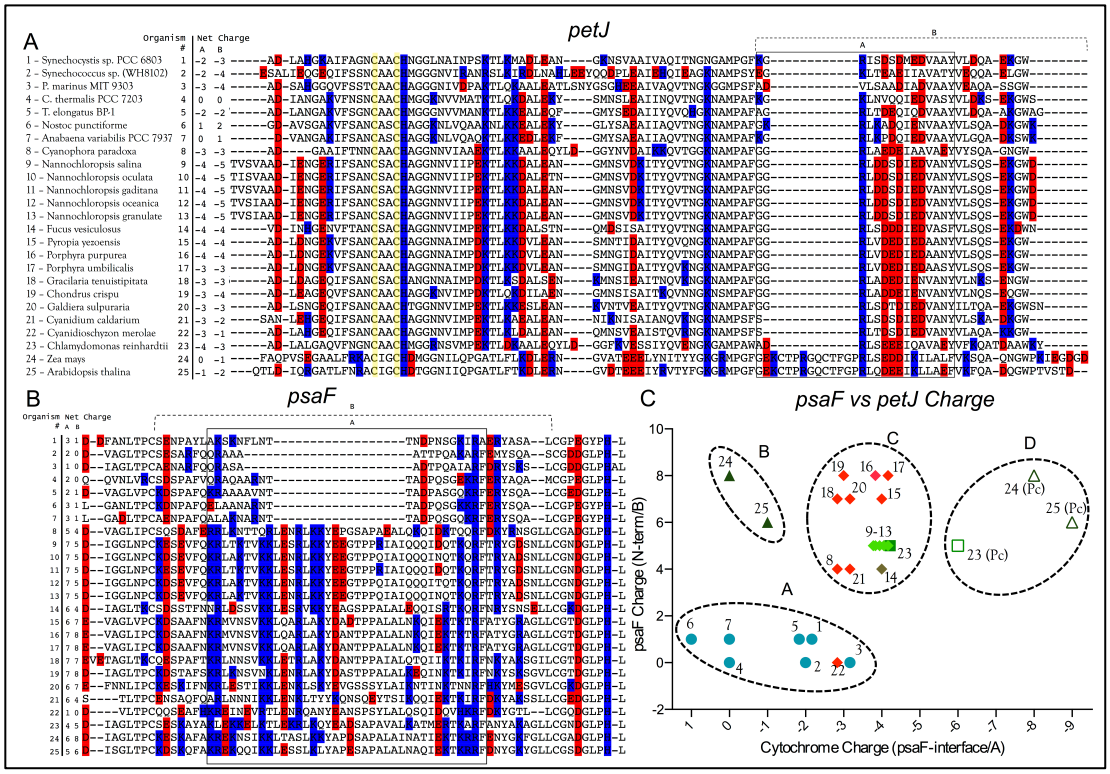

Figure 3-17. Cyt c_6 (petJ) vs psaF charge analysis from various photosynthetic organisms

A) PetJ alignment from cyanobacteria(1-7), algae(8-23), and plants (24-25). Heme coordinating cysteines are highlighted in yellow. Potential psaF interacting interface region are boxed (A & B) with their charges shown on the left. B) PsaF alignment from cyanobacteria(1-7), algae(8-23), and plants (24-25). Charged residues are highlighted red (acidic) and blue (basic). Regions A and B are potential cytochrome interaction sites as indicated by (Vanselow et al. 2009) and their net charges are shown on the left. C) Plot of cytochrome charge (region A) vs psaF charge (region B). Cyanobacteria are represented as circles, algae as diamonds and squares, and plants as triangles. Plastocyanin are shown in open square and triangles.

more efficient reduction of the PSI complex. We designed mutations to the subunit of PSI (psaF) that is responsible for docking cytochrome c_6 to the luminal surface of PSI. This was done after an N-terminal psaF alignment was made comparing cyanobacteria to higher plant and algal species (Figure 3-18A). It is shown from this alignment that cyanobacteria, more specifically *T. elongatus* lack a patch of basic, lysine rich residues which seems to contribute to the elongation of the cytochrome binding area of the psaF subunits in algae and higher plants. The mutations made would incorporate this patch from an algal species (*Chlamydomonas reinhardtii*) into our strain of *T. elongatus*.

After we constructed the modified PSI (psaF-Chlamy) DNA for homologous recombination in T. elongatus, a thermal stable kanamycin gene was inserted as a selectable marker (Figure 3-19). The DNA was then transformed into *T. elongatus* via electroporation and transformants were selected and segregated through numerous rounds of increasing kanamycin concentration. DNA was once again extracted for sequencing and our clone was confirmed (Figure 3-20). Once a sufficient amount of this mutant *T. elongatus* was grown and harvested, PSI was then isolated and the higher size shift of psaF was confirmed by MALDI (Figure 3-21).

H. Surface Charge Changes to Cytochrome

Also working off the complementary of this PSI/cytochrome docking site, we also made DNA constructs to mutate *T. elongatus*' cytochrome c_6 to mimic the

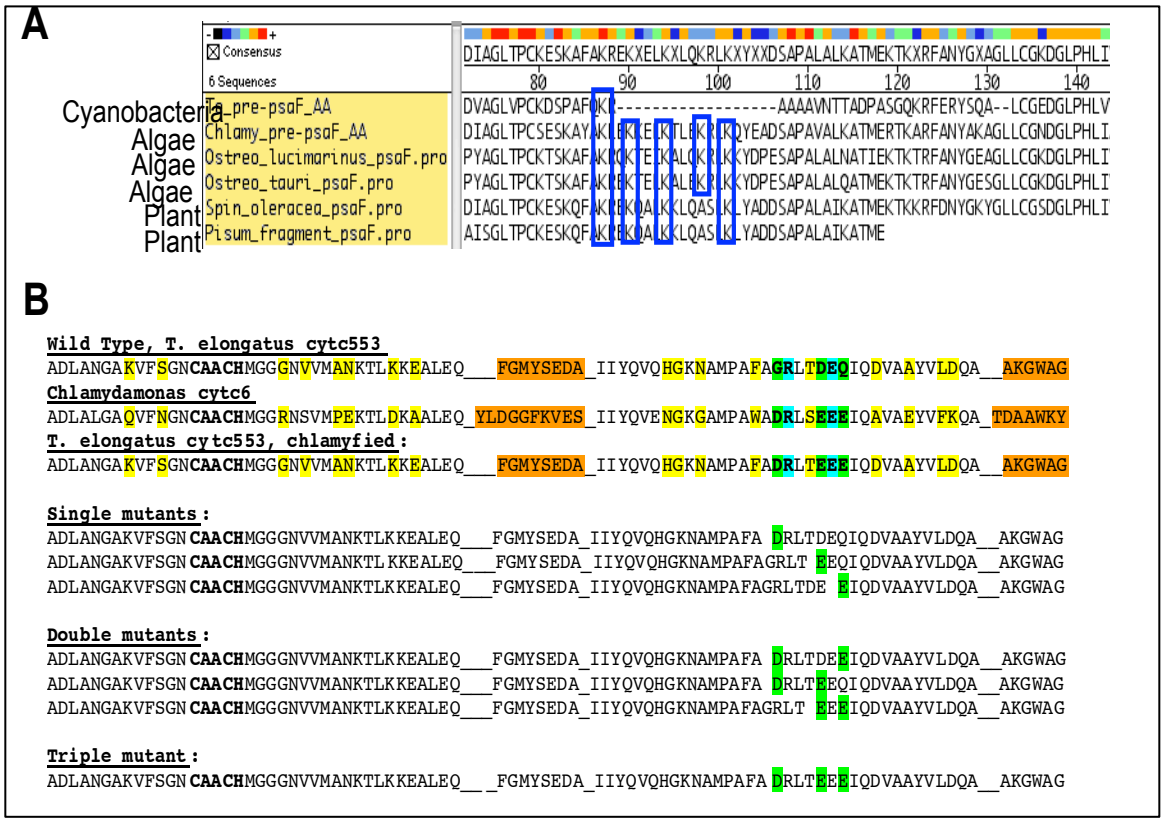

Figure 3-18. Partial psaF/cyt c_6 alignments for electrostatic mutants production

A) N-terminal alignment of psaF from cyanobacteria, algae, and plants. Potential basic lysine residues for cloning are shown in blue boxes B) Proposed cyt c_6 mutants that would add acidic residues from algal cyt c_6 to cyanobacteria cyt c_6. Three single, three double, and one triple mutant cyt c_6 sequences are shown. Thank you Natalie Myers for this figure.

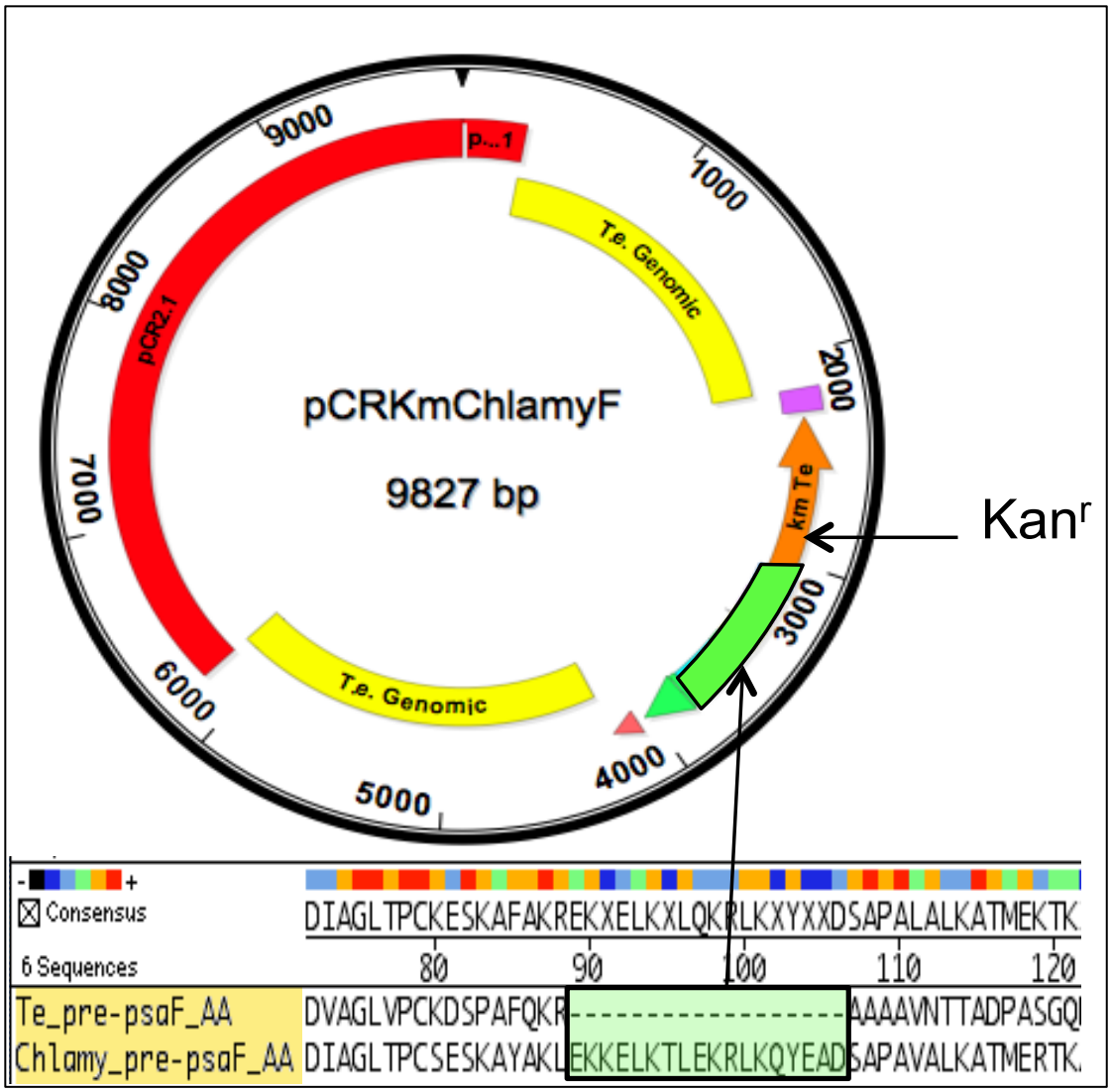

Figure 3-19. Homologous recombination cloning scheme for psaF in *T. elongatus*

Residues (18) from *Chlamydomonas* psaF were inserted into a cloning vector containing wild type *T. elongatus* psaF sequence along with about 2 kb of flanking genomic DNA. The "Chlamy" psaF insert also included a kanamyacin (kmTe) resistant cassette for mutant selection.

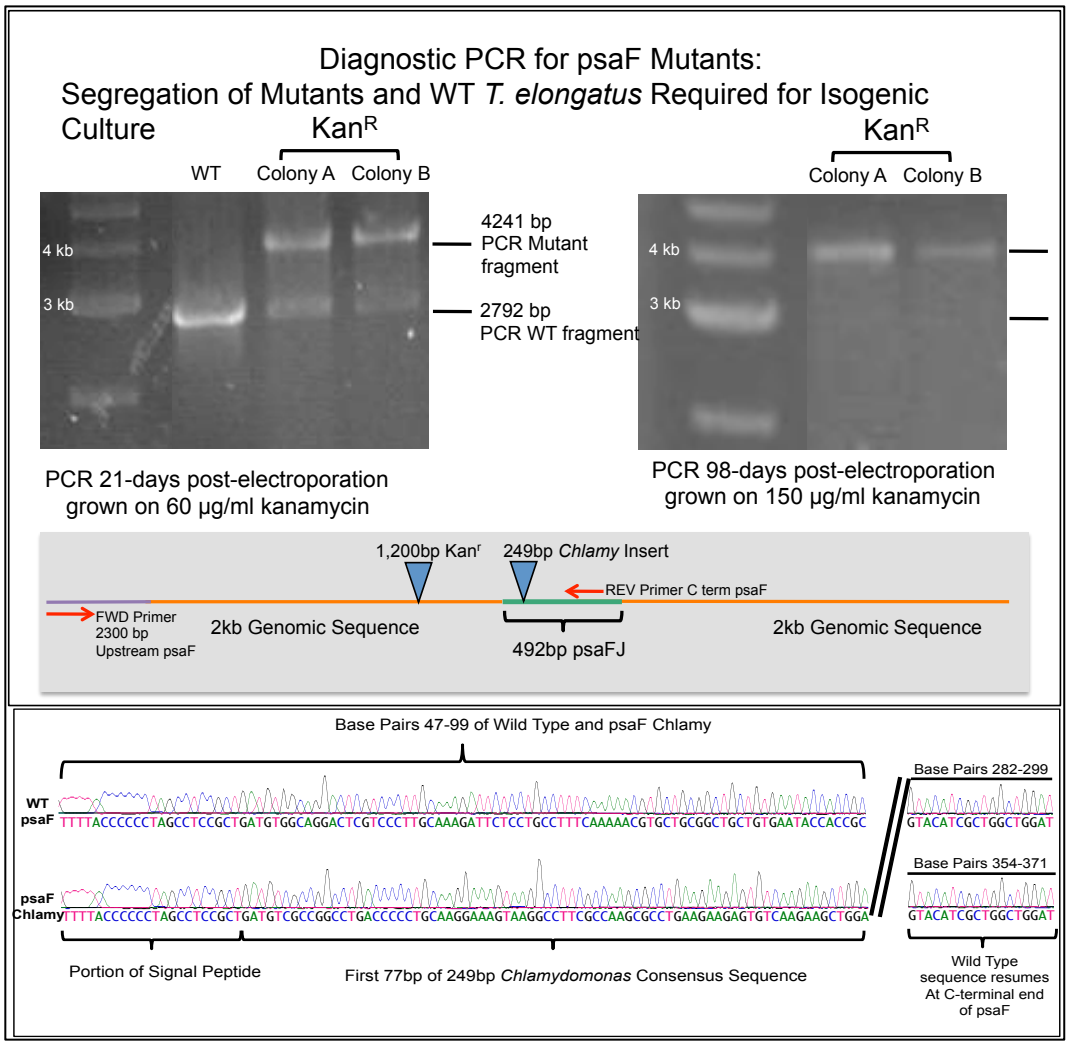

Figure 3-20. Homologous recombination cloning confirmation (post electroporation) for psaF-*Chlamy* in *T. elongatus*

At 21 days post electroporation, colony PCR (top left) shows WT band of *T. elongatus* psaF around 3 kb and colonies A and B from kanamycin plates show both the WT and mutant bands of psaF (4 kb). At 98 days post electroporation, sequential generations of colony A and B show only the mutant psaF band. Primers used for colony PCR are shown below gel pictures. DNA sequencing results (bottom) confirms that the psaF-Chlamy mutant was successfully made for *T. elongatus.*

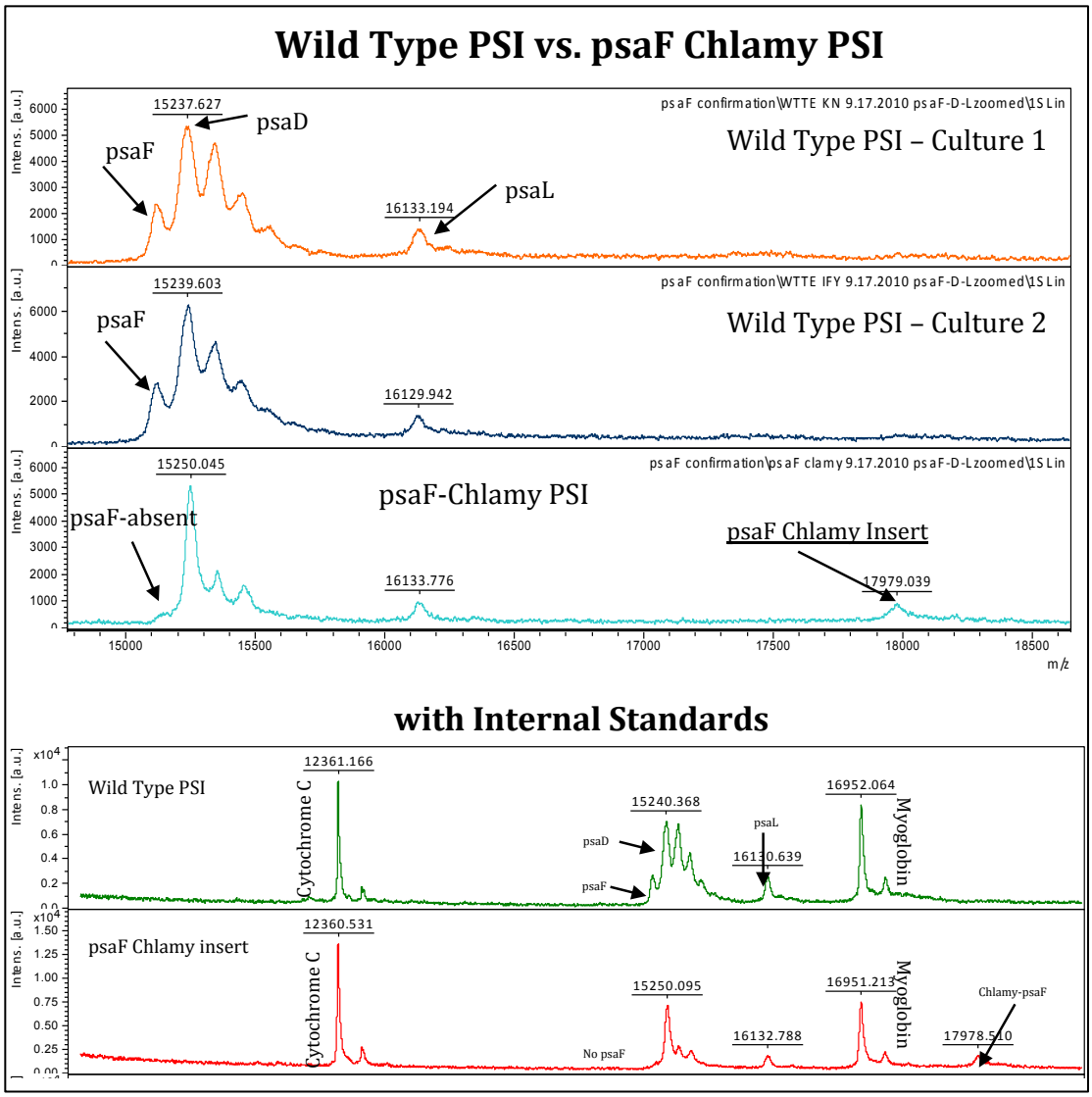

Figure 3-21. MALDI conformation of psaF-Chlamy PSI

Two *T. elongatus* cultures grown from different labs are used for PSI (top 2 panels). The third panel shows the WT psaF peak missing, while a new psaF-Chlamy appears which are not seen in either WT panels. The same confirmation is shown at the bottom two panels, just with internal standards added.

cytochrome of *C. reinhardtii* by introducing acidic residues that supposedly would interact with the newly formed basic patch on psaF-Chlamy (Figure 3-18B). This was done with as a single addition of an acidic residue at each of the three sites (single mutants), with two additions of acidic residues (double mutants) and finally a triple mutant with all three sites mutated to introduce an acidic residue. These mutants were also recombinantly expressed in E. coli and purified as described previously.

I. JTS-10 Flash Photolysis of Electrostatic Mutants

Results show that with more added acidic residues added to cytochrome, the rate for psaF-Chlamy PSI re-reduction is slower (Figure 3-22). The triple mutant, shows the slowest recovery rate, followed by the single and double mutants, with the wild type remaining the fastest. From these results, we speculate that the added residues have created an electrostatic interaction that is too strong for the cytochrome to quickly detach from PSI for re-reduction by ascorbate. This is exemplified by the probable multiple P_{700+} turnover events caused by the actinic flashes in the millisecond timescale.

J. Conclusions

We started this project with the initial primary aim of understanding the relationship between the electron transfer rate and surface charges on the protein pair (PsaF-cyt c_6). We showed that we were able to first characterize the cyt c_6 in *T.*

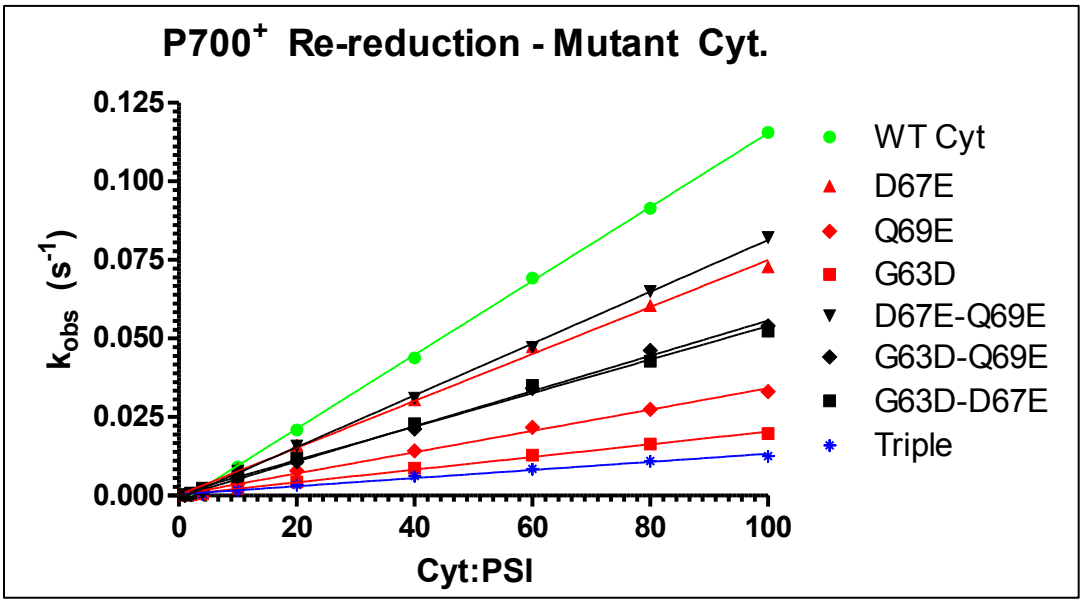

Figure 3-22. Re-reduction rates of electrostatic mutant cyt c_6s with psaF-Chlamy PSI

Single phase k_{obs} rates are shown for simplicity. Wild type and mutant cytochromes used to reduce psaF-Chlamy PSI at 8 different cyt:P_{700} ratios (1, 2, 4, 10, 20, 40, 60, 80, and 100:1) are shown with WT in green, single mutants in red, double mutants in black, and triple mutant in blue.

elongatus by finding the intracellular molar ratio of cyt c_6 to PSI via quantitative Western Blot analysis, showing us about a 2:1 of cyt c_6 to PSI *in vivo.* This allowed us to use ratios that were close to this value in our initial LED flash-photolysis assays where the kinetics of the electron transfer were measured. With the ability to modulate the system via illumination, temperature, pH, and ionic strength, we felt comfortable in being able to modulate this system in increasing the electron transfer. As we compared the LED system versus the more widely used laser systems, an added kinetic phase was seen in the LED system. We attribute this to the nature of the duration of the assays where the protein pair was exposed to the actinic light. With a longer light duration, multiple turn-over events of P_{700} oxidation and reduction by cyt c_6 must occur, further complicating the kinetic result output. We rationalized this with Figure 3-16, where a schematic of the kinetic model was proposed.

The results from our electrostatic mutations were almost the exact opposite of what we initial expected, but after more consideration of our kinetic model, we are able to interpret the results as having a light artifact that was contributed to our LED instrumentation. The electrostatic mutations that were added to our WT cyt c_6 and PsaF possibly did what we had initially intended, to allow reduced cyt c_6 to find PsaF quicker, but it might have worked too well. The longer light cycle and added turn over events of P_{700} ox-red did not allow the mutated cyt c_6 to disassociate from the mutated PsaF once the initial electron transfer occurred. This now oxidized cytc6, may still be bound to PsaF, while the light cycle was still on, blocking the free and reduced population of cyt c_6 access to now oxidized P_{700}. This was shown with

the apparent “stickiness” of this interaction, where more electrostatic mutations made the rate seem slower. This however, has not been tested by the single turn-over laser flash-photolysis system, where the results may appear faster with more electrostatic mutations. We aim to proceed with these assays as our next step.

Chapter 4

Other Cytochrome/PSI Strategies for Applied Photosynthesis

A. Introduction

Along with our electrostatic mutants of cyt c_6 and PsaF, we also wanted to explore other methods and approaches of increasing the electron transfer rate by either cyt c_6 or PSI modifications. We discuss here how our electrostatic mutation results gave us an idea for another strategy, where we generated a "molecular battery pack" where a poly-cytochrome cloning method was used. We next explore the broader scope of this PSI-donor pair by looking at a wide collection of photosynthetic organisms via a bioinformatics approach. This then allowed us to carefully compare the surface charge composition of the PSI-donor pair and relate it to their electron transport rates.

B. Poly-cytochrome Strategy

From the previous section, we concluded that our triple mutant cytochrome gave a slower PSI re-reduction because it was binding too tightly to psaF, not allowing the cytochrome to be reduced by ascorbate. From this, we developed a strategy to allow for quick re-reduction of bound cytochromes. This involved linking wild type

cytochromes to the C-term of the "Triple" mutant cytochrome that showed the slowest P_{700+} re-recovery rate. With the cytochromes linked side by side, we hoped that the cytochrome furthest away from PSI can be reduced by ascorbate and transfer that electron to the adjacent cytochrome's heme group, eventually leading to the "Triple" mutant cytochrome (Figure 4-1).

Linkage Strategies

To make these constructs, we implemented a cloning scheme that would allow successive rounds of mutagenesis, adding one more wild type cytochrome each time. Using the XhoI restriction site at the C-terminus of the "Triple" mutant cytochrome, we inserted WT cytochrome using SalI and XhoI (SalI_WT_XhoI), abolishing the XhoI site on the C-terminus of the "Triple" mutant, leaving only one XhoI site at the C-terminus of the WT cytochrome (_Triple-WT_XhoI). This allowed us to successively clone in WT cytochromes with the same strategy (Figure 4-2A,B).

After proteins were made and verified (Figure 4-2C), we looked at the P_{700} re-reduction rates. Results show that Poly-cyt-2 was more than twice as fast as the "Triple" mutant alone, yet Poly-cyt-3,4, and 5, got successively slower (Figure 4-3A). In order to investigate whether the slow rate was caused by mis-folding or clumping of the Poly-cyts, we added Urea to loosen any potential aggregation. The results with urea showed a very similar trend from 0 to 5M concentrations (4-3B). Our next plan would be to repeat this strategy with wild type cytochrome as the ends, leaving off the potentially rate-limiting "Triple" mutant cytochrome.

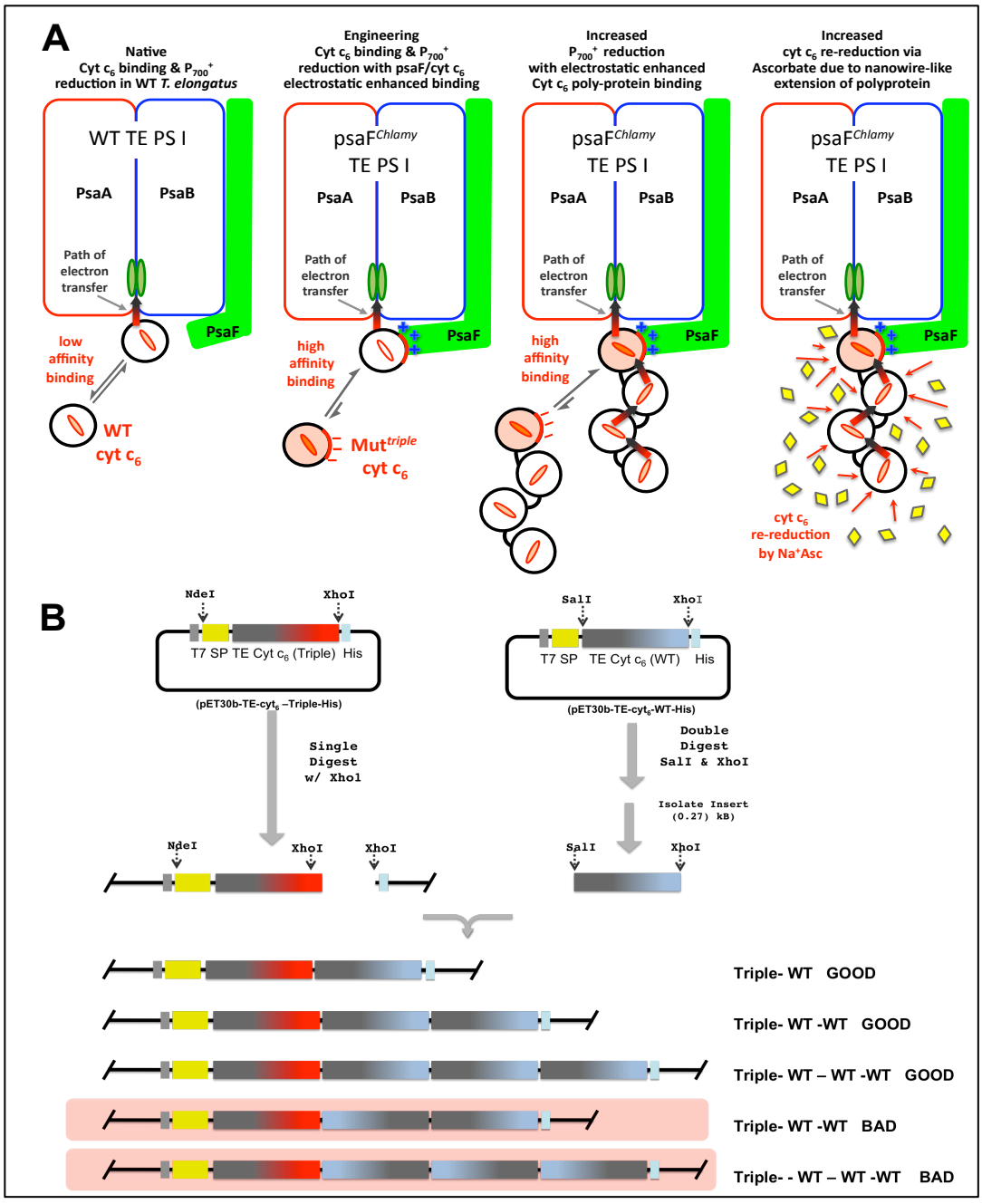

Figure 4-1. Poly-cytochrome design and cloning strategy.

A) Schematic of how the "high affinity binding" Triple-mutant cytochrome, binding tightly to PsaF, can serve as the front end of a molecular "battery pack" where each trailing cytochrome would transfer electrons to the adjacent cytochrome, finally reducing P700. B)Cloning strategy using the restriction enzymes *Nde1, Xho1*, and *Sal1* to successively drop in another cytochrome to each poly-cytochrome.

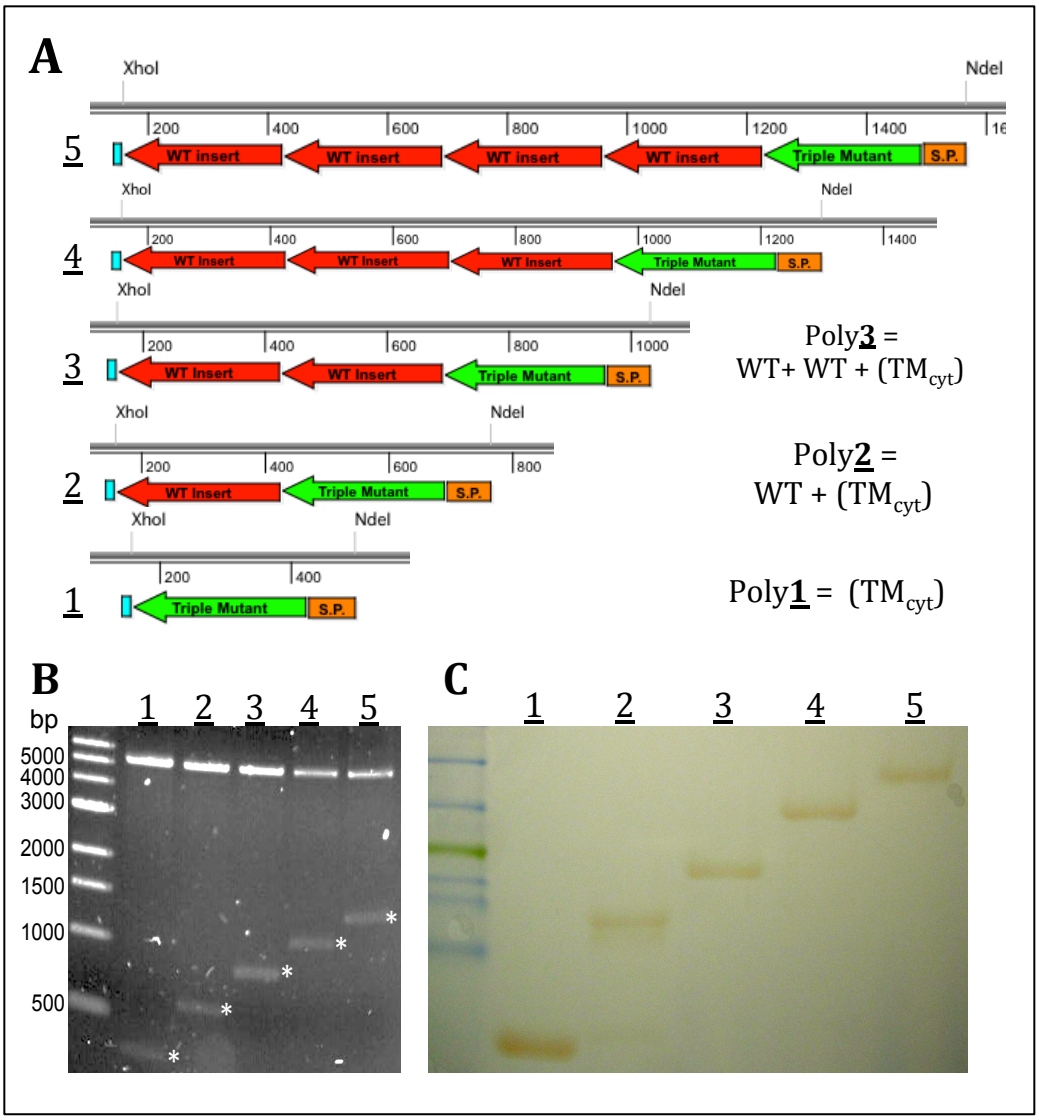

Figure 4-2. Poly-cytochrome cloning and purification confirmation.

A) Progressive cloning scheme that incorporates a WT Cyt sequence to the C-term of previous Poly-cyt. For Poly-2, a WT sequence was inserted after the C-term of the "electrostatic triple mutant cytochrome" (TM_{cyt}). B) Colony PCR on successful Poly-cyt cloning, showing Poly1-5, each about 250 bp higher than the last. C) SDS PAGE showing a heme stain of each poly-cyt.

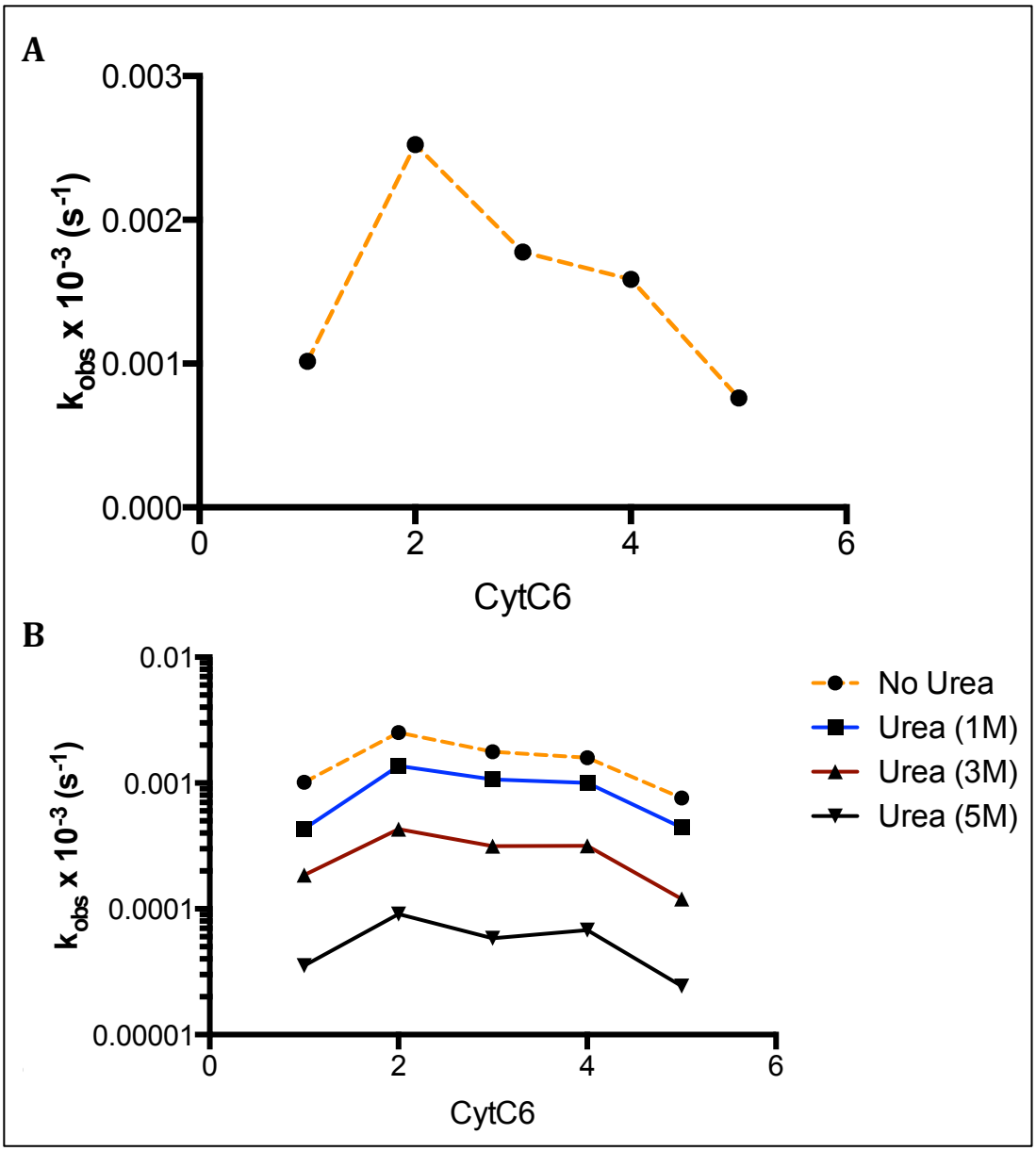

Figure 4-3. P_{700} reduction kinetics by poly-cyts.

A) The k_{obs} rates for a 1:1 molar ratio of poly-cyt:P700 for each poly cyt. Poly-cyt2 shows the fastest P_{700} reduction, but decreasing with each successive poly-cyt. B) Urea was incorporated into each flash-photolysis assay for each poly-cyt. The more urea, the slower each sample seems to get.

C. Bioinformatics of PSI-donor Pair

From a list of 96 photosynthetic species, we categorized them into groups that contained a known sequence of cytochrome c_6 (Table 4-1), plastocyanin (Table 4-3), or both (Table 4-2). The "only cyt" group contained 15 algae and 17 cyanobacteria. The "only plastocyanin" group contained 7 algae, 2 cyanobacteria, and 15 plants. The group with both cytochrome c and plastocyanin was comprised of 3 algae, 2 plants, and 35 cyanobacteria. With this list, we aligned the psaF protein sequences and found a conserved motif from "DIAG" at the N-terminus to "GLPHL", which covers the portion exposed to the lumen space. This portion was selected by looking at the crystal structure of known cyanobacteria and algal PSI's. With a window covering the "DIAG" to "GLPHL" motif, we analyzed the sequences to gather the total number of residues, number of charged residues (segregated into basic and acidic), and the percent charge. Plants and algae have about 70 total residues, while cyanobacteria contain around 50. The number and percentage of charged residues shows that cyanobacteria are have the lowest, followed by algae, and then plants with the most. In breaking down the charge composition, plants and algae appear to contain more basic than acidic for all three groups (Figure 4-4).

We then repeated the analysis with the electron donors. We selected a conserved window of residues by looking at previous literature that identified the binding site of cyt/PC to PSI, aligning the sequences and matching to crystal structures. For the majority of the sequences (93/96), the conserved window gave 16 residues. Looking at the "only cyt" group, the algal sequences have a higher percent charged than cyanobacteria (Figure 4-5). The "only PC" group shows that

Table 4-1. Organisms containing only cyt c_6 used for bioinformatics of psaF/e- donor charge analysis from plants, algae, and cyanobacteria.

Contains only Cytc_6			
Organism	**Cyanos**	**Algae**	**Plants**
Acaryochloris marina MBIC11017	✓		
Acaryochloris sp. CCMEE 5410	✓		
Arthrospira platensis NIES-39	✓		
Arthrospira sp. PCC 8005	✓		
Cyanobium sp. PCC 7001	✓		
Cyanothece sp. PCC 7425	✓		
Gloeobacter violaceus PCC 7421	✓		
Microcoleus chthonoplastes PCC 7420	✓		
Microcoleus vaginatus FGP-2	✓		
Nostoc sp. PCC 7120	✓		
Oscillatoria sp. PCC 6506	✓		
Synechococcus sp. CB0101	✓		
Synechococcus sp. CB0205	✓		
Synechococcus sp. PCC 7002	✓		
Synechococcus sp. RCC307	✓		
Thermosynechococcus elongatus BP-1	✓		
Trichodesmium erythraeum IMS101	✓		
Aureococcus anophagefferens		✓	
Bigelowiella natans		✓	
Cyanidioschyzon merolae strain 10D		✓	
Cyanophora paradoxa		✓	
Ectocarpus siliculosus		✓	
Fucus vesiculosus		✓	
Gracilaria tenuistipitata var. liui		✓	
Guillardia theta		✓	
Heterosigma akashiwo		✓	
Phaeodactylum tricornutum		✓	
Porphyra purpurea		✓	
Porphyra umbilicalis		✓	
Pyropia yezoensis		✓	
Thalassiosira pseudonana CCMP1335		✓	
Vaucheria litorea		✓	

Table 4-2. Organisms containing both cyt c_6 and plastocyanin used for bioinformatics of psaF/ e^- donor charge analysis from plants, algae, and cyanobacteria

Contains Both Cytc_6 and Plastocyanin			
Organism	**Cyanos**	**Algae**	**Plants**
Nostoc azollae 0708	✓		
Anabaena variabilis ATCC 29413	✓		
Crocosphaera watsonii WH 0003	✓		
Cyanothece sp. ATCC 51472	✓		
Cyanothece sp. CCY0110	✓		
Cyanothece sp. PCC 7424	✓		
Cyanothece sp. PCC 7822	✓		
Cyanothece sp. PCC 8802	✓		
Cylindrospermopsis raciborskii CS-505	✓		
Fischerella sp. JSC-11	✓		
Lyngbya sp. PCC 8106	✓		
Microcystis aeruginosa PCC 7941	✓		
Microcystis aeruginosa PCC 9701	✓		
Microcystis aeruginosa PCC 9808	✓		
Moorea producens 3L (Lyngbya majuscule)	✓		
Nodularia spumigena CCY9414	✓		
Nostoc punctiforme PCC 73102	✓		
Raphidiopsis brookii D9	✓		
Synechococcus elongatus PCC 7942	✓		
Synechococcus sp. BL107	✓		
Synechococcus sp. CC9311	✓		
Synechococcus sp. CC9605	✓		
Synechococcus sp. CC9902	✓		
Synechococcus sp. JA-2-3B'a(2-13)	✓		
Synechococcus sp. JA-3-3Ab	✓		
Synechococcus sp. PCC 7335	✓		
Synechococcus sp. RS9916	✓		
Synechococcus sp. RS9917	✓		
Synechococcus sp. WH 5701	✓		
Synechococcus sp. WH 7803	✓		
Synechococcus sp. WH 7805	✓		
Synechococcus sp. WH 8016	✓		
Synechococcus sp. WH 8102	✓		
Synechococcus sp. WH 8109	✓		
Synechocystis sp. PCC 6803 substr.PCC-P	✓		
Chlamydomonas reinhardtii		✓	
Chlorella variabilis		✓	
Coccomyxa subellipsoidea C-169		✓	
Sorghum bicolor			✓
Zea mays			✓

Table 4-3. Organisms containing only plastocyanin used for bioinformatics of psaF/ e^- donor charge analysis from plants, algae, and cyanobacteria.

Contains only Plastocyanin			
Organism	**Cyanos**	**Algae**	**Plants**
Cyanobacterium UCYN-A	✓		
Microcystis sp. T1-4	✓		
Chlamydomonas incerta		✓	
Micromonas pusilla CCMP1545		✓	
Micromonas sp. RCC299		✓	
Ostreococcus lucimarinus CCE9901		✓	
Ostreococcus tauri		✓	
Paulinella chromatophora		✓	
Volvox carteri f. nagariensis		✓	
Arabidopsis lyrata subsp. Lyrata			✓
Arabidopsis thaliana			✓
Brachypodium distachyon			✓
Glycine max			✓
Hordeum vulgare subsp. vulgare			✓
Medicago truncatula			✓
Nicotiana tabacum			✓
Oryza sativa Japonica Group			✓
Physcomitrella patens subsp. patens			✓
Picea sitchensis			✓
Populus trichocarpa			✓
Ricinus communis			✓
Selaginella moellendorffii			✓
Spinacia oleracea			✓
Vitis vinifera			✓

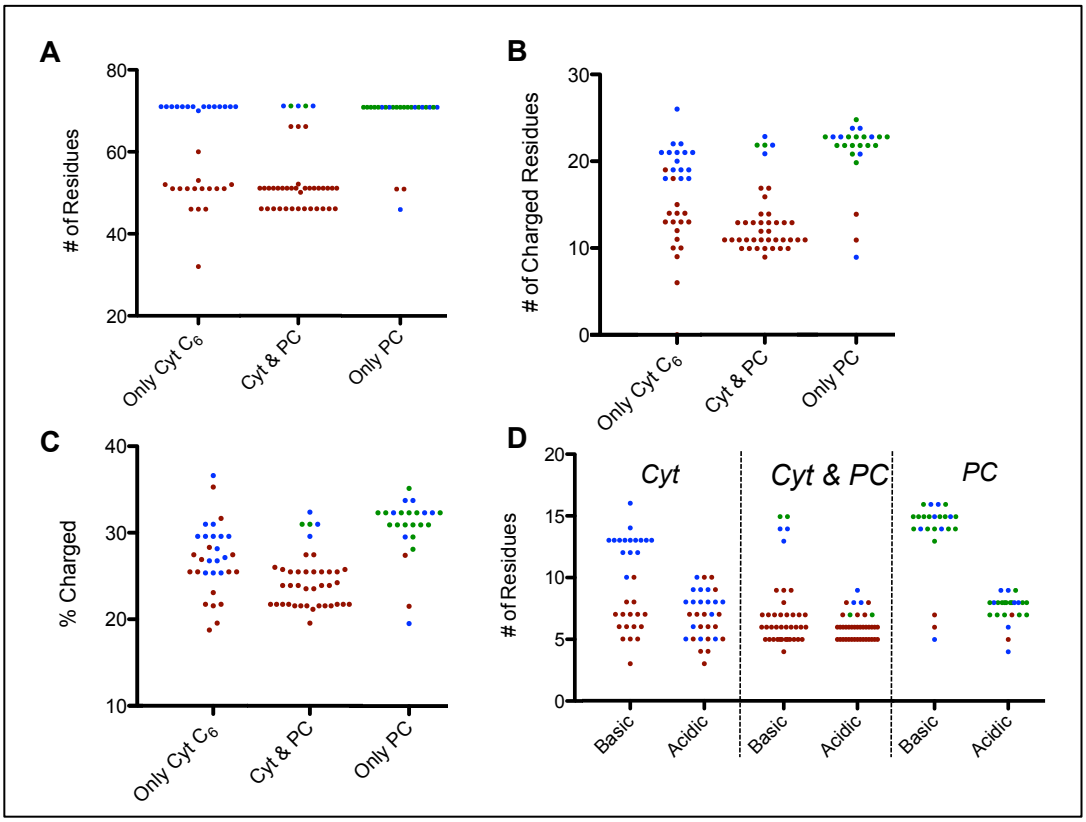

Figure 4-4. Bioinformatics of psaF charge analysis from plants, algae, and cyanobacteria.

Color key: Red-cyanobacteria, Blue-algae, Green-plants
Organisms from Tables 1-Only cyt c_6, 2-Both cyt c_6 and 3-Only PC.

A) The total number of residues for psaF are shown for each group. B) The total number of those residues in A) that are charged. C) The percentage of psaF residues that are charged: B) divided by A). D) Breaking down those residues that are charged into basic and acidic for each group.

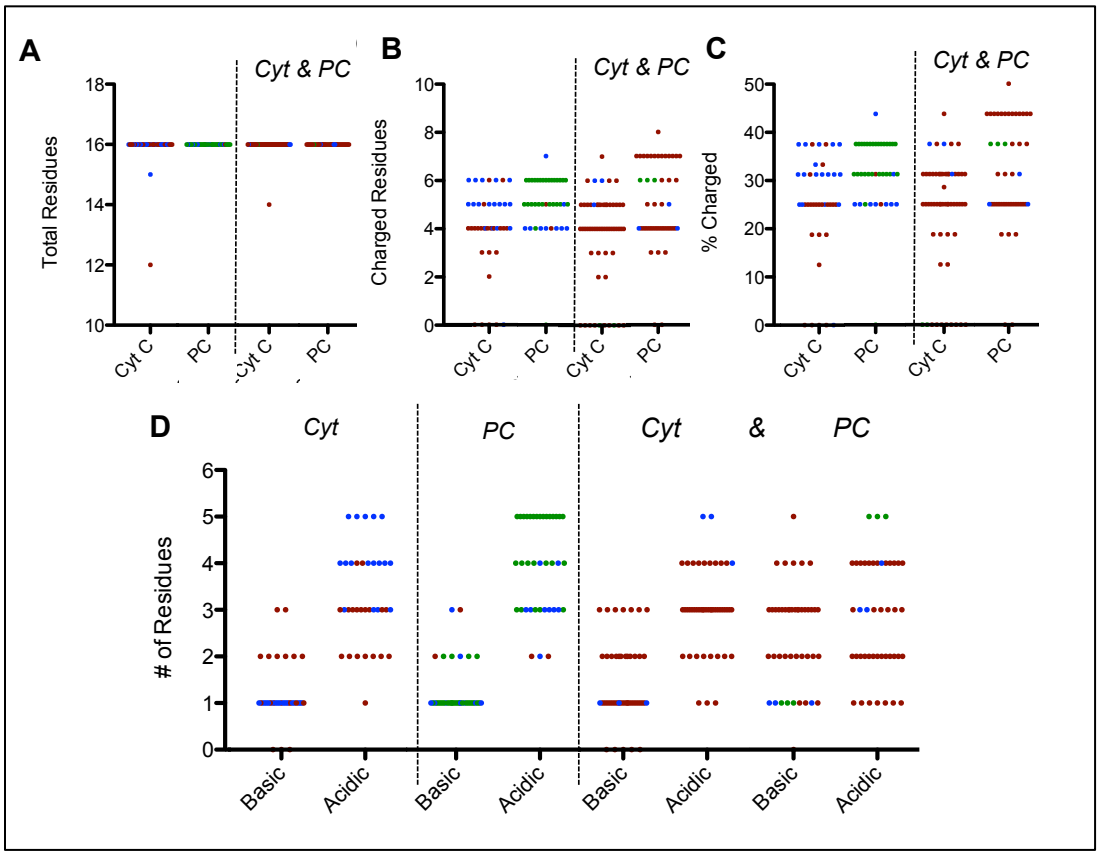

Figure 4-5. Bioinformatics of e^- donor charge analysis from plants, algae, and cyanobacteria.

Color key: Red-cyanobacteria, Blue-algae, Green-plants
Organisms from Tables 1-Only cyt c_6, 2-Both cyt c_6 and 3-Only PC.

A) The total number of residues for cytc/pc are shown for each group. B) The total number of those residues in A) that are charged. C) The percentage of cyt c_6/pc residues that are charged: B) divided by A). D) Breaking down those residues that are charged into basic and acidic for each group.

plants have a higher percent charged than algae or cyanobacteria. This suggested that charged residues are more prevalent in the more evolved species. With charge distribution, we see that in the groups of "only cyt" and "only PC", the more evolved species have more acidic than basic residues (Figure 4-5). The trend for this analysis suggests that the more evolved eukaryotes have a higher percent charged for both the lumen exposed portion of psaF and also for the donors proteins. For psaF, the higher plants and algae have more basic residues than that of the cyanobacteria. For the donors, plants and algae have more acidic residues than that of cyanobacteria. This shows that the basic residues on psaF and acidic residues on the donors may form an electrostatic interaction that only came about in algae and higher plants. This may be due to the spacial organization of the lumen space of the thylakoid membrane during the formation of the chloroplast in endosymbiosis. We next will expand the data set to have a more even distribution of prokaryotes versus eukaryotes, leading to the comparison of known electron transfer rates of the PSI/cyt pair to find an "optimal" charge distribution for fast electron transport.

D. PSI-donor Surface Charge Composition vs. e^- Transport Rate

As part of the electron transfer chain in photosynthesis, a soluble carrier (either cytochrome c or plastocyanin) accepts an electron from the Cytb6f complex and shuttles it to Photosystem I, allowing for the reduction of the special pair chlorophyll P_{700}. The interaction between cytochrome c_6 and PSI is known to occur near or at the psaF subunit of PSI. This protein pair has been investigated in

previous literature to show that an electrostatic interaction (acidic on cytochrome and basic on psaF) has emerged from cyanobacteria (very little or none) to algae and plants (prominent interaction), which affects their electron transfer rate. In order to investigate this transition, we aim to focus on the interacting interface between the cytochrome and psaF, and their charge content. Ten cytochromes (Table 4-4) were chosen from a selected group of about 100, with the criteria of covering a wide range of surface charge properties. These include protein pI, psaF-interface net charge, number of psaF-interface acidic residues and total protein net charge (Figure 4-6). From the coding sequences, the cytochromes were synthesized, sub-cloned into the pet30B expression vector behind a His-tag, and transformed into an *E. coli* expression strain along with a CCM heme maturase vector. Purification was the same as other cytochromes mentioned previously. An SDS-PAGE showing an example purification is shown in Figure 4-7A, along with the other purified Vcyts (Figure 4-7B).

Following the completion of cytochrome production (Figure 4-7), a reduced spectra was gathered for each Vcyt to confirm it's absorbance signatures (Figure 4-8). Electron transfer activity was analyzed via photo-flash photolysis using purified PSI from cyanobacteria (Syn. 6803 and *T. elongatus*) and a plant (spinach). Example P_{700} reduction curves by Vcyts using *Syn. 6803* are shown (Figure 4-9). The reduction rates by all cyts are shown (Figure 4-9C) for *Syn. 6803*, *T. elongatus* (Figure 4-9B), and spinach (Figure 4-9D). The x-scale is arranged by increasing positive net charge of each cytochrome. As spinach PSI has the most positive psaF, we do not really see a true trend with the charges of the cytochromes tested. Yet for

Table 4-4. The Uniprot entry IDs cyt c_6(petJ) for sequences used for Vcyts bioinformatics analysis.

Cyt c_6/PetJ	
Organism	**Uniprot Entry ID**
Arthrospira platensis NIES-39	D5A3R9
Bigelowiella natans	Q7XYQ4
Nostoc sp. PCC 7120	P0A3X7
Trichodesmium erythraeum IMS101	Q111R3
Fischerella sp. JSC-11	G6FNJ4
Nostoc azollae 0708	D7E5B2
Cyanophora paradoxa	Q9LEN1
Chlamydomonas reinhardii	P08197
Nostoc punctiform	B2IVD6
Synechocystis 6803	P46445

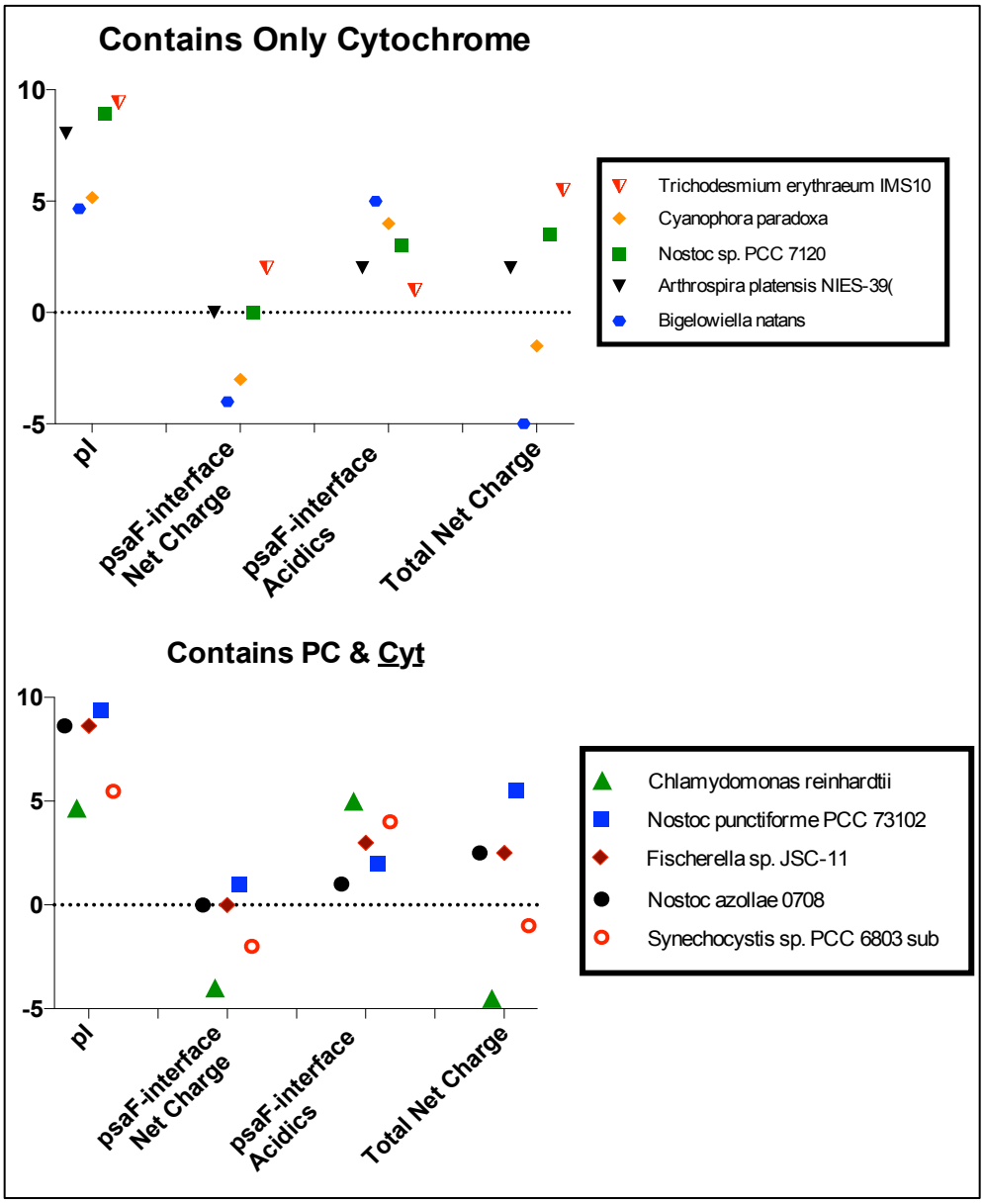

Figure 4-6. Bioinformatics of cytochrome c_6 charge analysis for Variable-cytochromes (Vcyts) cloning selection.

Sequences of cyt c_6s were gathered from Uniprot, IDs shown in Table 5. From a list of about 100 photosynthetic organisms, 10 were selected that gave a wide range of each criteria (pI, psaF-interface net charge, psaF-interface acidics, and total protein net charge. (Top graph) - Organisms that contained only cyt c_6 sequences. (Bottom graph) –Organism that have both cyt c_6 and plastocyanin.

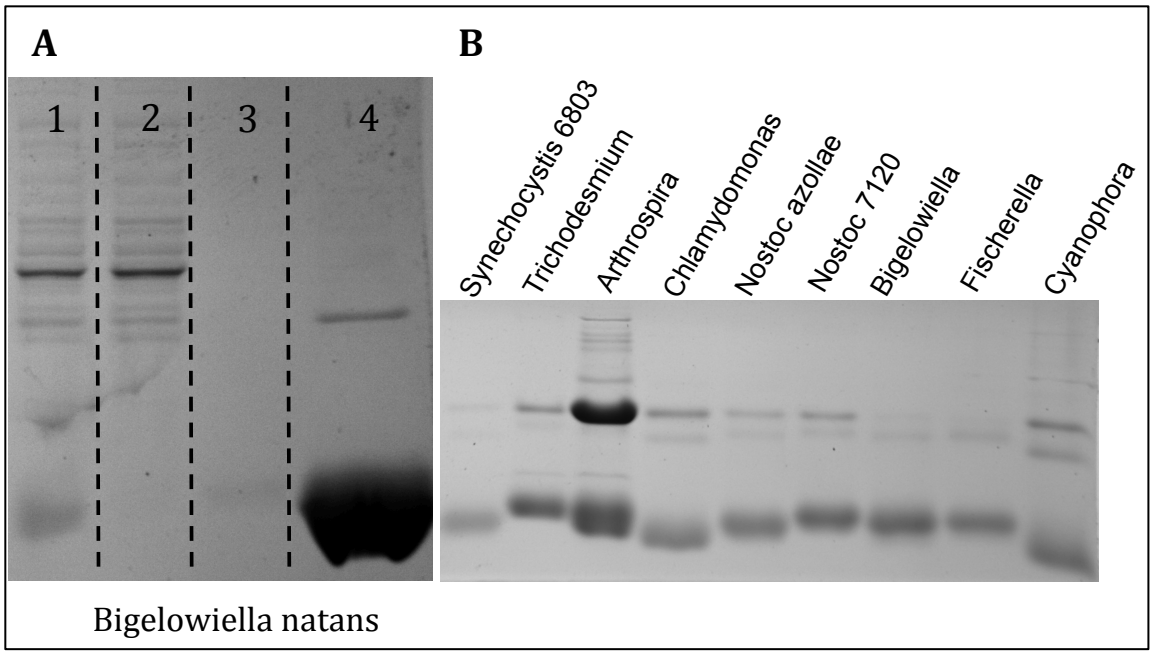

Figure 4-7. Purified cytochrome c_6s from the selected Variable Cyts.

A) SDS PAGE of purified cyt c_6. Lane 1: Flow through; Lane 2: Initial column wash; Lane 3: Final wash with 1 mM immidazole; Lane 4: Elution with 20 mM immidazole. B) Final elution for each of the Vcyts.

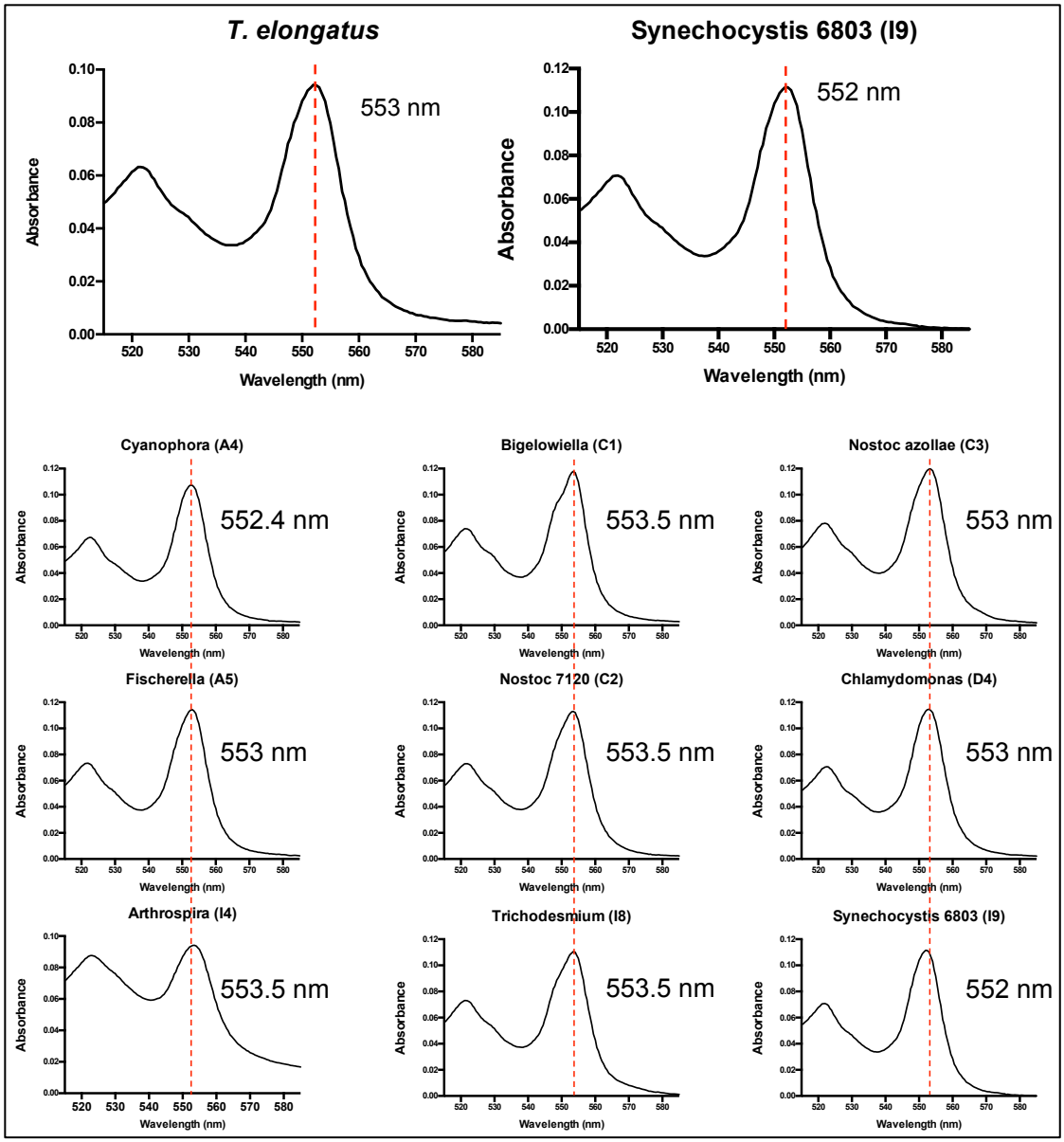

Figure 4-8. Reduced spectra of purified cytochromes from the selected Variable Cytochromes.

Slight peak shifts are seen with each purified Vcyt (still between 552-554 nm). Reduced cyt c_6 peaks are shown from two well characterized "model" cyanobacteria (*T. elongatus and Synechocystis 6803*) as a reference (Top).

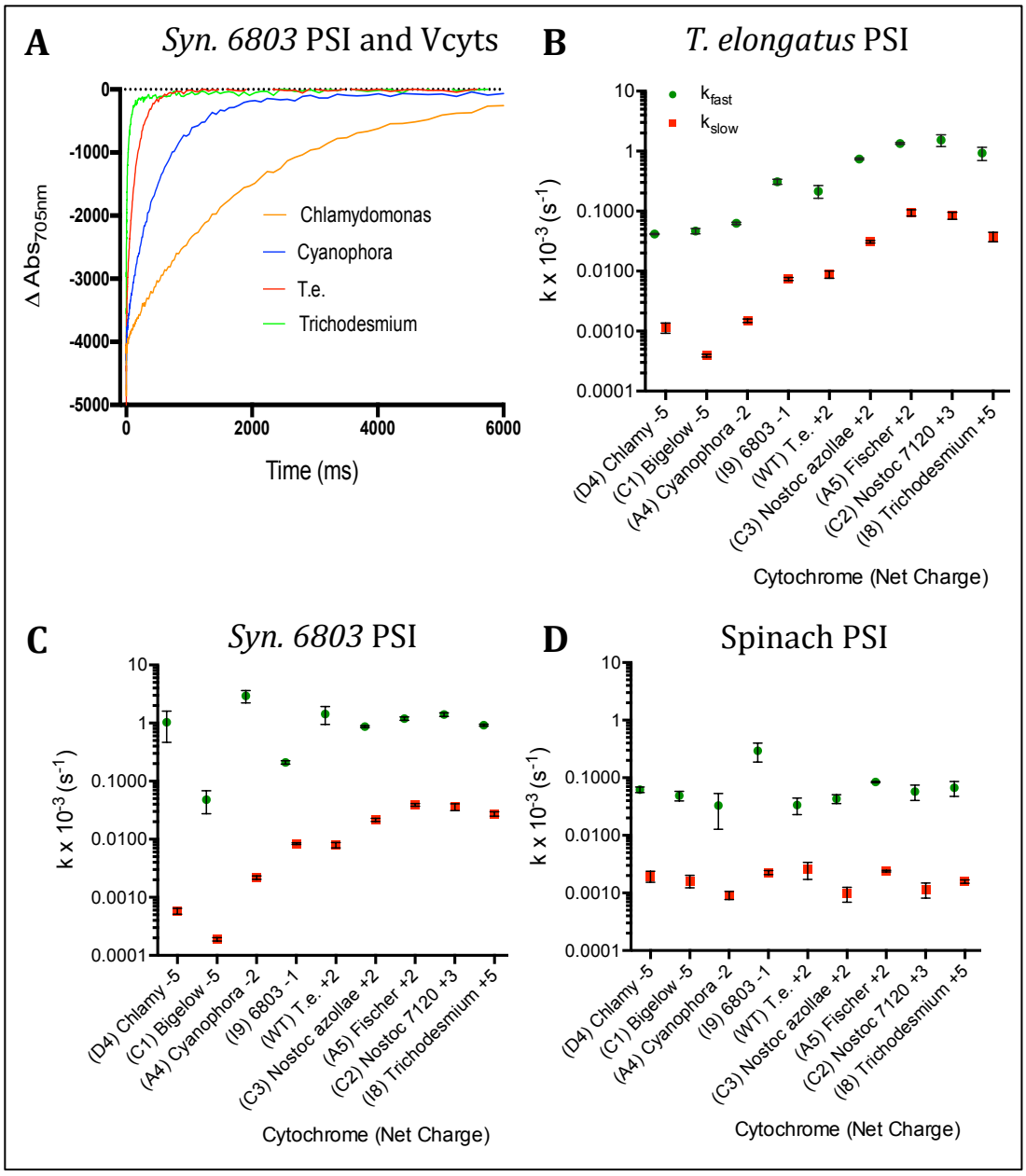

Figure 4-9. Reduction of PSI by Variable Cytochromes.

A) Example P_{700} reduction curves by Vcyts using *Syn. 6803* PSI. B) *T. elongatus* PSI reduced by equal molar ratios of each Vcyt. Recombinant *T. elongatus* cyt c_6 is included for reference. X-scale is arranged by increasing positive net charge of each cytochrome. The same was done for Syn. 6803 PSI (C) and spinach PSI (D).

the less charged cyanobacteria, we see that the more positive the cytochrome, the faster the PSI reduction rate gets. We will have to apply more variables and parameters to be able to tease out any true correlation.

E. Conclusions

We showed here various approaches towards the aim of increasing electron transport for bio-energy applications. By using the electrostatic mutants generated in Chapter 3, we were able to create a poly-cytochrome strategy that utilized a successive cloning scheme in creating faster electron transport. The results showed that we were successful in increasing the rate of electron transport with the linkage of cytochromes, but the more "links" we added, the slower the rate appeared. This we concluded was due to potential mis-folding of the poly-proteins to where even high concentrations of urea would not alleviate. This strategy can be further fined tuned by different linkage lengths, mixing different affinity cytochromes for each "link", and adjusting the buffer conditions to allow proper folding of the poly-proteins.

The bioinformatics investigation gave us a broad overview of the PSI-donor pair, which allowed us to break down charge compositions and test many "Variable" cytochromes. By mix-matching Variable cytochromes and testing with different PSI's that we had available, we saw some trends of that gave us clues for future directions. We will continue to explore the data set for other parameters and criteria (pH, temperature, concentrations, etc.) that might help shed more light.

Chapter 5

Differential PsaF Recognition via Western Blot

A. Introduction

With the aims of expanding our data sets from the previous chapter and collection of PSI, we searched for commercially available cyanobacteria antibodies, which gave us a very limited selection. These cyanobacteria antibodies also were not generated with a specificity for cyanobacteria, but also recognizing algal and plant PSI's. They also were made to recognize either the core complexes (PsaA and PsaB) or stromal subunits (PsaC, PsaD, and PsaE), which for our projects involving the lumen exposed PsaF, proved to be no value. We set out with the initial goal of generating a universal cyanobacterial antibody. This was done by making PsaF-specific peptides from sequence alignments using a wide range of cyanobacteria. After these alignments were done, we saw different groupings show up for the lengths used to cover the "conserved region" of PsaF that we selected. The final results of the preliminary findings of this project showed us how our two final PsaF antibodies reacted and recognized different cyanobacteria.

B. PsaF Antigen Design

Most photosynthetic antibodies that are available commercially have been designed using plant-based antigens. In order to make a universal cyanobacteria antibody, we selected the lumen-exposed (lumen-exposed) portion of psaF. A

protein sequence alignment was done with all available cyanobacteria that had a psaF annotated sequence. This gave a two distinct consensus groups, one of 45 (Table 5-1) residues and another with 50 (Table 5-2) residues. We selected a motif that consisted of DVAG- XXX -GLPHL, where the most common residues were used to fill in the "XXX". The two resulting consensus sequences are shown in Figures 5-1 and 5-2.

C. PsaF Antibody Specificity

These two consensus sequences were then codon optimized for *E. coli* expression. Peptides for these two sequences (psaF-peptide A, psaF-peptide B) were then synthesized and cloned into the IMPACT System expression vector, utilizing an Intein tag for purification (Figure 5-3). We analyzed the antigenicity plots for Peptide A and B consensus sequences. Each sequence (A & B) was also BLASTED against *T. elongatus* and *Syn. 6803* psaF sequences to ensure recognition of "model" cyanobacteria. Peptide A was 60% identical to *T. elongatus*, while only 37% identical to *Syn. 6803*. Peptide B was 73 and 71% identical to *T. elongatus* and *Syn. 6803* psaF sequences, respectively. The peptides were purified (SDS PAGE on right of Figure 5-3), and sent for antibodies production by Pocono Rabbit Farm and Laboratory, Inc. (PRF&L).

Table 5-1. Uniprot Entry ID for psaF sequences used in alignment of cyanobacterial lumen-exposed psaF (N-Term) for peptide synthesis – Peptide A

psaF (lengths 45-47)		
#	**Organism**	**Uniprot Entry ID**
1	Synechococcus sp. BL107	Q05YP9
2	Synechococcus sp. CC9311	Q0I866
3	Synechococcus sp. CC9605	Q3ALX4
4	Synechococcus sp. CC9902	Q3AWM3
5	Synechococcus sp. JA-2-3B'a(2-13)	Q2JI24
6	Synechococcus sp. JA-3-3Ab	Q2JXH0
7	Synechococcus sp. PCC 7335	B4WP24
8	Synechococcus sp. RS9916	Q05WR1
9	Synechococcus sp. RS9917	A3Z5Y5
10	Synechococcus sp. WH 5701	A3YY20
11	Synechococcus sp. WH 7803	A5GMV5
12	Synechococcus sp. WH 7805	A4CRT9
13	Synechococcus sp. WH 8016	G4FJE2
14	Synechococcus sp. WH 8102	Q7U572
15	Synechococcus sp. WH 8109	W0GSG2
16	Cyanobium sp. PCC 7001	B5INN5
17	Prochlorococcus marinus SS120	Q9X7I4
18	Prochlorococcus marinus MED4	Q7V2K7

Table 5-2. Uniprot Entry ID for psaF sequences used in alignment of cyanobacterial lumen-exposed psaF (N-Term) for peptide synthesis – Peptide B

psaF (lengths 48-51)		
#	Organism	Uniprot Entry ID
19	Nostoc azollae 0708	D7DZ81
20	Nostoc punctiforme 29133	B2J589
21	Raphidiopsis brookii D9	D4TNU2
22	Nodularia spumigena CCY9414	A0ZBQ3
23	Oscillatoria sp. PCC 6506	D8FZQ8
24	Anabaena 7120	P58564
25	Anabaena variabilis ATCC 29413	P31091
26	Cyanothece sp. CCY0110	A3IQ52
27	Cyanothece sp. PCC 7424	B7K766
28	Cyanothece sp. PCC 7822	E0UAY2
29	Crocosphaera watsonii WH 0003	G5IXP3
30	Synechocystis sp. PCC 6803	P29256
31	Cyanothece ATCC 51142	B1WVQ3
32	Cyanothece sp. PCC 7425	B8HVK4
33	Cyanothece 8801	B7K086
34	Microcystis aeruginosa NIES-843	B0JUV3
35	Microcystis aeruginosa PCC 7941	I4GHL6
36	Microcystis aeruginosa PCC 9701	I4IXF2
37	Microcystis aeruginosa PCC 9808	I4I635
38	Synechococcus elongatus PCC 7942	Q31NT9
39	Fischerella sp. JSC-11	G6FY36
40	Thermosynechococcus elongatus BP-1	P0A401
41	Acaryochloris marina MBIC11017	B0C7S7
42	Trichodesmium erythraeum IMS101	Q115B4
43	Arthrospira platensis NIES-39	D5A278
44	Arthrospira sp. PCC 8005	H1WAX7
45	Cylindrospermopsis raciborskii CS-505	D4TDK0
46	Gloeobacter violaceus PCC 7421	Q7NH05
47	Lyngbya sp. PCC 8106	A0YZL3
48	Prochlorococcus marinus MIT9313	Q7V659
49	Prochlorococcus marinus MIT9312	Q31C65
50	Prochlorococcus marinus MIT9303	A2C7G1

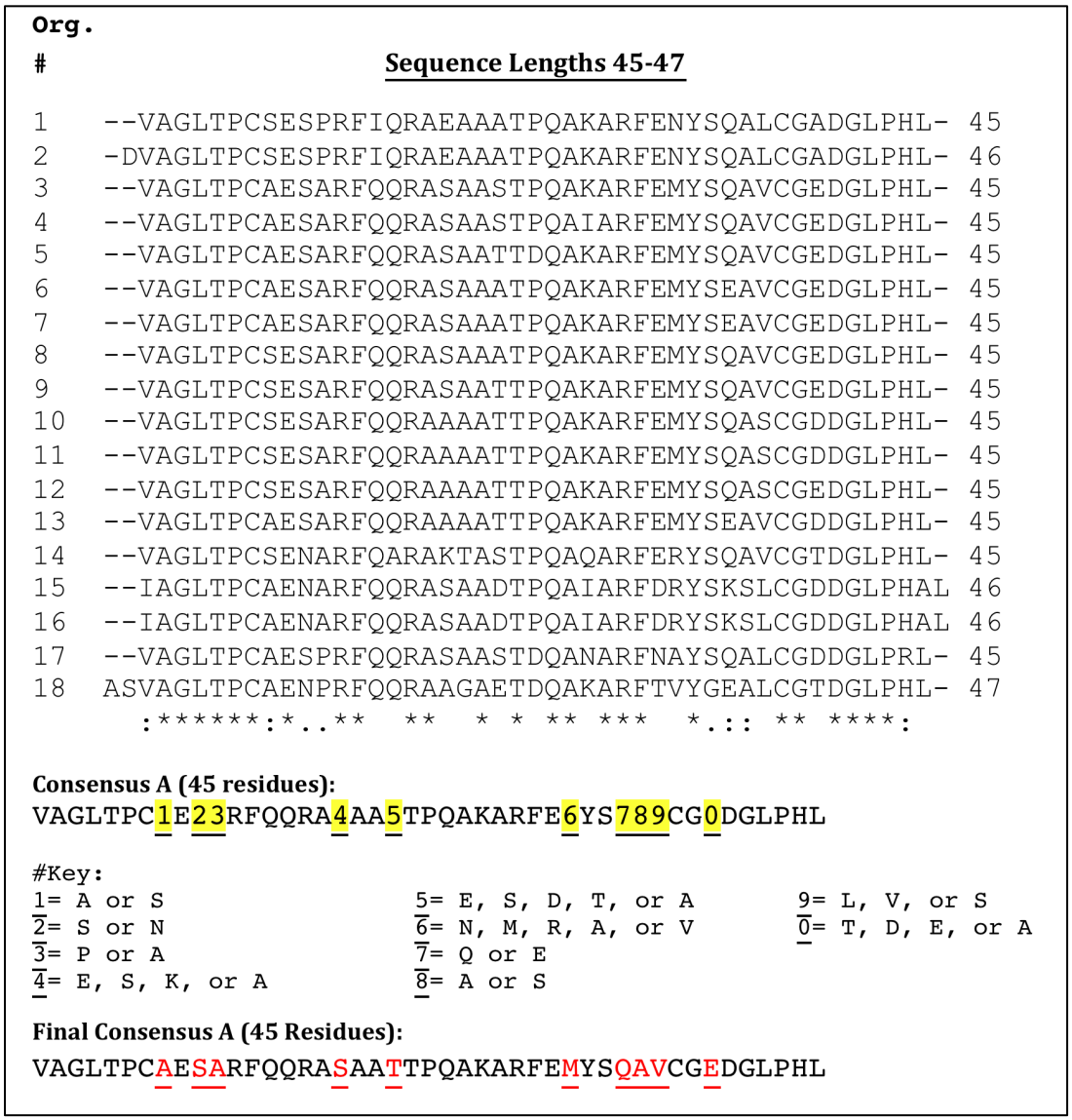

Figure 5-1. Alignment of cyanobacterial lumen-exposed psaF (N-Term) for peptide synthesis – Peptide A

Organisms used here (listed in Table 5-1) have 45-47 residues for the predicted lumen-exposed region of psaF. A consensus sequence of 45 residues resulted, where numbers in yellow represents the available residues found for that position, but not calculated as truly "conserved". The final consensus shows residues (in red) that were the most frequently found for those positions.

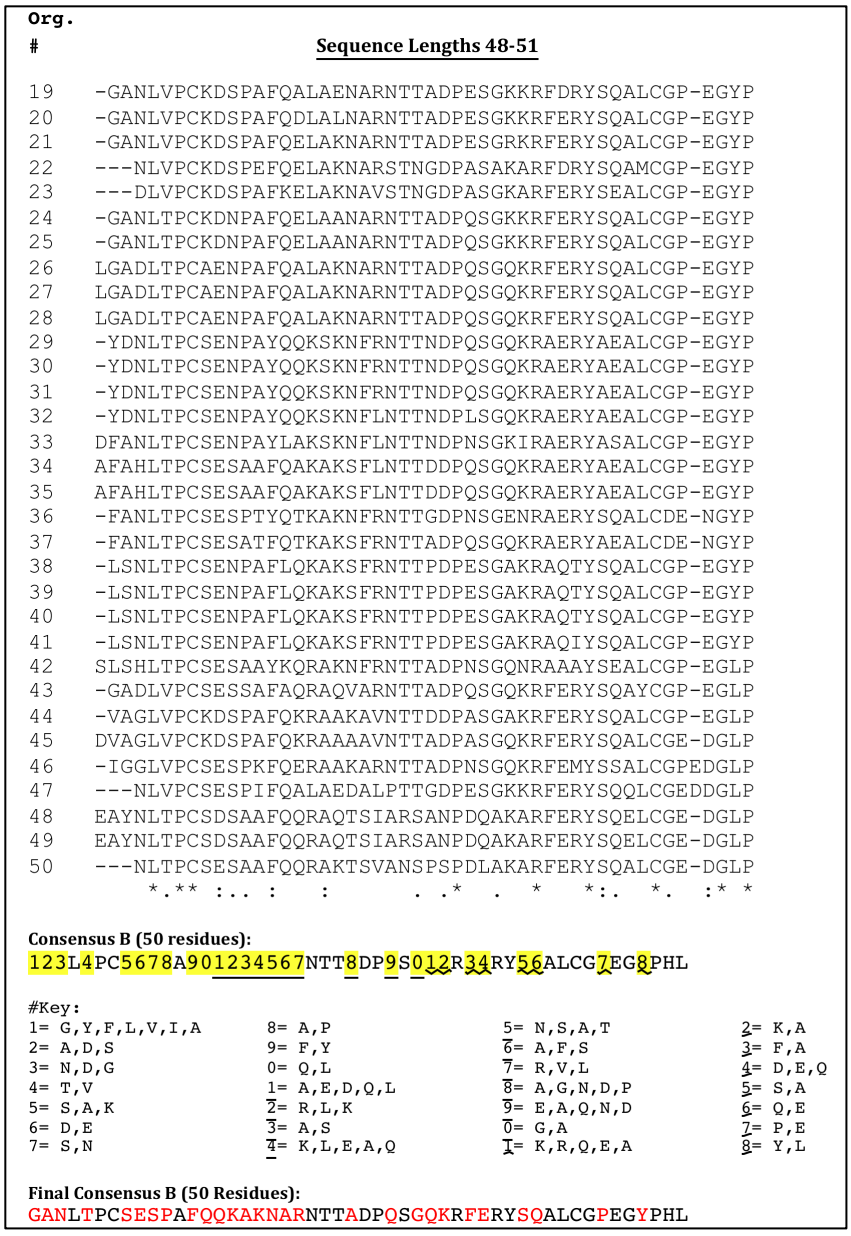

Figure 5-2. Alignment of cyanobacterial lumen-exposed psaF (N-Term) for peptide synthesis – Peptide B

Organisms used here (listed in Table 5-2) have 48-51 residues for the predicted lumen-exposed region of psaF. A consensus sequence of 50 residues resulted, where numbers in yellow represents the available residues found for that position, but not calculated as truly "conserved". The final consensus shows residues (in red) that were the most frequently found for those positions.

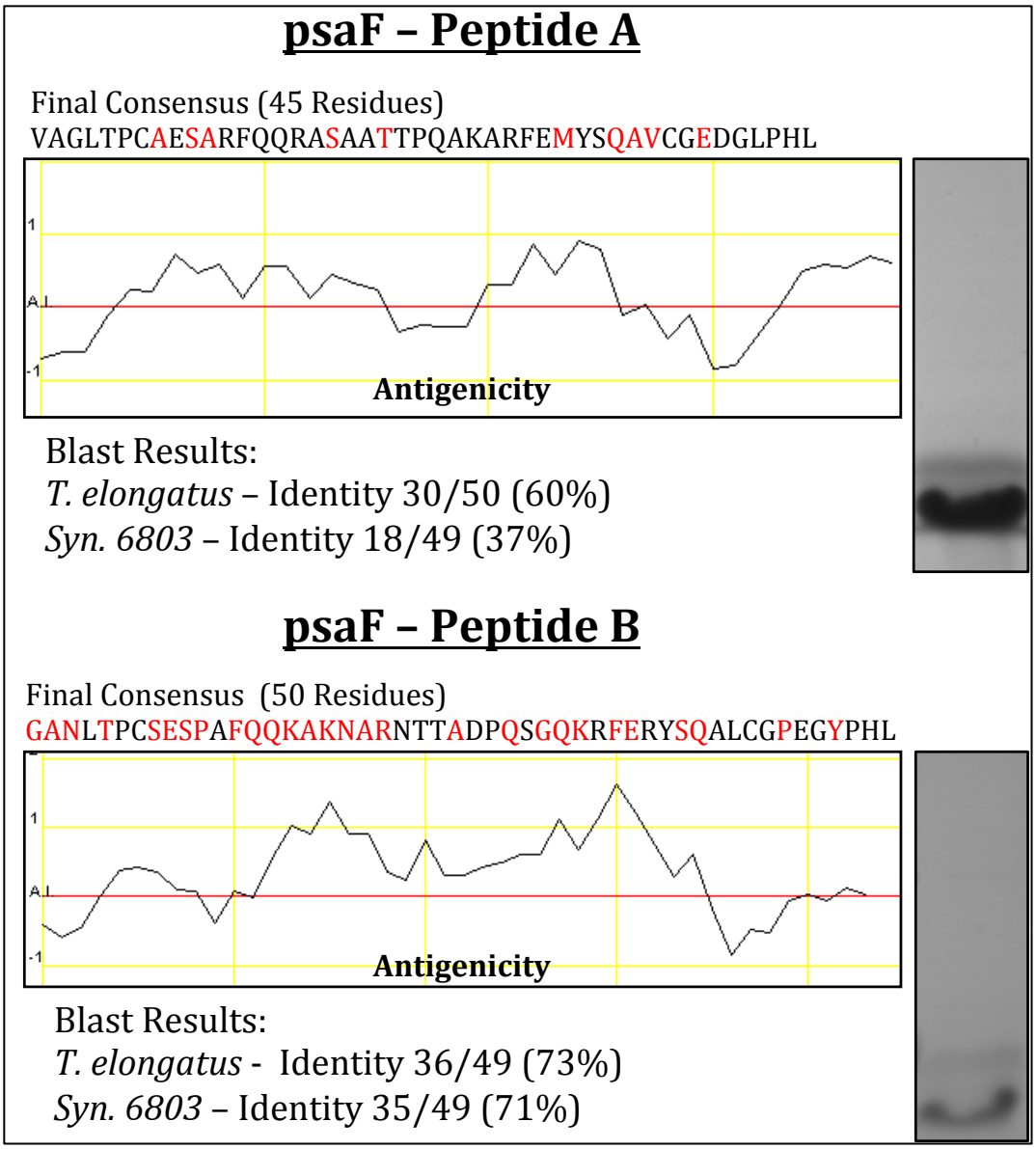

Figure 5-3. Peptides A-B antigenicity analysis for psaF-antibodies production.

Antigenicity plots for Peptide A and B consensus sequences. Each sequence (A & B) was also Blasted against *T. elongatus* and *Syn. 6803* psaF sequences to ensure recognition of "model" cyanobacteria.
Peptide A was 60% identical to *T. elongatus*, while only 37% identical to *Syn. 6803*. Peptide B was 73 and 71% identical to *T. elongatus* and *Syn. 6803* psaF sequences, respectively. The IMPACT System (Intein-tag) was used for final purification of peptides (SDS-PAGE on right), which were then sent for antibodies production by Pocono Rabbit Farm and Laboratory, Inc. (PRF&L).

D. Differential Recognition by various cyanobacteria

The Western Blot comparison method for differential psaF recognition by psaF antibodies generated by Peptides A and B are shown in Figure 5-4. Whole cell cyanobacteria (concentrated liquid culture) were mixed with SSB, heated, pelleted, and remaining supernatant were saved as samples ready to be loaded SDS-PAGE samples. Samples (1-8) were equally loaded and ran on two identical SDS-PAGE gels. The two gels were then transferred to a membrane and blocked exactly the same way, proceeding with a defined Western Blot protocol, with the primary antibody being the only difference. Final exposed blot (top) lanes were then compared side-by-side, with the end goal of identifying any differences in the expected psaF band around 15 kDa (bottom). The resulting psaF antibodies comparisons are shown for each panel, with *T. elongatus* included as a signal reference (Figure 5-5). The results are shown in Table 5-3, where we interpreted each band as nonspecific, doublet, or absent.

E. Antibody Dependent Phylogenetic Tree Groupings

Figure 5-6 shows a Phylogenetic tree generated from the psaF sequence alignment from Table 5-3. ClustalW was used for sequence alignment, along with Muscle, which gave the same result. Neighbor-Joining parameter was used to generate the tree from "MEGA v.6.06" alignment software. It is very difficult for us to make any conclusions since this type of analysis requires more cyanobacteria with available sequenced genomes, along with many different batches of liquid

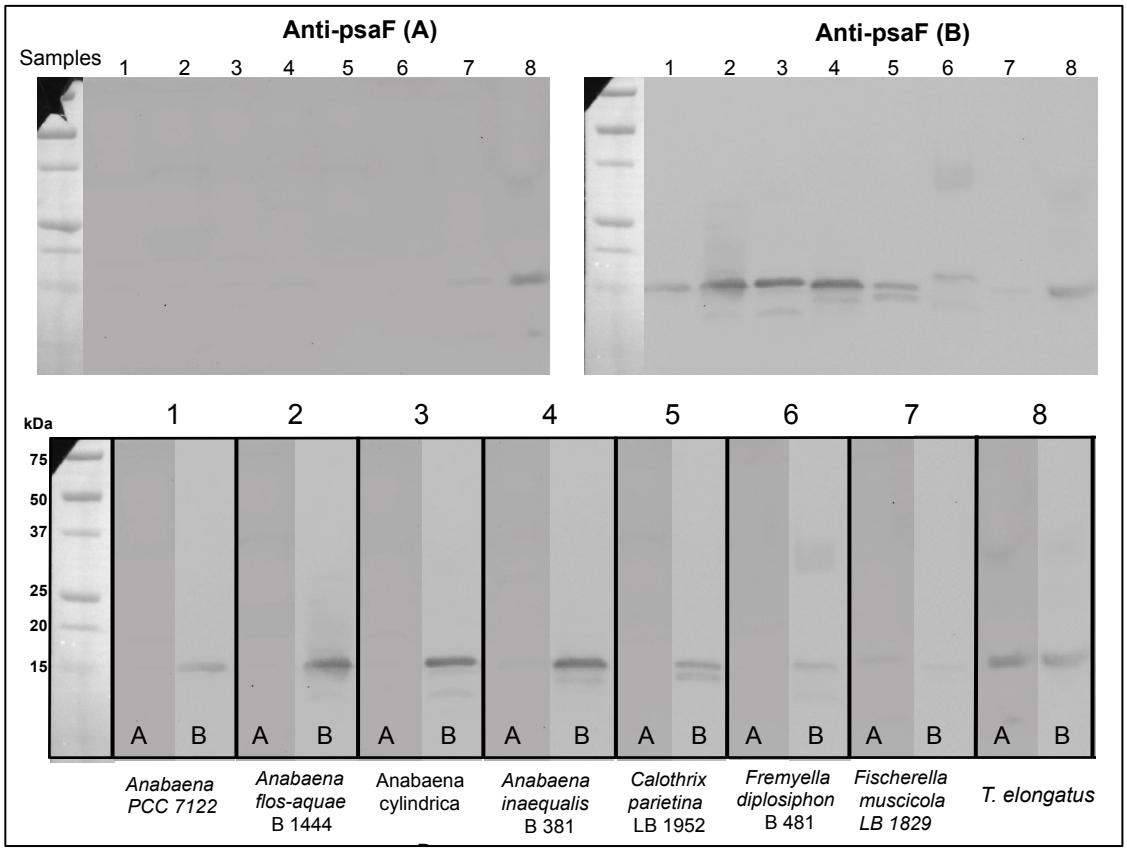

Figure 5-4. Western Blot comparison method for differential psaF recognition by psaF antibodies generated by Peptides A and B.

Whole cell cyanobacteria (concentrated liquid culture) were mixed with SSB , heated, spun down, and remaining supernatant were saved as samples ready to be loaded SDS-PAGE samples.

Samples (1-8) were equally loaded and ran on two identical SDS PAGE gels. The two gels were then transferred to a membrane and blocked exactly the same way, proceeding with a defined Western Blot protocol, with the primary antibody being the only difference. Final exposed blot (top) lanes were then compared side-by-side, with the end goal of identifying any differences in the expected psaF band around 15 kDa (bottom).

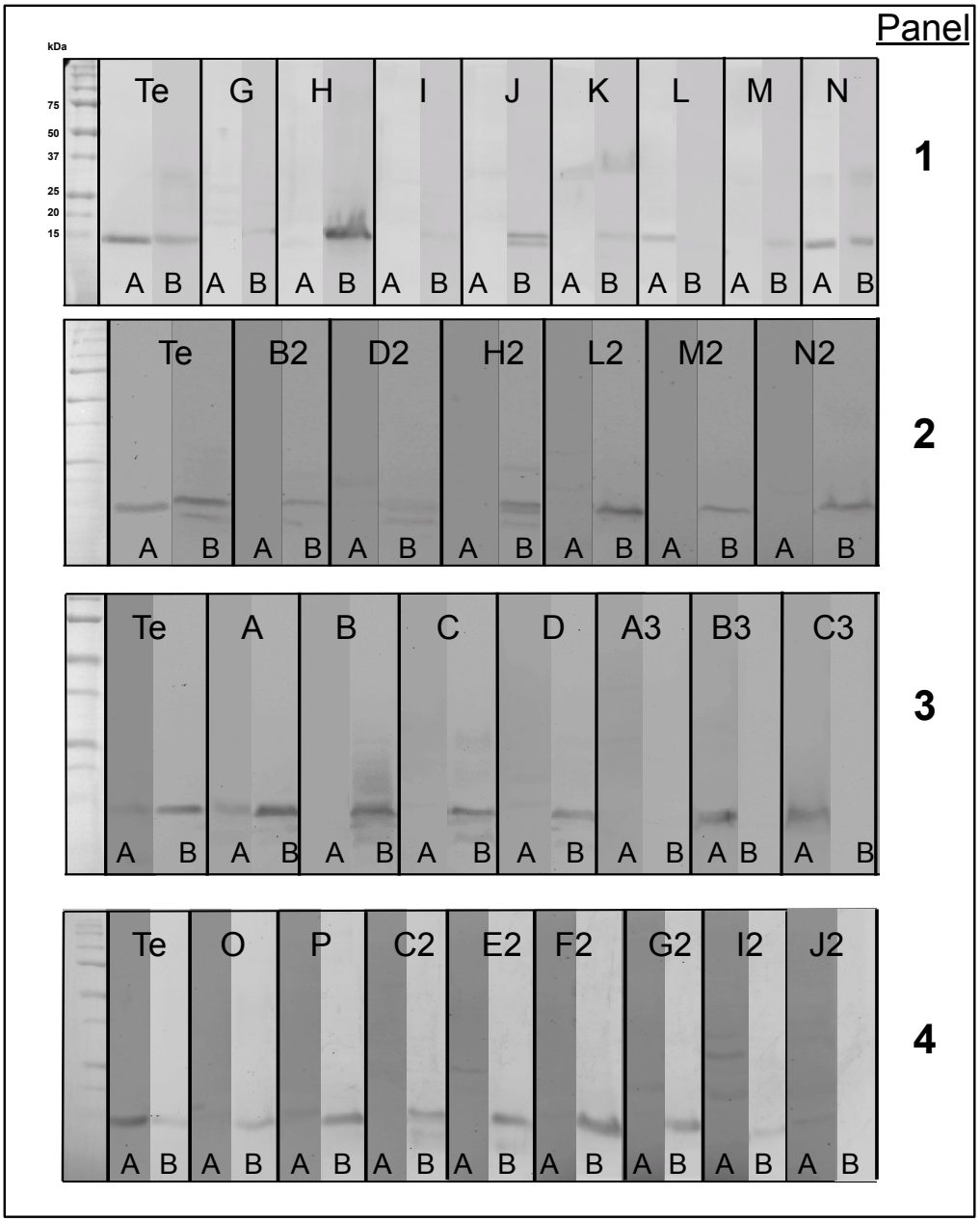

Figure 5-5. Results of Western Blot comparison for differential psaF recognition by psaF antibodies (A & B).

Resulting psaF antibodies comparisons are shown for each panel, with *T. elongatus* (T.e.) ran from each "batch run" as a detection signal reference.
Panel 1 – Samples: Te, G, H, I, J, K, L, M, N
Panel 2 – Samples: Te, B2, D2, H2, L2, M2, N2
Panel 3 – Samples: Te, A, B, C, D, A3, B3, C3
Panel 4 – Samples: Te, O, P, C2, E2, F2, G2, I2, J2

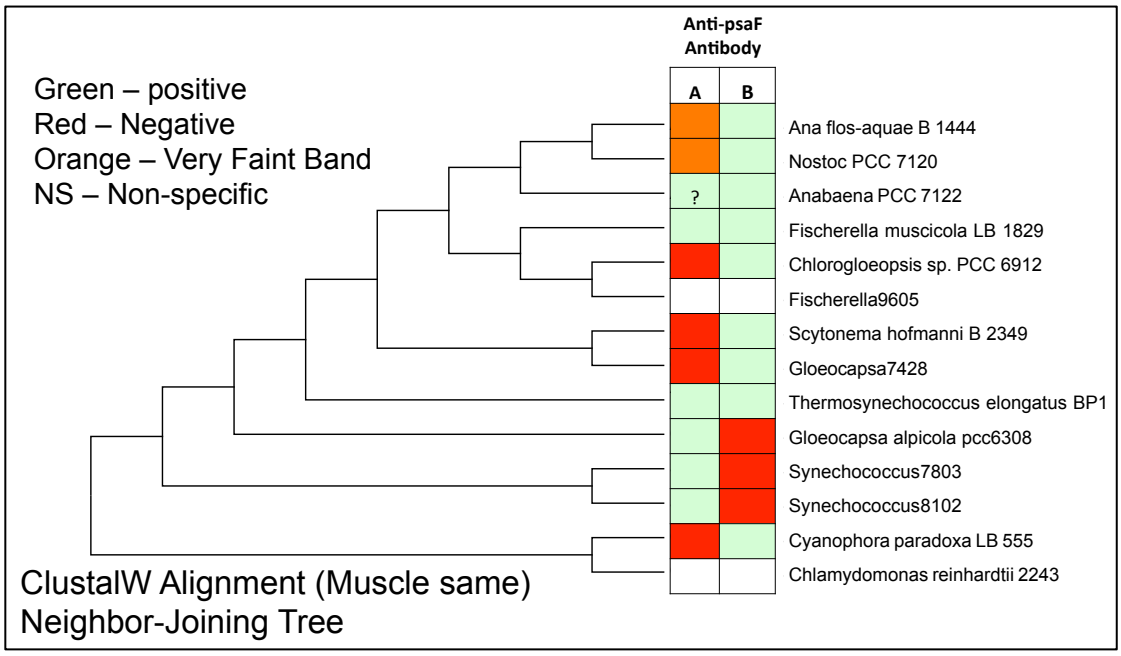

Figure 5-6. Phylogenetic tree of psaF sequence alignment from Table 5-3

ClustalW was used for sequence alignment, along with Muscle, which gave the same result. Neighbor-Joining parameter was used to generate the tree from "MEGA v.6.06" alignment software.

Table 5-3. Results of Western Blot comparison for differential psaF recognition by psaF antibodies (A & B).

Color Key:

Green- positive, Red- negative, Orange – faint band, NS – non-specific band(s)

Genome availability is also shown in yellow.

			Anti-psaF	
		Genome?	A	B
A	*Anabaena PCC 7122*	known		
B	*Anabaena flos-aquae* B 1444	known		
C	*Anabaena flos-aquae* LB 2558	unknown		NS
E	*Anabaena inaequalis* B 381	unknown		Doublet
F	*Calothrix parietina* LB 1952	unknown		Doublet
G	*Cyanophora biloba* LB 2766	unknown	NS	
H	*Cylindrospermum licheniforme* B 2014	unknown	Lower?	
I	*Cyanophora paradoxa* LB 555	known?		
J	*Fremyella diplosiphon* B 481	unknown		Doublet
K	*Fischerella muscicola LB 1829*	known		
L	*Gloeocapsa alpicola LB 1598*	known		
M	*Gloeotrichia ghosi* LB 1920	unknown		
N	*Scytonematopsis contorta* 2963	unknown		
O	*Spirirestis rafaelensis* B 2660	unknown		
P	*Tolypothrix distorta var. symplocoides* B 424	unknown		
A2	*Nodularia harveyana* B 2093	unknown		
B2	*Scytonema hofmanni* B 2349	known		NS
C2	*Fischerella ambigua* 1903	unknown		Doublet?
D2	*Mastigocladus* sp B2965	unknown		Doublet?
E2	*Scytonema crispum* LB 1556	unknown	NS	
F2	*Nodularia PCC 73104*	unknown		
G2	*Nostoc PCC 7120*	known	NS	
H2	*Hapalosiphon welwitschii B 1830*	unknown		Doublet?
I2	*Aphanothece* sp. SP25	unknown	NS	
J2	*Plectonema boryanum B 482*	unknown	NS	
K2	*Pseudanabaena* sp B SP48	unknown		
L2	*Calothrix membranacea* B 379	unknown		
M2	*Gloeocapsa* pcc 7428	known		
N2	*Chlorogloeopsis sp.* PCC 6912	known		
O2	*Fischerella* pcc 9605	known		
P2	*Chlamydomonas reinhardtii* 2243	known		
B3	Synechosystis 7803	known		
C3	Synechosystis 8102	known?		

culture that was grown with various parameters that might trigger the expression of one version of psaF over another, if the organism has multiple copies of this gene.

F. Conclusions

By generating a sequence alignment, using a "conserved" motif of lumen-exposed PsaF and using those for antibody production, we created two antibodies that allowed for differential recognition of cyanobacteria. The preliminary results show us that with a wider and broader set of photosynthetic organisms, we can use these antibodies as a initial screen for PSI recognition. The phylogenetic tree we generated showed a preliminary grouping that may eventually help in classifying newly discovered or unclassified/unsequenced cyanobacteria. This future project can employ various growth conditions to see if multiple copies of *psaF* in these organisms can be differentially expressed.

Chapter 6

Conclusions and Future Directions

As we mentioned previously, the collection of bio-hybrid devices listed in Chapter 1, either with the goal of evolving molecular hydrogen or to generate a photocurrent, utilize PSI's ability to energize electrons via light input so that they can flow freely through the reaction center, allowing them to be fed to acceptors on the stromal side. The energetics and rate of which these electrons travel through the internal cofactors of PSI have been thoroughly discussed and worked on by many groups in the last decade, with the potential to increase this rate for applied photosynthesis. The majority of our work here however, focuses on the preceding steps of how the electrons can even be donated to PSI, allowing it to be processed through the complex.

At the start of this project, we started with a well characterized, model cyanobacterium, *Thermosynechococcus elongatus BP-1*. This thermophilic cyanobacterium, with a fully sequenced genome (Nakamura, Kaneko et al. 2002), and available PSI crystal structure (PDB ID- 1JB0)(Byrdin, Jordan et al. 2002), gave us a thermo-tolerant platform in which we were able to manipulate in various aspects, toward the goal of increasing electron transfer. Previous literature have reported fast electron transfer rates in plant and algae systems, which were attributed to the increased electrostatic interactions between the electron donor and the lumen exposed, N-terminal portion of the PsaF subunit of PSI (Hippler, Drepper et al. 1998, Sommer, Drepper et al. 2006). These protein surface

interactions have been shown to be due to increased positively charged residues on PsaF and negatively charged residues on the electron donors, cyt c_6 or PC (Hippler, Drepper et al. 1998, Sommer, Drepper et al. 2006). This gave us an idea to where we thought it would be very advantageous to be able to increase the rate of electron transfer to P_{700}, but also easily manipulate other features of PSI by working with a basic cyanobacteria PSI background. Before starting to think about increasing the electron transport rate, we first had to be sure that we had the ability to well characterize our WT electron donor/PSI system with our own instrumentation.

We originally aimed at understanding the relationship between the electron transfer rate and surface charges on the protein pair (PsaF-cyt c_6). Our secondary aim of increasing electron transport for bio-energy applications directed us to looking at the differences between these photosynthetic electron transfer rates and the system that they were in (cyanobacteria, algae, or plants). In order to show that we can accurately measure these rates with our instrumentation (LED-flashphotolysis), WT proteins from *T. elongatus* were used (purified PSI and recombinant cyt c_6).

We showed that we were able to first characterize the cyt c_6 in *T. elongatus* by finding the intracellular molar ratio of cyt c_6 to PSI via quantitative Western Blot analysis, showing us about a 2:1 of cyt c_6 to PSI *in vivo.* This allowed us to use physiologically relevant ratios in our initial LED flash-photolysis assays where the kinetics of the electron transfer were measured. With the ability to modulate the system via illumination, temperature, pH, and ionic strength, we felt comfortable in being able to modulate this system in increasing the electron transfer. As we

compared the LED system versus the more widely used laser systems, an added kinetic phase was seen in the LED system. We attribute this to the nature of the duration of the assays where the protein pair was exposed to the actinic light. With a longer light duration, multiple turn-over events of P_{700} oxidation and reduction by cyt c_6 must occur, further complicating the kinetic result output. We rationalized this with Figure 3-16, where a schematic of the kinetic model was proposed.

The results from our electrostatic mutations were almost the exact opposite of what we initial expected, but after more consideration of our kinetic model, we are able to interpret the results as having a light artifact that was contributed to our LED instrumentation. The electrostatic mutations that were added to our WT cyt c_6 and PsaF possibly did what we had initially intended, to allow reduced cyt c_6 to find PsaF quicker, but it might have worked too well. The longer light cycle and added turn over events of P_{700} ox-red did not allow the mutated cyt c_6 to disassociate from the mutated PsaF once the initial electron transfer occurred. This now oxidized cytc6, may still be bound to PsaF, while the light cycle was still on, blocking the free and reduced population of cyt c_6 access to now oxidized P_{700}. This was shown with the apparent "stickiness" of this interaction, where more electrostatic mutations made the rate seem slower. This however, has not been tested by the single turn-over laser flash-photolysis system, where the results may appear faster with more electrostatic mutations. We aim to proceed with these assays as our next step.

Along with our electrostatic mutants of cyt c_6 and PsaF, we also wanted to explore other methods and approaches of increasing the electron transfer rate by either cyt c_6 or PSI modifications. We discuss here how our electrostatic mutation

results gave us an idea for another strategy, where we generated a "molecular battery pack" where a poly-cytochrome cloning method was used. We next explore the broader scope of this PSI-donor pair by looking at a wide collection of photosynthetic organisms via a bioinformatics approach. This then allowed us to carefully compare the surface charge composition of the PSI-donor pair and relate it to their electron transport rates.

By using the electrostatic mutants generated in Chapter 3, we were able to create a poly-cytochrome strategy that utilized a successive cloning scheme in creating faster electron transport. The results showed that we were successful in increasing the rate of electron transport with the linkage of cytochromes, but the more "links" we added, the slower the rate appeared. This we concluded was due to potential mis-folding of the poly-proteins to where even high concentrations of urea would not alleviate. This strategy can be further fined tuned by different linkage lengths, mixing different affinity cytochromes for each "link", and adjusting the buffer conditions to allow proper folding of the poly-proteins.

The bioinformatics investigation gave us a broad overview of the PSI-donor pair, which allowed us to break down charge compositions and test many "Variable" cytochromes. By mix-matching Variable cytochromes and testing with different PSI's that we had available, we saw some trends of that gave us clues for future directions. We will continue to explore the data set for other parameters and criteria (pH, temperature, concentrations, etc.) that might help shed more light on how, if at all, the surface charge composition may affect electron transfer rates among photosynthetic organisms.

In order to expand our data set and collection of PSI, we initially had the goal of generating a universal cyanobacterial antibody. This was done by making PsaF-specific peptides from sequence alignments using a wide range of cyanobacteria. After these alignments were done, we saw different groupings show up for the lengths used to cover the "conserved region" of PsaF that we selected. The final parts of this project came by chance as we saw how our two final PsaF antibodies reacted and recognized different cyanobacteria. We see that by generating a sequence alignment, using a "conserved" motif of lumen-exposed PsaF and using those for antibody production, we created two antibodies that allowed for differential recognition of cyanobacteria. This final results show us that with a wider and broader set of photosynthetic organisms, we can use these antibodies as a initial screen for PSI recognition. The phylogenetic tree showed a preliminary grouping that may eventually help in classifying newly discovered or unclassified/unsequenced cyanobacteria. These future project can employ various growth conditions to see if multiple copies of *psaF* in these organisms can be differentially expressed.

We here have reviewed a vast array of usages and applications for PSI, but have only begun the process of incorporating this green potential into what is realistically feasible to reach the market. While this work focuses mainly on one protein pair, there is much greater potential in photosynthesis that has yet to be explored. To truly aim for a sustainable future, I believe that much more of our time, effort, and money should be invested into something that could revolutionize the future for our future generations. Despite a relatively small number of laboratories

worldwide working on applied photosynthesis, the collective progress is very encouraging. In a short span of less than 10 years, the performance of these PSI based devices has increased more than 10,000 fold. Moreover, this work has been accomplished with a fraction of the research support that other areas of bioenergy research have enjoyed for the past decade. On the other hand, there are still many challenges in funding for PSI biohybrid-based research, along with breaking the major "bottle-necks" that really make it an affordable investment.

List of References

Agalarov, R., M. Byrdin, F. Rappaport, G. Shen, D. A. Bryant, A. van der Est and J. H. Golbeck (2008). "Removal of the PsaF polypeptide biases electron transfer in favor of the PsaB branch of cofactors in Triton X-100 photosystem I complexes from Synechococcus sp. PCC 7002." Photochem Photobiol **84**(6): 1371-1380.

Albertsson, P. A. (1995). "The structure and function of the chloroplast photosynthetic membrane - a model for the domain organization." Photosynth Res **46**(1-2): 141-149.

Ali, K., S. Santabarbara, P. Heathcote, M. C. Evans and S. Purton (2006). "Bidirectional electron transfer in photosystem I: replacement of the symmetry-breaking tryptophan close to the PsaB-bound phylloquinone A1B with a glycine residue alters the redox properties of A1B and blocks forward electron transfer at cryogenic temperatures." Biochim Biophys Acta **1757**(12): 1623-1633.

Almog, O., G. Shoham, D. Michaeli and R. Nechushtai (1991). "Monomeric and trimeric forms of photosystem I reaction center of Mastigocladus laminosus: crystallization and preliminary characterization." Proc Natl Acad Sci U S A **88**(12): 5312-5316.

Amunts, A., O. Drory and N. Nelson (2007). "The structure of a plant photosystem I supercomplex at 3.4 A resolution." Nature **447**(7140): 58-63.

Amunts, A., O. Drory and N. Nelson (2007). "The structure of a plant photosystem I supercomplex at 3.4 angstrom resolution." Nature **447**(7140): 58-63.

Amunts, A. and N. Nelson (2008). "Functional organization of a plant Photosystem I: Evolution of a highly efficient photochemical machine." Plant Physiology and Biochemistry **46**(3): 228-237.

Amunts, A. and N. Nelson (2009). "Plant photosystem I design in the light of evolution." Structure **17**(5): 637-650.

Amunts, A. and N. Nelson (2009). "Plant Photosystem I Design in the Light of Evolution." Structure (London, England : 1993) **17**(5): 637-650.

Amunts, A., H. Toporik, A. Borovikova and N. Nelson (2010). "Structure determination and improved model of plant photosystem I." J Biol Chem **285**(5): 3478-3486.

Andersen, B., H. V. Scheller and B. L. Moller (1992). "The PSI-E subunit of photosystem I binds ferredoxin:NADP+ oxidoreductase." FEBS Lett **311**(2): 169-173.

Ansari, S. A. and Q. Husain (2012). "Potential applications of enzymes immobilized on/in nano materials: A review." Biotechnology Advances **30**(3): 512-523.

Antonkine, M. L., G. H. Liu, D. Bentrop, D. A. Bryant, I. Bertini, C. Luchinat, J. H. Golbeck and D. Stehlik (2002). "Solution structure of the unbound, oxidized photosystem I subunit PsaC, containing [4Fe-4S] clusters F-A and F-B: a conformational change occurs upon binding to photosystem I." Journal of Biological Inorganic Chemistry **7**(4-5): 461-472.

Arblaster, J. W. (1989). " "Densities of osmium and iridium: recalculations based upon a review of the latest crystallographic data"." Platinum Metals Review **33**(1): 14-16.

Aro, E. M., I. Virgin and B. Andersson (1993). "Photoinhibition of Photosystem II. Inactivation, protein damage and turnover." Biochim Biophys Acta **1143**(2): 113-134.

Aspinwall, C. L., M. Sarcina and C. W. Mullineaux (2004). "Phycobilisome mobility in the cyanobacterium Synechococcus sp PCC7942 is influenced by the trimerisation of Photosystem I." Photosynthesis Research **79**(2): 179-187.

Badura, A., D. Guschin, T. Kothe, M. J. Kopczak, W. Schuhmann and M. Rogner (2011). "Photocurrent generation by photosystem 1 integrated in crosslinked redox hydrogels." Energy & Environmental Science **4**(7): 2435-2440.

Baker, D. R., A. K. Manocchi, S. Pendley, J. J. Sumner, M. Hurley, K. Xu, B. D. Bruce and C. A. Lundgren (2012). "Photosystem I based solar cell for on-site hydrogen production." Abstracts of Papers of the American Chemical Society **243**.

Balme, A., M. Hervas, L. A. Campos, J. Sancho, M. A. De la Rosa and J. A. Navarro (2001). "A comparative study of the thermal stability of plastocyanin, cytochrome c(6) and Photosystem I in thermophilic and mesophilic cyanobacteria." Photosynth Res **70**(3): 281-289.

Barber, J. and B. Andersson (1992). "Too much of a good thing: light can be bad for photosynthesis." Trends Biochem Sci **17**(2): 61-66.

Beissinger, M., H. Sticht, M. Sutter, A. Ejchart, W. Haehnel and P. Rosch (1998). "Solution structure of cytochrome c(6) from the thermophilic cyanobacterium Synechococcus elongatus." Embo Journal **17**(1): 27-36.

Bellafiore, S., F. Barneche, G. Peltier and J. D. Rochaix (2005). "State transitions and light adaptation require chloroplast thylakoid protein kinase STN7." Nature **433**(7028): 892-895.

Ben-Shem, A., F. Frolow and N. Nelson (2003). "Crystal structure of plant photosystem I." Nature **426**(6967): 630-635.

Ben-Shem, A., F. Frolow and N. Nelson (2004). "Evolution of photosystem I - from symmetry through pseudo-symmetry to asymmetry." FEBS Lett **564**(3): 274-280.

Ben-Shem, A., F. Frolow and N. Nelson (2004). "Evolution of photosystem I - from symmetry through pseudosymmetry to asymmetry." FEBS Letters **564**(3): 274-280.

Ben-Shem, A., F. Frolow and N. Nelson (2004). "Light-harvesting features revealed by the structure of plant photosystem I." Photosynth Res **81**(3): 239-250.

Bender, S. L. and B. A. Barry (2008). "Light-induced dynamics in photosystem I electron transfer." Biophys J **95**(8): 3927-3934.

Berry, E. A., M. Guergova-Kuras, L. S. Huang and A. R. Crofts (2000). "Structure and function of cytochrome bc complexes." Annu Rev Biochem **69**: 1005-1075.

Berthold, T., E. D. von Gromoff, S. Santabarbara, P. Stehle, G. Link, O. G. Poluektov, P. Heathcote, C. F. Beck, M. C. Thurnauer and G. Kothe (2012). "Exploring the electron transfer pathways in photosystem I by high-time-resolution electron paramagnetic resonance: observation of the B-side radical pair P700(+)A1B(-) in whole cells of the deuterated green alga Chlamydomonas reinhardtii at cryogenic temperatures." J Am Chem Soc **134**(12): 5563-5576.

Bibby, T. S., I. Mary, J. Nield, F. Partensky and J. Barber (2003). "Low-light-adapted Prochlorococcus species possess specific antennae for each photosystem." Nature **424**(6952): 1051-1054.

Blankenship, R. E. (2010). "Early evolution of photosynthesis." Plant Physiol **154**(2): 434-438.

Blankenship, R. E., D. M. Tiede, J. Barber, G. W. Brudvig, G. Fleming, M. Ghirardi, M. R. Gunner, W. Junge, D. M. Kramer, A. Melis, T. A. Moore, C. C. Moser, D. G. Nocera, A. J. Nozik, D. R. Ort, W. W. Parson, R. C. Prince and R. T. Sayre (2011). "Comparing photosynthetic and photovoltaic efficiencies and recognizing the potential for improvement." Science **332**(6031): 805-809.

Boekema, E. J., A. Hifney, A. E. Yakushevska, M. Piotrowski, W. Keegstra, S. Berry, K. P. Michel, E. K. Pistorius and J. Kruip (2001). "A giant chlorophyll-protein complex induced by iron defciency in cyanobacteria." Nature **412**(6848): 745-748.

Bonardi, V., P. Pesaresi, T. Becker, E. Schleiff, R. Wagner, T. Pfannschmidt, P. Jahns and D. Leister (2005). "Photosystem II core phosphorylation and photosynthetic acclimation require two different protein kinases." Nature **437**(7062): 1179-1182.

Bottcher, B., P. Graber and E. J. Boekema (1992). "The structure of Photosystem I from the thermophilic cyanobacterium Synechococcus sp. determined by electron microscopy of two-dimensional crystals." Biochim Biophys Acta **1100**(2): 125-136.

Brecht, M., M. Hussels, E. Schlodder and N. V. Karapetyan (2012). "Red antenna states of Photosystem I trimers from Arthrospira platensis revealed by single-

molecule spectroscopy." Biochimica Et Biophysica Acta-Bioenergetics **1817**(3): 445-452.

Brettel, K. and J. H. Golbeck (1995). "Spectral and kinetic characterization of electron acceptor A1 in a Photosystem I core devoid of iron-sulfur centers F X, F B and F A." Photosynth Res **45**(3): 183-193.

Brettel, K. and W. Leibl (2001). "Electron transfer in photosystem I." Biochim Biophys Acta **1507**(1-3): 100-114.

Byrdin, M., P. Jordan, N. Krauss, P. Fromme, D. Stehlik and E. Schlodder (2002). "Light harvesting in photosystem I: modeling based on the 2.5-A structure of photosystem I from Synechococcus elongatus." Biophys J **83**(1): 433-457.

Byrdin, M., S. Santabarbara, F. Gu, W. V. Fairclough, P. Heathcote, K. Redding and F. Rappaport (2006). "Assignment of a kinetic component to electron transfer between iron-sulfur clusters F(X) and F(A/B) of Photosystem I." Biochim Biophys Acta **1757**(11): 1529-1538.

Cardona, T., A. Sedoud, N. Cox and A. W. Rutherford (2012). "Charge separation in photosystem II: a comparative and evolutionary overview." Biochim Biophys Acta **1817**(1): 26-43.

Carmeli, I., L. Frolov, C. Carmeli and S. Richter (2007). "Photovoltaic activity of photosystem I-based self-assembled monolayer." Journal of the American Chemical Society **129**(41): 12352-+.

Carmeli, I., I. Lieberman, L. Kraversky, Z. Y. Fan, A. O. Govorov, G. Markovich and S. Richter (2010). "Broad Band Enhancement of Light Absorption in Photosystem I by Metal Nanoparticle Antennas." Nano Letters **10**(6): 2069-2074.

Caruana, D. J. and S. Howorka (2010). "Biosensors and biofuel cells with engineered proteins." Molecular Biosystems **6**(9): 1548-1556.

Chapman, H. N., P. Fromme, A. Barty, T. A. White, R. A. Kirian, A. Aquila, M. S. Hunter, J. Schulz, D. P. DePonte, U. Weierstall, R. B. Doak, F. R. N. C. Maia, A. V. Martin, I. Schlichting, L. Lomb, N. Coppola, R. L. Shoeman, S. W. Epp, R. Hartmann, D. Rolles, A. Rudenko, L. Foucar, N. Kimmel, G. Weidenspointner, P. Holl, M. N. Liang, M. Barthelmess, C. Caleman, S. Boutet, M. J. Bogan, J. Krzywinski, C. Bostedt, S. Bajt, L. Gumprecht, B. Rudek, B. Erk, C. Schmidt, A. Homke, C. Reich, D. Pietschner, L. Struder, G. Hauser, H. Gorke, J. Ullrich, S. Herrmann, G. Schaller, F. Schopper, H. Soltau, K. U. Kuhnel, M. Messerschmidt, J. D. Bozek, S. P. Hau-Riege, M. Frank, C. Y. Hampton, R. G. Sierra, D. Starodub, G. J. Williams, J. Hajdu, N. Timneanu, M. M. Seibert, J. Andreasson, A. Rocker, O. Jonsson, M. Svenda, S. Stern, K. Nass, R. Andritschke, C. D. Schroter, F. Krasniqi, M. Bott, K. E. Schmidt, X. Y. Wang, I. Grotjohann, J. M. Holton, T. R. M. Barends, R. Neutze, S. Marchesini, R. Fromme, S. Schorb, D. Rupp, M. Adolph, T. Gorkhover, I. Andersson, H. Hirsemann, G. Potdevin,

H. Graafsma, B. Nilsson and J. C. H. Spence (2011). "Femtosecond X-ray protein nanocrystallography." Nature **470**(7332): 73-U81.

Chen, J., S. L. Bender, J. M. Keough and B. A. Barry (2009). "Tryptophan as a probe of photosystem I electron transfer reactions: a UV resonance Raman study." J Phys Chem B **113**(33): 11367-11370.

Chen, P. H., H. L. Liu, Y. J. Chen, H. Cheng, W. L. Lin, C. H. Yeh and C. H. Chang (2012). "Enhancing CO2 bio-mitigation by genetic engineering of cyanobacteria." Energy & Environmental Science **5**(8): 8318-8327.

Chitnis, P. R. (2001). "PHOTOSYSTEM I: Function and Physiology." Annu Rev Plant Physiol Plant Mol Biol **52**: 593-626.

Chitnis, P. R., D. Purvis and N. Nelson (1991). "Molecular-Cloning and Targeted Mutagenesis of the Gene Psaf Encoding Subunit-Iii of Photosystem-I from the Cyanobacterium Synechocystis-Sp Pcc 6803." Journal of Biological Chemistry **266**(30): 20146-20151.

Chitnis, P. R., P. A. Reilly, M. C. Miedel and N. Nelson (1989). "Structure and targeted mutagenesis of the gene encoding 8-kDa subunit of photosystem I from the cyanobacterium Synechocystis sp. PCC 6803." J Biol Chem **264**(31): 18374-18380.

Chitnis, P. R., P. A. Reilly and N. Nelson (1989). "Insertional inactivation of the gene encoding subunit II of photosystem I from the cyanobacterium Synechocystis sp. PCC 6803." J Biol Chem **264**(31): 18381-18385.

Chitnis, P. R., Q. Xu, V. P. Chitnis and R. Nechushtai (1995). "Function and Organization of Photosystem-I Polypeptides." Photosynthesis Research **44**(1-2): 23-40.

Chitnis, V. P. and P. R. Chitnis (1993). "PsaL subunit is required for the formation of photosystem I trimers in the cyanobacterium Synechocystis sp. PCC 6803." FEBS Letters **336**(2): 330-334.

Chitnis, V. P., Q. Xu, L. Yu, J. H. Golbeck, H. Nakamoto, D. L. Xie and P. R. Chitnis (1993). "Targeted inactivation of the gene psaL encoding a subunit of photosystem I of the cyanobacterium Synechocystis sp. PCC 6803." Journal of Biological Chemistry **268**(16): 11678-11684.

Choquet, Y. and O. Vallon (2000). "Synthesis, assembly and degradation of thylakoid membrane proteins." Biochimie **82**(6-7): 615-634.

Ciesielski, P. N., D. E. Cliffel and G. K. Jennings (2011). "Kinetic Model of the Photocatalytic Effect of a Photosystem I Monolayer on a Planar Electrode Surface." Journal of Physical Chemistry A **115**(15): 3326-3334.

Ciesielski, P. N., C. J. Faulkner, M. T. Irwin, J. M. Gregory, N. H. Tolk, D. E. Cliffel and G. K. Jennings (2010). "Enhanced Photocurrent Production by Photosystem I Multilayer Assemblies." Advanced Functional Materials **20**(23): 4048-4054.

Ciesielski, P. N., F. M. Hijazi, A. M. Scott, C. J. Faulkner, L. Beard, K. Emmett, S. J. Rosenthal, D. Cliffel and G. K. Jennings (2010). "Photosystem I - Based biohybrid photoelectrochemical cells." Bioresource Technology **101**(9): 3047-3053.

Ciesielski, P. N., A. M. Scott, C. J. Faulkner, B. J. Berron, D. E. Cliffel and G. K. Jennings (2008). "Functionalized Nanoporous Gold Leaf Electrode Films for the Immobilization of Photosystem I." Acs Nano **2**(12): 2465-2472.

Ciobanu, M., H. A. Kincaid, V. Lo, A. D. Dukes, G. K. Jennings and D. E. Cliffel (2007). "Electrochemistry and photoelectrochemistry of photosystem I adsorbed on hydroxyl-terminated monolayers." Journal of Electroanalytical Chemistry **599**(1): 72-78.

Cramer, W. A. and A. Trebst (1991). "Membrane protein structure prediction: cytochrome b." Trends Biochem Sci **16**(6): 207.

Das, R., P. J. Kiley, M. Segal, J. Norville, A. A. Yu, L. Y. Wang, S. A. Trammell, L. E. Reddick, R. Kumar, F. Stellacci, N. Lebedev, J. Schnur, B. D. Bruce, S. G. Zhang and M. Baldo (2004). "Integration of photosynthetic protein molecular complexes in solid-state electronic devices." Nano Letters **4**(6): 1079-1083.

Dau, H., I. Zaharieva and M. Haumann (2012). "Recent developments in research on water oxidation by photosystem II." Curr Opin Chem Biol **16**(1-2): 3-10.

De la Cerda, B., A. Diaz-Quintana, J. A. Navarro, M. Hervas and M. A. De la Rosa (1999). "Site-directed mutagenesis of cytochrome c6 from Synechocystis sp. PCC 6803. The heme protein possesses a negatively charged area that may be isofunctional with the acidic patch of plastocyanin." J Biol Chem **274**(19): 13292-13297.

De la Rosa, M. A., J. A. Navarro, A. Diaz-Quintana, B. De la Cerda, F. P. Molina-Heredia, A. Balme, S. Murdoch Pdel, I. Diaz-Moreno, R. V. Duran and M. Hervas (2002). "An evolutionary analysis of the reaction mechanisms of photosystem I reduction by cytochrome c(6) and plastocyanin." Bioelectrochemistry **55**(1-2): 41-45.

Deisenhofer, J., O. Epp, K. Miki, R. Huber and H. Michel (1984). "X-Ray Structure-Analysis of a Membrane-Protein Complex - Electron-Density Map at 3a Resolution and a Model of the Chromophores of the Photosynthetic Reaction Center from Rhodopseudomonas-Viridis." Journal of Molecular Biology **180**(2): 385-398.

Deisenhofer, J., O. Epp, K. Miki, R. Huber and H. Michel (1985). "Structure of the Protein Subunits in the Photosynthetic Reaction Center of Rhodopseudomonas-Viridis at 3a Resolution." Nature **318**(6047): 618-624.

Depege, N., S. Bellafiore and J. D. Rochaix (2003). "Role of chloroplast protein kinase Stt7 in LHCII phosphorylation and state transition in Chlamydomonas." Science **299**(5612): 1572-1575.

Diaz, A., F. Navarro, M. Hervas, J. A. Navarro, S. Chavez, F. J. Florencio and M. A. De la Rosa (1994). "Cloning and correct expression in E. coli of the petJ gene encoding cytochrome c6 from Synechocystis 6803." FEBS Lett **347**(2-3): 173-177.

Drepper, F., M. Hippler, W. Nitschke and W. Haehnel (1996). "Binding dynamics and electron transfer between plastocyanin and photosystem I." Biochemistry **35**(4): 1282-1295.

Duran, R. V., M. Hervas, B. De la Cerda, M. A. De la Rosa and J. A. Navarro (2006). "A laser flash-induced kinetic analysis of in vivo photosystem I reduction by site-directed mutants of plastocyanin and cytochrome c(6) in Synechocystis sp PCC 6803." Biochemistry **45**(3): 1054-1060.

Efrati, A., O. Yehezkeli, R. Tel-Vered, D. Michaeli, R. Nechushtai and I. Willner (2012). "Electrochemical switching of photoelectrochemical processes at CdS QDs and photosystem I-modified electrodes." ACS Nano **6**(10): 9258-9266.

El-Mohsnawy, E., M. J. Kopczak, E. Schlodder, M. Nowaczyk, H. E. Meyer, B. Warscheid, N. V. Karapetyan and M. Rogner (2010). "Structure and function of intact photosystem 1 monomers from the cyanobacterium Thermosynechococcus elongatus." Biochemistry **49**(23): 4740-4751.

Ellis, R. J. and A. P. Minton (2006). "Protein aggregation in crowded environments." Biol Chem **387**(5): 485-497.

Evans, B. R., H. M. O'Neill, S. A. Hutchens, B. D. Bruce and E. Greenbaum (2004). "Enhanced photocatalytic hydrogen evolution by covalent attachment of plastocyanin to photosystem I." Nano Letters **4**(10): 1815-1819.

Falzone, C. J., Y. H. Kao, J. D. Zhao, K. L. Maclaughlin, D. A. Bryant and J. T. J. Lecomte (1994). "H-1 and N-15 Nmr Assignments of Psae, a Photosystem-I Subunit from the Cyanobacterium Synechococcus Sp Strain Pcc-7002." Biochemistry **33**(20): 6043-6051.

Farah, J., G. Frank, H. Zuber and J. D. Rochaix (1995). "Cloning and sequencing of a cDNA clone encoding the photosystem I PsaD subunit from Chlamydomonas reinhardtii." Plant Physiol **107**(4): 1485-1486.

Faulkner, C. J., S. Lees, P. N. Ciesielski, D. E. Cliffel and G. K. Jennings (2008). "Rapid assembly of photosystem I monolayers on gold electrodes." Langmuir **24**(16): 8409-8412.

Feissner, R. E., C. L. Richard-Fogal, E. R. Frawley, J. A. Loughman, K. W. Earley and R. G. Kranz (2006). "Recombinant cytochromes c biogenesis systems I and II and analysis of haem delivery pathways in Escherichia coli." Mol Microbiol **60**(3): 563-577.

Ferreira, K. N., T. M. Iverson, K. Maghlaoui, J. Barber and S. Iwata (2004). "Architecture of the photosynthetic oxygen-evolving center." Science **303**(5665): 1831-1838.

Ford, R. C. and A. Holzenburg (1988). "Investigation of the structure of trimeric and monomeric photosystem I reaction centre complexes." EMBO J **7**(8): 2287-2293.

Fotiadis, D., D. J. Muller, G. Tsiotis, L. Hasler, P. Tittmann, T. Mini, P. Jeno, H. Gross and A. Engel (1998). "Surface analysis of the photosystem I complex by electron and atomic force microscopy." J Mol Biol **283**(1): 83-94.

Frazao, C., C. M. Soares, M. A. Carrondo, E. Pohl, Z. Dauter, K. S. Wilson, M. Hervas, J. A. Navarro, M. A. De la Rosa and G. M. Sheldrick (1995). "Ab initio determination of the crystal structure of cytochrome c6 and comparison with plastocyanin." Structure **3**(11): 1159-1169.

Frolov, L., Y. Rosenwaks, C. Carmeli and I. Carmeli (2005). "Fabrication of a photoelectronic device by direct chemical binding of the photosynthetic reaction center protein to metal surfaces." Advanced Materials **17**(20): 2434-+.

Frolov, L., Y. Rosenwaks, S. Richter, C. Carmeli and I. Carmeli (2008). "Photoelectric junctions between GaAs and photosynthetic reaction center protein." Journal of Physical Chemistry C **112**(35): 13426-13430.

Frolov, L., O. Wilner, C. Carmeli and I. Carmeli (2008). "Fabrication of oriented multilayers of photosystem I proteins on solid surfaces by auto-metallization." Advanced Materials **20**(2): 263-+.

Fromme, P., P. Jordan and N. Krauss (2001). "Structure of photosystem I." Biochim Biophys Acta **1507**(1-3): 5-31.

Fromme, P., A. Melkozernov, P. Jordan and N. Krauss (2003). "Structure and function of photosystem I: interaction with its soluble electron carriers and external antenna systems." FEBS Lett **555**(1): 40-44.

Garczarek, L., G. W. M. van der Staay, J. C. Thomas and F. Partensky (1998). "Isolation and characterization of photosystem I from two strains of the marine oxychlorobacterium Prochlorococcus." Photosynthesis Research **56**(2): 131-141.

Gerster, D., J. Reichert, H. Bi, J. V. Barth, S. M. Kaniber, A. W. Holleitner, I. Visoly-Fisher, S. Sergani and I. Carmeli (2012). "Photocurrent of a single photosynthetic protein." Nature Nanotechnology **7**(10): 673-676.

Giera, W., K. Gibasiewicz, V. M. Ramesh, S. Lin and A. Webber (2009). "Electron transfer from A to A(1) in Photosystem I from Chlamydomonas reinhardtii occurs in both the A and B branch with 25-30-ps lifetime." Phys Chem Chem Phys **11**(25): 5186-5191.

Golbeck, J. H. (1999). "A comparative analysis of the spin state distribution of in vitro and in vivo mutants of PsaC - A biochemical argument for the sequence of electron transfer in Photosystem I as F-X -> F-A -> F-B -> ferredoxin/flavodoxin." Photosynthesis Research **61**(2): 107-144.

Goni, G., A. Serrano, S. Frago, M. Hervas, J. R. Peregrina, M. A. De la Rosa, C. Gomez-Moreno, J. A. Navarro and M. Medina (2008). "Flavodoxin-mediated electron transfer from photosystem I to ferredoxin-NADP+ reductase in Anabaena: role of flavodoxin hydrophobic residues in protein-protein interactions." Biochemistry **47**(4): 1207-1217.

Grieco, M., M. Tikkanen, V. Paakkarinen, S. Kangasjarvi and E. M. Aro (2012). "Steady-state phosphorylation of light-harvesting complex II proteins preserves photosystem I under fluctuating white light." Plant Physiol **160**(4): 1896-1910.

Groth, G. and K. Schirwitz (1999). "Rapid purification of membrane extrinsic F1-domain of chloroplast ATP synthase in monodisperse form suitable for 3D-crystallization." Eur J Biochem **260**(1): 15-21.

Gunther, D. (2013). "Pueraria lobata (Kudzu) Photosystem I Improves the Photoelectrochemical Performance of Silicon." Industrial Biotechnology **9**(1): 37-41.

Gunther, D., G. LeBlanc, D. Prasai, J. R. Zhang, D. E. Cliffel, K. I. Bolotin and G. K. Jennings (2013). "Photosystem I on graphene as a highly transparent, photoactive electrode." Langmuir **29**(13): 4177-4180.

Hagemann, G. E., N. Gad'on, A. Garcia, G. Drews and M. H. Tadros (1995). "The light-harvesting complex II (B800-850) of Rhodobacter sulfidophilus: characterization and formation under different growth conditions." FEMS Microbiol Lett **126**(1): 7-11.

Haldrup, A., H. Naver and H. V. Scheller (1999). "The interaction between plastocyanin and photosystem I is inefficient in transgenic Arabidopsis plants lacking the PSI-N subunit of photosystem I." Plant J **17**(6): 689-698.

Hankamer, B., J. Barber and E. J. Boekema (1997). "Structure and Membrane Organization of Photosystem Ii in Green Plants." Annu Rev Plant Physiol Plant Mol Biol **48**: 641-671.

Hankamer, B., J. Nield, D. Zheleva, E. Boekema, S. Jansson and J. Barber (1997). "Isolation and biochemical characterisation of monomeric and dimeric photosystem

II complexes from spinach and their relevance to the organisation of photosystem II in vivo." Eur J Biochem **243**(1-2): 422-429.

Hastings, G., S. Hoshina, A. N. Webber and R. E. Blankenship (1995). "Universality of energy and electron transfer processes in photosystem I." Biochemistry **34**(47): 15512-15522.

Hastings, G., L. J. Reed, S. Lin and R. E. Blankenship (1995). "Excited state dynamics in photosystem I: effects of detergent and excitation wavelength." Biophys J **69**(5): 2044-2055.

Hatanaka, H., K. Sonoike, M. Hirano and S. Katoh (1993). "Small subunits of Photosystem I reaction center complexes from Synechococcus elongatus. I. Is the psaF gene product required for oxidation of cytochrome c-553?" Biochim Biophys Acta **1141**(1): 45-51.

Hatanaka, H., R. Tanimura, S. Katoh and F. Inagaki (1997). "Solution structure of ferredoxin from the thermophilic cyanobacterium Synechococcus elongatus and its thermostability." Journal of Molecular Biology **268**(5): 922-933.

Hauska, G., T. Schoedl, H. Remigy and G. Tsiotis (2001). "The reaction center of green sulfur bacteria." Biochimica Et Biophysica Acta-Bioenergetics **1507**(1-3): 260-277.

Heidorn, T., D. Camsund, H. H. Huang, P. Lindberg, P. Oliveira, K. Stensjo and P. Lindblad (2011). "Synthetic Biology in Cyanobacteria: Engineering and Analyzing Novel Functions." Methods in Enzymology, Vol 497: Synthetic Biology, Methods for Part/Device Characterization and Chassis Engineering, Pt A **497**: 539-579.

Hervas, M., M. A. De la Rosa and G. Tollin (1992). "A comparative laser-flash absorption spectroscopy study of algal plastocyanin and cytochrome c552 photooxidation by photosystem I particles from spinach." Eur J Biochem **203**(1-2): 115-120.

Hervas, M., A. Diaz-Quintana, C. A. Kerfeld, D. W. Krogmann, M. A. De la Rosa and J. A. Navarro (2005). "Cyanobacterial Photosystem I lacks specificity in its interaction with cytochrome c(6) electron donors." Photosynth Res **83**(3): 329-333.

Hervas, M. and J. A. Navarro (2011). "Effect of crowding on the electron transfer process from plastocyanin and cytochrome c6 to photosystem I: a comparative study from cyanobacteria to green algae." Photosynth Res **107**(3): 279-286.

Hervas, M., J. A. Navarro and M. A. De La Rosa (2003). "Electron transfer between membrane complexes and soluble proteins in photosynthesis." Acc Chem Res **36**(10): 798-805.

Hervas, M., J. A. Navarro, A. Diaz, H. Bottin and M. A. De la Rosa (1995). "Laser-flash kinetic analysis of the fast electron transfer from plastocyanin and cytochrome c6 to

photosystem I. Experimental evidence on the evolution of the reaction mechanism." Biochemistry **34**(36): 11321-11326.

Hervas, M., J. M. Ortega, J. A. Navarro, M. A. Delarosa and H. Bottin (1994). "Laser Flash Kinetic-Analysis of Synechocystis Pcc-6803 Cytochrome C(6) and Plastocyanin Oxidation by Photosystem-I." Biochimica Et Biophysica Acta-Bioenergetics **1184**(2-3): 235-241.

Hippler, M., F. Drepper, J. Farah and J. D. Rochaix (1997). "Fast electron transfer from cytochrome c6 and plastocyanin to photosystem I of Chlamydomonas reinhardtii requires PsaF." Biochemistry **36**(21): 6343-6349.

Hippler, M., F. Drepper, W. Haehnel and J. D. Rochaix (1998). "The N-terminal domain of PsaF: precise recognition site for binding and fast electron transfer from cytochrome c6 and plastocyanin to photosystem I of Chlamydomonas reinhardtii." Proc Natl Acad Sci U S A **95**(13): 7339-7344.

Hippler, M., J. Reichert, M. Sutter, E. Zak, L. Altschmied, U. Schroer, R. G. Herrmann and W. Haehnel (1996). "The plastocyanin binding domain of photosystem I." EMBO J **15**(23): 6374-6384.

Hippler, M., A. Riedel, U. Schroer, W. Nitschke and W. Haehnel (1996). "Light-induced charge separation between plastocyanin and the iron-sulfur clusters FA and FB in the complex of plastocyanin and photosystem I." Arch Biochem Biophys **330**(2): 414-418.

Hiyama, T. and B. Ke (1972). "Difference spectra and extinction coefficients of P 700." Biochim Biophys Acta **267**(1): 160-171.

Holland, H. D. (2006). "The oxygenation of the atmosphere and oceans." Philos Trans R Soc Lond B Biol Sci **361**(1470): 903-915.

Hoover, D. M., C. L. Drennan, A. L. Metzger, C. Osborne, C. H. Weber, K. A. Pattridge and M. L. Ludwig (1999). "Comparisons of wild-type and mutant flavodoxins from Anacystis nidulans. Structural determinants of the redox potentials." Journal of Molecular Biology **294**(3): 725-743.

Ihalainen, J. A., P. E. Jensen, A. Haldrup, I. H. van Stokkum, R. van Grondelle, H. V. Scheller and J. P. Dekker (2002). "Pigment organization and energy transfer dynamics in isolated photosystem I (PSI) complexes from Arabidopsis thaliana depleted of the PSI-G, PSI-K, PSI-L, or PSI-N subunit." Biophys J **83**(4): 2190-2201.

Ihara, M., H. Nakamoto, T. Kamachi, I. Okura and M. Maeda (2006). "Photoinduced hydrogen production by direct electron transfer from photosystem I cross-linked with cytochrome c3 to [NiFe]-hydrogenase." Photochem Photobiol **82**(6): 1677-1685.

Iwuchukwu, I. J., E. Iwuchukwu, R. Le, C. Paquet, R. Sawhney, B. Bruce and P. Frymier (2011). "Optimization of photosynthetic hydrogen yield from platinized photosystem I complexes using response surface methodology." International Journal of Hydrogen Energy **36**(18): 11684-11692.

Iwuchukwu, I. J., M. Vaughn, N. Myers, H. O'Neill, P. Frymier and B. D. Bruce (2010). "Self-organized photosynthetic nanoparticle for cell-free hydrogen production." Nat Nanotechnol **5**(1): 73-79.

Iwuchukwu, I. J., M. Vaughn, N. Myers, H. O'Neill, P. Frymier and B. D. Bruce (2010). "Self-organized photosynthetic nanoparticle for cell-free hydrogen production." Nat Nano **5**(1): 73-79.

Iwuchukwu, I. J., M. Vaughn, N. Myers, H. O'Neill, P. Frymier and B. D. Bruce (2010). "Self-organized photosynthetic nanoparticle for cell-free hydrogen production." Nature Nanotechnology **5**(1): 73-79.

Izawa, S. (1980). "Acceptors and donors and chloroplast electron transport." Methods in Enzymology **69**: 413-434.

Jansson, S., B. Andersen and H. V. Scheller (1996). "Nearest-neighbor analysis of higher-plant photosystem I holocomplex." Plant Physiol **112**(1): 409-420.

Jensen, P. E., R. Bassi, E. J. Boekema, J. P. Dekker, S. Jansson, D. Leister, C. Robinson and H. V. Scheller (2007). "Structure, function and regulation of plant photosystem I." Biochim Biophys Acta **1767**(5): 335-352.

Jensen, P. E., M. Gilpin, J. Knoetzel and H. V. Scheller (2000). "The PSI-K subunit of photosystem I is involved in the interaction between light-harvesting complex I and the photosystem I reaction center core." J Biol Chem **275**(32): 24701-24708.

Jordan, P., P. Fromme, H. T. Witt, O. Klukas, W. Saenger and N. Krauss (2001). "Three-dimensional structure of cyanobacterial photosystem I at 2.5 A resolution." Nature **411**(6840): 909-917.

Jordan, P., P. Fromme, H. T. Witt, O. Klukas, W. Saenger and N. Krauss (2001). "Three-dimensional structure of cyanobacterial photosystem I at 2.5 angstrom resolution." Nature **411**(6840): 909-917.

Kaftan, D., V. Brumfeld, R. Nevo, A. Scherz and Z. Reich (2002). "From chloroplasts to photosystems: in situ scanning force microscopy on intact thylakoid membranes." EMBO J **21**(22): 6146-6153.

Kana, R., E. Kotabova, M. Lukes, S. Papacek, C. Matonoha, L. N. Liu, O. Prasil and C. W. Mullineaux (2014). "Phycobilisome Mobility and Its Role in the Regulation of Light Harvesting in Red Algae." Plant Physiol **165**(4): 1618-1631.

Kaniber, S. M., M. Brandstetter, F. C. Simmel, I. Carmeli and A. W. Holleitner (2010). "On-Chip Functionalization of Carbon Nanotubes with Photosystem I." Journal of the American Chemical Society **132**(9): 2872-+.

Karapetyan, N. V. (2004). "The dynamics of excitation energy in photosystem I of cyanobacteria: Transfer in the antenna, capture by the reaction site, and dissipation." Biofizika **49**(2): 212-226.

Karapetyan, N. V., A. R. Holzwarth and M. Rogner (1999). "The photosystem I trimer of cyanobacteria: molecular organization, excitation dynamics and physiological significance." Febs Letters **460**(3): 395-400.

Kawakami, K., Y. Umena, N. Kamiya and J. R. Shen (2011). "Structure of the catalytic, inorganic core of oxygen-evolving photosystem II at 1.9 A resolution." J Photochem Photobiol B **104**(1-2): 9-18.

Ke, B. (1973). "Primary Electron-Acceptor of Photosystem I." Biochimica Et Biophysica Acta **301**(1): 1-33.

Keren, N., R. Aurora and H. B. Pakrasi (2004). "Critical roles of bacterioferritins in iron storage and proliferation of cyanobacteria." Plant Physiol **135**(3): 1666-1673.

Kerfeld, C. A. and D. W. Krogmann (1998). "PHOTOSYNTHETIC CYTOCHROMES c IN CYANOBACTERIA, ALGAE, AND PLANTS." Annu Rev Plant Physiol Plant Mol Biol **49**: 397-425.

Kiley, P., X. Zhao, M. Vaughn, M. A. Baldo, B. D. Bruce and S. Zhang (2005). "Self-assembling peptide detergents stabilize isolated photosystem I on a dry surface for an extended time." PLoS Biol **3**(7): e230.

Kiley, P., X. J. Zhao, M. Vaughn, M. A. Baldo, B. D. Bruce and S. G. Zhang (2005). "Self-assembling peptide detergents stabilize isolated photosystem I on a dry surface for an extended time." Plos Biology **3**(7): 1180-1186.

Kincaid, H. A., T. Niedringhaus, M. Ciobanu, D. E. Cliffel and G. K. Jennings (2006). "Entrapment of photosystem I within self-assembled films." Langmuir **22**(19): 8114-8120.

Kirchhoff, H. (2008). "Molecular crowding and order in photosynthetic membranes." Trends Plant Sci **13**(5): 201-207.

Kirilovsky, D. L., A. G. Boussac, F. J. van Mieghem, J. M. Ducruet, P. R. Setif, J. J. Yu, W. F. Vermaas and A. W. Rutherford (1992). "Oxygen-evolving photosystem II preparation from wild type and photosystem II mutants of Synechocystis sp. PCC 6803." Biochemistry **31**(7): 2099-2107.

Ko, B. S., B. Babcock, G. K. Jennings, S. G. Tilden, R. R. Peterson, D. Cliffel and E. Greenbaum (2004). "Effect of surface composition on the adsorption of photosystem I onto alkanethiolate self-assembled monolayers on gold." Langmuir **20**(10): 4033-4038.

Kopnov, F., I. Cohen-Ofri and D. Noy (2011). "Electron Transport between Photosystem II and Photosystem I Encapsulated in Sol-Gel Glasses." Angewandte Chemie-International Edition **50**(51): 12347-12350.

Kruip, J., D. Bald, E. Boekema and M. Rögner (1994). "Evidence for the existence of trimeric and monomeric Photosystem I complexes in thylakoid membranes from cyanobacteria." Photosynthesis Research **40**(3): 279-286.

Kruip, J., E. J. Boekema, D. Bald, A. F. Boonstra and M. Rogner (1993). "Isolation and Structural Characterization of Monomeric and Trimeric Photosystem-I Complexes (P700-Center-Dot-Fa/Fb and P700-Center-Dot-Fx) from the Cyanobacterium Synechocystis Pcc-6803." Journal of Biological Chemistry **268**(31): 23353-23360.

Kruip, J., P. R. Chitnis, B. Lagoutte, M. Rogner and E. J. Boekema (1997). "Structural organization of the major subunits in cyanobacterial photosystem 1. Localization of subunits PsaC, -D, -E, -F, and -J." J Biol Chem **272**(27): 17061-17069.

Kubota, H., I. Sakurai, K. Katayama, N. Mizusawa, S. Ohashi, M. Kobayashi, P. P. Zhang, E. M. Aro and H. Wada (2010). "Purification and characterization of photosystem I complex from Synechocystis sp PCC 6803 by expressing histidine-tagged subunits." Biochimica Et Biophysica Acta-Bioenergetics **1797**(1): 98-105.

LeBlanc, G., G. Chen, E. A. Gizzie, G. K. Jennings and D. E. Cliffel (2012). "Enhanced Photocurrents of Photosystem I Films on p-Doped Silicon." Advanced Materials **24**(44): 5959-5962.

LeBlanc, G., G. Chen, G. K. Jennings and D. E. Cliffel (2012). "Photoreduction of Catalytic Platinum Particles Using Immobilized Multilayers of Photosystem I." Langmuir **28**(21): 7952-7956.

LeBlanc, G., G. P. Chen, E. A. Gizzie, G. K. Jennings and D. E. Cliffel (2012). "Enhanced Photocurrents of Photosystem I Films on p-Doped Silicon." Advanced Materials **24**(44): 5959-+.

Lee, I., J. W. Lee and E. Greenbaum (1997). "Biomolecular electronics: Vectorial arrays of photosynthetic reaction centers." Physical Review Letters **79**(17): 3294-3297.

Lelong, C., P. Setif, B. Lagoutte and H. Bottin (1994). "Identification of the amino acids involved in the functional interaction between photosystem I and ferredoxin from Synechocystis sp. PCC 6803 by chemical cross-linking." J Biol Chem **269**(13): 10034-10039.

Li, H. and J. C. Liao (2013). "Engineering a cyanobacterium as the catalyst for the photosynthetic conversion of CO2 to 1,2-propanediol." Microbial Cell Factories **12**.

Li, M., D. A. Semchonok, E. J. Boekema and B. D. Bruce (2014). "Characterization and evolution of tetrameric photosystem I from the thermophilic cyanobacterium Chroococcidiopsis sp TS-821." Plant Cell **26**(3): 1230-1245.

Li, N., J. D. Zhao, P. V. Warren, J. T. Warden, D. A. Bryant and J. H. Golbeck (1991). "PsaD is required for the stable binding of PsaC to the photosystem I core protein of Synechococcus sp. PCC 6301." Biochemistry **30**(31): 7863-7872.

Li, Y., A. van der Est, M. G. Lucas, V. M. Ramesh, F. Gu, A. Petrenko, S. Lin, A. N. Webber, F. Rappaport and K. Redding (2006). "Directing electron transfer within Photosystem I by breaking H-bonds in the cofactor branches." Proc Natl Acad Sci U S A **103**(7): 2144-2149.

Liebl, U., M. Mockensturmwilson, J. T. Trost, D. C. Brune, R. E. Blankenship and W. Vermaas (1993). "Single Core Polypeptide in the Reaction-Center of the Photosynthetic Bacterium Heliobacillus-Mobilis - Structural Implications and Relations to Other Photosystems." Proceedings of the National Academy of Sciences of the United States of America **90**(15): 7124-7128.

Lindberg, P., S. Park and A. Melis (2010). "Engineering a platform for photosynthetic isoprene production in cyanobacteria, using Synechocystis as the model organism." Metabolic Engineering **12**(1): 70-79.

Liu, W. S., J. S. Yuan and C. N. Stewart (2013). "Advanced genetic tools for plant biotechnology." Nature Reviews Genetics **14**(11): 781-793.

Lubner, C. E., R. Grimme, D. A. Bryant and J. H. Golbeck (2010). "Wiring Photosystem I for Direct Solar Hydrogen Production." Biochemistry **49**(3): 404-414.

Lubner, C. E., P. Knorzer, P. J. N. Silva, K. A. Vincent, T. Happe, D. A. Bryant and J. H. Golbeck (2010). "Wiring an [FeFe]-Hydrogenase with Photosystem I for Light-Induced Hydrogen Production." Biochemistry **49**(48): 10264-10266.

Lushy, A., L. Verchovsky and R. Nechushtai (2002). "The stable assembly of newly synthesized PsaE into the photosystem I complex occurring via the exchange mechanism is facilitated by electrostatic interactions." Biochemistry **41**(37): 11192-11199.

Lyons, T. W., C. T. Reinhard and N. J. Planavsky (2014). "The rise of oxygen in Earth's early ocean and atmosphere." Nature **506**(7488): 307-315.

Makita, H. and G. Hastings (2015). "Directionality of electron transfer in cyanobacterial photosystem I at 298 and 77K." FEBS Lett **589**(13): 1412-1417.

Mangels, D., J. Kruip, S. Berry, M. Rogner, E. J. Boekema and F. Koenig (2002). "Photosystem I from the unusual cyanobacterium Gloeobacter violaceus." Photosynthesis Research **72**(3): 307-319.

Mannan, R. M., W. Z. He, S. U. Metzger, J. Whitmarsh, R. Malkin and H. B. Pakrasi (1996). "Active photosynthesis in cyanobacterial mutants with directed modifications in the ligands for two iron-sulfur clusters in the PsaC protein of photosystem I." Embo Journal **15**(8): 1826-1833.

Manocchi, A. K., D. R. Baker, S. S. Pendley, K. Nguyen, M. M. Hurley, B. D. Bruce, J. J. Sumner and C. A. Lundgren (2013). "Photocurrent generation from surface assembled photosystem I on alkanethiol modified electrodes." Langmuir **29**(7): 2412-2419.

Manocchi, A. K., D. R. Baker, J. J. Sumner, S. S. Pendley, M. M. Hurley, K. Xu, B. D. Bruce and C. A. Lundgren (2012). "Surface-assembled Photosystem I as a biomolecular reactor toward solar energy conversion." Abstracts of Papers of the American Chemical Society **244**.

Marton, I., A. Zuker, E. Shklarman, V. Zeevi, A. Tovkach, S. Roffe, M. Ovadis, T. Tzfira and A. Vainstein (2010). "Nontransgenic Genome Modification in Plant Cells." Plant Physiology **154**(3): 1079-1087.

Masukawa, H., M. Kitashima, K. Inoue, H. Sakurai and R. P. Hausinger (2012). "Genetic Engineering of Cyanobacteria to Enhance Biohydrogen Production from Sunlight and Water." Ambio **41**: 169-173.

Matsumoto, K., M. Vaughn, B. D. Bruce, S. Koutsopoulos and S. G. Zhang (2009). "Designer Peptide Surfactants Stabilize Functional Photosystem-I Membrane Complex in Aqueous Solution for Extended Time." Journal of Physical Chemistry B **113**(1): 75-83.

Matsumoto, K., S. Zhang and S. Koutsopoulos (2010). "Enhanced electron transfer activity of photosystem I by polycations in aqueous solution." Biomacromolecules **11**(11): 3152-3157.

Mazor, Y., I. Greenberg, H. Toporik, O. Beja and N. Nelson (2012). "The evolution of photosystem I in light of phage-encoded reaction centres." Philosophical Transactions of the Royal Society B-Biological Sciences **367**(1608): 3400-3405.

McConnell, M. D., J. Sun, R. Siavashi, A. Webber, K. E. Redding, J. H. Golbeck and A. van der Est (2015). "Species-dependent alteration of electron transfer in the early stages of charge stabilization in Photosystem I." Biochim Biophys Acta **1847**(4-5): 429-440.

Medina, M. (2009). "Structural and mechanistic aspects of flavoproteins: photosynthetic electron transfer from photosystem I to NADP(+)." Febs Journal **276**(15): 3942-3958.

Medina, M., A. Diaz, M. Hervas, J. A. Navarro, C. Gomez-Moreno, M. A. de la Rosa and G. Tollin (1993). "A comparative laser-flash absorption spectroscopy study of Anabaena PCC 7119 plastocyanin and cytochrome c6 photooxidation by photosystem I particles." Eur J Biochem **213**(3): 1133-1138.

Mershin, A., K. Matsumoto, L. Kaiser, D. Yu, M. Vaughn, M. K. Nazeeruddin, B. D. Bruce, M. Graetzel and S. Zhang (2012). "Self-assembled photosystem-I biophotovoltaics on nanostructured TiO(2)and ZnO." Sci Rep **2**: 234.

Mershin, A., K. Matsumoto, L. Kaiser, D. Y. Yu, M. Vaughn, M. K. Nazeeruddin, B. D. Bruce, M. Graetzel and S. G. Zhang (2012). "Self-assembled photosystem-I biophotovoltaics on nanostructured TiO2 and ZnO." Scientific Reports **2**.

Millsaps, J. F., B. D. Bruce, J. W. Lee and E. Greenbaum (2001). "Nanoscale photosynthesis: Photocatalytic production of hydrogen by platinized photosystem I reaction centers." Photochemistry and Photobiology **73**(6): 630-635.

Minagawa, J. (2011). "State transitions--the molecular remodeling of photosynthetic supercomplexes that controls energy flow in the chloroplast." Biochim Biophys Acta **1807**(8): 897-905.

Minai, L., Y. Cohen, P. R. Chitnis and R. Nechushtai (1996). "The precursor of PsaD assembles into the photosystem I complex in two steps." Proc Natl Acad Sci U S A **93**(13): 6338-6342.

Minai, L., A. Fish, M. Darash-Yahana, L. Verchovsky and R. Nechushtai (2001). "The assembly of the PsaD subunit into the membranal photosystem I complex occurs via an exchange mechanism." Biochemistry **40**(43): 12754-12760.

Miyachi, M., Y. Yamanoi, Y. Shibata, H. Matsumoto, K. Nakazato, M. Konno, K. Ito, Y. Inoue and H. Nishihara (2010). "A photosensing system composed of photosystem I, molecular wire, gold nanoparticle, and double surfactants in water." Chem Commun (Camb) **46**(15): 2557-2559.

Miyachi, M., Y. Yamanoi, T. Yonezawa, H. Nishihara, M. Iwai, M. Konno, M. Iwai and Y. Inoue (2009). "Surface immobilization of PSI using vitamin K1-like molecular wires for fabrication of a bio-photoelectrode." J Nanosci Nanotechnol **9**(3): 1722-1726.

Moal, G. and B. Lagoutte (2012). "Photo-induced electron transfer from photosystem I to NADP(+): characterization and tentative simulation of the in vivo environment." Biochim Biophys Acta **1817**(9): 1635-1645.

Molina-Heredia, F. P., A. Balme, M. Hervas, J. A. Navarro and M. A. De la Rosa (2002). "A comparative structural and functional analysis of cytochrome cM cytochrome c6 and plastocyanin from the cyanobacterium Synechocystis sp. PCC 6803." FEBS Lett **517**(1-3): 50-54.

Molina-Heredia, F. P., A. Diaz-Quintana, M. Hervas, J. A. Navarro and M. A. De La Rosa (1999). "Site-directed mutagenesis of cytochrome c(6) from Anabaena species PCC 7119. Identification of surface residues of the hemeprotein involved in photosystem I reduction." J Biol Chem **274**(47): 33565-33570.

Molina-Heredia, F. P., J. Wastl, J. A. Navarro, D. S. Bendall, M. Hervas, C. J. Howe and M. A. De La Rosa (2003). "Photosynthesis: a new function for an old cytochrome?" Nature **424**(6944): 33-34.

Morris, E. P., B. Hankamer, D. Zheleva, G. Friso and J. Barber (1997). "The three-dimensional structure of a photosystem II core complex determined by electron crystallography." Structure **5**(6): 837-849.

Muh, F., C. Glockner, J. Hellmich and A. Zouni (2012). "Light-induced quinone reduction in photosystem II." Biochim Biophys Acta **1817**(1): 44-65.

Muhlenhoff, U. and F. Chauvat (1996). "Gene transfer and manipulation in the thermophilic cyanobacterium Synechococcus elongatus." Molecular & General Genetics **252**(1-2): 93-100.

Mukherjee, D., M. May, M. Vaughn, B. D. Bruce and B. Khomami (2010). "Controlling the Morphology of Photosystem I Assembly on Thiol-Activated Au Substrates." Langmuir **26**(20): 16048-16054.

Mukherjee, D., M. Vaughn, B. Khomami and B. D. Bruce (2011). "Modulation of cyanobacterial photosystem I deposition properties on alkanethiolate Au substrate by various experimental conditions." Colloids and Surfaces B: Biointerfaces **88**(1): 181-190.

Mukherjee, D., M. Vaughn, B. Khomami and B. D. Bruce (2011). "Modulation of cyanobacterial photosystem I deposition properties on alkanethiolate Au substrate by various experimental conditions." Colloids and Surfaces B-Biointerfaces **88**(1): 181-190.

Mula, S., A. Savitsky, K. Mobius, W. Lubitz, J. H. Golbeck, M. D. Mamedov, A. Y. Semenov and A. van der Est (2012). "Incorporation of a high potential quinone reveals that electron transfer in Photosystem I becomes highly asymmetric at low temperature." Photochem Photobiol Sci **11**(6): 946-956.

Muller, M. G., C. Slavov, R. Luthra, K. E. Redding and A. R. Holzwarth (2010). "Independent initiation of primary electron transfer in the two branches of the photosystem I reaction center." Proc Natl Acad Sci U S A **107**(9): 4123-4128.

Mullineaux, C. W. (2014). "Electron transport and light-harvesting switches in cyanobacteria." Front Plant Sci **5**: 7.

Mullineaux, C. W. and J. F. Allen (1990). "State 1-State 2 transitions in the cyanobacterium Synechococcus 6301 are controlled by the redox state of electron carriers between Photosystems I and II." Photosynth Res **23**(3): 297-311.

Mustardy, L., K. Buttle, G. Steinbach and G. Garab (2008). "The three-dimensional network of the thylakoid membranes in plants: quasihelical model of the granum-stroma assembly." Plant Cell **20**(10): 2552-2557.

Naithani, S., J. M. Hou and P. R. Chitnis (2000). "Targeted inactivation of the psaK1, psaK2 and psaM genes encoding subunits of Photosystem I in the cyanobacterium Synechocystis sp PCC 6803." Photosynthesis Research **63**(3): 225-236.

Nakamoto, H. (1995). "Targeted inactivation of the gene psaI encoding a subunit of photosystem I of the cyanobacterium Synechocystis sp PCC 6803." Plant and Cell Physiology **36**(8): 1579-1587.

Nakamura, A., T. Suzawa, Y. Kato and T. Watanabe (2011). "Species Dependence of the Redox Potential of the Primary Electron Donor P700 in Photosystem I of Oxygenic Photosynthetic Organisms Revealed by Spectroelectrochemistry." Plant and Cell Physiology **52**(5): 815-823.

Nakamura, A., T. Suzawa, Y. Kato and T. Watanabe (2011). "Species dependence of the redox potential of the primary electron donor p700 in photosystem I of oxygenic photosynthetic organisms revealed by spectroelectrochemistry." Plant Cell Physiol **52**(5): 815-823.

Nakamura, Y., T. Kaneko, S. Sato, M. Ikeuchi, H. Katoh, S. Sasamoto, A. Watanabe, M. Iriguchi, K. Kawashima, T. Kimura, Y. Kishida, C. Kiyokawa, M. Kohara, M. Matsumoto, A. Matsuno, N. Nakazaki, S. Shimpo, M. Sugimoto, C. Takeuchi, M. Yamada and S. Tabata (2002). "Complete genome structure of the thermophilic cyanobacterium Thermosynechococcus elongatus BP-1." DNA Res **9**(4): 123-130.

Naver, H., A. Haldrup and H. V. Scheller (1999). "Cosuppression of photosystem I subunit PSI-H in Arabidopsis thaliana. Efficient electron transfer and stability of photosystem I is dependent upon the PSI-H subunit." J Biol Chem **274**(16): 10784-10789.

Naver, H., M. P. Scott, J. H. Golbeck, B. L. Moller and H. V. Scheller (1996). "Reconstitution of barley photosystem I with modified PSI-C allows identification of domains interacting with PSI-D and PSI-A/B." J Biol Chem **271**(15): 8996-9001.

Nelson, N. (2009). "Plant Photosystem I - The Most Efficient Nano-Photochemical Machine." Journal of Nanoscience and Nanotechnology **9**(3): 1709-1713.

Nelson, N. (2011). "Photosystems and global effects of oxygenic photosynthesis." Biochimica Et Biophysica Acta-Bioenergetics **1807**(8): 856-863.

Nelson, N. (2013). "Evolution of photosystem I and the control of global enthalpy in an oxidizing world." Photosynthesis Research **116**(2-3): 145-151.

Nelson, N. and A. Ben-Shem (2005). "The structure of photosystem I and evolution of photosynthesis." Bioessays **27**(9): 914-922.

Nelson, N. and C. F. Yocum (2006). "Structure and function of photosystems I and II." Annu Rev Plant Biol **57**: 521-565.

Newman, B. J. and J. C. Gray (1988). "Characterisation of a full-length cDNA clone for pea ferredoxin-NADP(+) reductase." Plant Mol Biol **10**(6): 511-520.

Nguyen, K. and B. D. Bruce (2014). "Growing green electricity: progress and strategies for use of photosystem I for sustainable photovoltaic energy conversion." Biochim Biophys Acta **1837**(9): 1553-1566.

Nikandrov, V. V., Y. V. Borisova, E. A. Bocharov, M. A. Usachev, G. V. Nizova, V. A. Nadtochenko, E. P. Lukashev, B. V. Trubitsin, A. N. Tikhonov, V. N. Kurashov, M. D. Mamedov and A. Y. Semenov (2012). "Photochemical properties of photosystem 1 immobilized in a mesoporous semiconductor matrix." High Energy Chemistry **46**(3): 200-205.

Nugent, J. H. A. (1996). "Oxygenic photosynthesis - Electron transfer in photosystem I and photosystem II." European Journal of Biochemistry **237**(3): 519-531.

Nusbaumer, H., S. M. Zakeeruddin, J. E. Moser and M. Gratzel (2003). "An alternative efficient redox couple for the dye-sensitized solar cell system." Chemistry-a European Journal **9**(16): 3756-3763.

O'neill, H. and E. Greenbaum (2005). "Spectroscopy and photochemistry of spinach Photosystem I entrapped and stabilized in a hybrid organosilicate glass." Chemistry of Materials **17**(10): 2654-2661.

Olive, J., F. A. Wollman, P. Bennoun and M. Recouvreur (1981). "Ultrastructure of thylakoid membranes in C. reinhardtii: evidence for variations in the partition coefficient of the light-harvesting complex-containing particles upon membrane fracture." Arch Biochem Biophys **208**(2): 456-467.

Oliver, J. W. K., I. M. P. Machado, H. Yoneda and S. Atsumi (2013). "Cyanobacterial conversion of carbon dioxide to 2,3-butanediol." Proceedings of the National Academy of Sciences of the United States of America **110**(4): 1249-1254.

Ort, D. R. and S. Izawa (1974). "Studies on the Energy-coupling Sites of Photophosphorylation: V. Phosphorylation Efficiencies (P/e(2)) Associated with Aerobic Photooxidation of Artificial Electron Donors." Plant Physiol **53**(3): 370-376.

Ortiz-Marquez, J. C. F., M. Do Nascimento, J. P. Zehr and L. Curatti (2013). "Genetic engineering of multispecies microbial cell factories as an alternative for bioenergy production." Trends in Biotechnology **31**(9): 521-529.

Pakrasi, H. B. (1995). "Genetic analysis of the form and function of photosystem I and photosystem II." Annual Review of Genetics **29**: 755-776.

Parmar, A., N. K. Singh, A. Pandey, E. Gnansounou and D. Madamwar (2011). "Cyanobacteria and microalgae: A positive prospect for biofuels." Bioresource Technology **102**(22): 10163-10172.

Patel, K., M. Bigler, J. Hill, B. Morgan, B. D. Bruce and N. Phambu (2013). "Raman investigation of the interaction of photosystem I with highly ordered pyrolytic graphite." Abstracts of Papers of the American Chemical Society **245**.

Pendley, S. S., M. M. Hurley, A. Mannochi, D. Baker, J. J. Sumner, C. Lundgren and B. D. Bruce (2012). "Re-engineering Photosystem I as a photocatalytic hydrogen producing reactor." Abstracts of Papers of the American Chemical Society **243**.

Perez Navarro, M., W. M. Ames, H. Nilsson, T. Lohmiller, D. A. Pantazis, L. Rapatskiy, M. M. Nowaczyk, F. Neese, A. Boussac, J. Messinger, W. Lubitz and N. Cox (2013). "Ammonia binding to the oxygen-evolving complex of photosystem II identifies the solvent-exchangeable oxygen bridge (mu-oxo) of the manganese tetramer." Proc Natl Acad Sci U S A **110**(39): 15561-15566.

Pesaresi, P., M. Pribil, T. Wunder and D. Leister (2011). "Dynamics of reversible protein phosphorylation in thylakoids of flowering plants: the roles of STN7, STN8 and TAP38." Biochim Biophys Acta **1807**(8): 887-896.

Polm, M. and K. Brettel (1998). "Secondary pair charge recombination in photosystem I under strongly reducing conditions: temperature dependence and suggested mechanism." Biophys J **74**(6): 3173-3181.

Proux-Delrouyre, V., C. Demaille, W. Leibl, P. Setif, H. Bottin and C. Bourdillon (2003). "Electrocatalytic investigation of light-induced electron transfer between cytochrome c6 and photosystem I." J Am Chem Soc **125**(45): 13686-13692.

Pulz, O. and W. Gross (2004). "Valuable products from biotechnology of microalgae." Applied Microbiology and Biotechnology **65**(6): 635-648.

Radakovits, R., R. E. Jinkerson, A. Darzins and M. C. Posewitz (2010). "Genetic Engineering of Algae for Enhanced Biofuel Production." Eukaryotic Cell **9**(4): 486-501.

Renaud, N., D. Powell, M. Zarea, B. Movaghar, M. R. Wasielewski and M. A. Ratner (2013). "Quantum interferences and electron transfer in photosystem I." J Phys Chem A **117**(29): 5899-5908.

Rochaix, J. D. (2011). "Regulation of photosynthetic electron transport." Biochim Biophys Acta **1807**(3): 375-383.

Rochaix, J. D. (2014). "Regulation and dynamics of the light-harvesting system." Annu Rev Plant Biol **65**: 287-309.

Rousseau, F., P. Setif and B. Lagoutte (1993). "Evidence for the involvement of PSI-E subunit in the reduction of ferredoxin by photosystem I." EMBO J **12**(5): 1755-1765.

Rousseau, F., P. Setif and B. Lagoutte (1993). "Evidence for the Involvement of Psi-E Subunit in the Reduction of Ferredoxin by Photosystem-I." Embo Journal **12**(5): 1755-1765.

Rutherford, A. W. and M. C. W. Evans (1980). "Direct Measurement of the Redox Potential of the Primary and Secondary Quinone Electron-Acceptors in Rhodopseudomonas-Sphaeroides (Wild-Type) by Electron-Paramagnetic-Res Spectrometry." Febs Letters **110**(2): 257-261.

Saenger, W., P. Jordan and N. Krauss (2002). "The assembly of protein subunits and cofactors in photosystem I." Curr Opin Struct Biol **12**(2): 244-254.

Santabarbara, S., B. Bullock, F. Rappaport and K. E. Redding (2015). "Controlling electron transfer between the two cofactor chains of photosystem I by the redox state of one of their components." Biophys J **108**(6): 1537-1547.

Santabarbara, S., M. Chen, A. W. Larkum and M. C. Evans (2007). "An electron paramagnetic resonance investigation of the electron transfer reactions in the chlorophyll d containing photosystem I of Acaryochloris marina." FEBS Lett **581**(8): 1567-1571.

Santabarbara, S., L. Galuppini and A. P. Casazza (2010). "Bidirectional electron transfer in the reaction centre of photosystem I." J Integr Plant Biol **52**(8): 735-749.

Santabarbara, S., P. Heathcote and M. C. Evans (2005). "Modelling of the electron transfer reactions in Photosystem I by electron tunnelling theory: the phylloquinones bound to the PsaA and the PsaB reaction centre subunits of PS I are almost isoenergetic to the iron-sulfur cluster F(X)." Biochim Biophys Acta **1708**(3): 283-310.

Santabarbara, S., P. Heathcote and M. C. W. Evans (2005). "Modelling of the electron transfer reactions in Photosystem I by electron tunnelling theory: The phylloquinones bound to the PsaA and the PsaB reaction centre subunits of PSI are

almost isoenergetic to the iron-sulfur cluster Fx." Biochimica Et Biophysica Acta-Bioenergetics **1708**(3): 283-310.

Santabarbara, S., A. Jasaitis, M. Byrdin, F. Gu, F. Rappaport and K. Redding (2008). "Additive effect of mutations affecting the rate of phylloquinone reoxidation and directionality of electron transfer within photosystem I." Photochem Photobiol **84**(6): 1381-1387.

Santabarbara, S., I. Kuprov, P. J. Hore, A. Casal, P. Heathcote and M. C. Evans (2006). "Analysis of the spin-polarized electron spin echo of the [P700+ A1-] radical pair of photosystem I indicates that both reaction center subunits are competent in electron transfer in cyanobacteria, green algae, and higher plants." Biochemistry **45**(23): 7389-7403.

Santabarbara, S., I. Kuprov, O. Poluektov, A. Casal, C. A. Russell, S. Purton and M. C. Evans (2010). "Directionality of electron-transfer reactions in photosystem I of prokaryotes: universality of the bidirectional electron-transfer model." J Phys Chem B **114**(46): 15158-15171.

Santabarbara, S., K. Reifschneider, A. Jasaitis, F. Gu, G. Agostini, D. Carbonera, F. Rappaport and K. E. Redding (2010). "Interquinone electron transfer in photosystem I as evidenced by altering the hydrogen bond strength to the phylloquinone(s)." J Phys Chem B **114**(28): 9300-9312.

Sauer, K., P. Mathis, S. Acker and J. A. van Best (1978). "Electron acceptors associated with P-700 in Triton solubilized photosystem I particles from spinach chloroplasts." Biochim Biophys Acta **503**(1): 120-134.

Sauer, K., P. Mathis, S. Acker and J. A. van Best (1979). "Absorption changes of P-700 reversible in milliseconds at low temperature in Triton-solubilized photosystem I particles." Biochim Biophys Acta **545**(3): 466-472.

Schenderlein, M., M. Cetin, J. Barber, A. Telfer and E. Schlodder (2008). "Spectroscopic studies of the chlorophyll d containing photosystem I from the cyanobacterium, Acaryochloris marina." Biochim Biophys Acta **1777**(11): 1400-1408.

Schlarb-Ridley, B. G., D. S. Bendall and C. J. Howe (2002). "Role of electrostatics in the interaction between cytochrome f and plastocyanin of the cyanobacterium Phormidium laminosum." Biochemistry **41**(10): 3279-3285.

Schlodder, E., M. Hussels, M. Cetin, N. V. Karapetyan and M. Brecht (2011). "Fluorescence of the various red antenna states in photosystem I complexes from cyanobacteria is affected differently by the redox state of P700." Biochim Biophys Acta **1807**(11): 1423-1431.

Schluchter, W. M., G. H. Shen, J. D. Zhao and D. A. Bryant (1996). "Characterization of psaI and psaL mutants of Synechococcus sp strain PCC 7002: A new model for state transitions in cyanobacteria." Photochemistry and Photobiology **64**(1): 53-66.

Semenov, A. Y., S. K. Chamorovsky and M. D. Mamedov (2004). "Electrogenic reactions in photosystem I complexes." Biofizika **49**(2): 227-238.

Semenov, A. Y., A. A. Petrova, M. D. Mamedov and V. A. Nadtochenko (2015). "Electron transfer in photosystem I containing native and modified quinone acceptors." Biochemistry (Mosc) **80**(6): 654-661.

Semenov, A. Y., I. V. Shelaev, F. E. Gostev, M. D. Mamedov, V. A. Shuvalov, O. M. Sarkisov and V. A. Nadtochenko (2012). "Primary steps of electron and energy transfer in photosystem I: effect of excitation pulse wavelength." Biochemistry (Mosc) **77**(9): 1011-1020.

Setif, P. (2001). "Ferredoxin and flavodoxin reduction by photosystem I." Biochimica Et Biophysica Acta-Bioenergetics **1507**(1-3): 161-179.

Setif, P., N. Fischer, B. Lagoutte, H. Bottin and J. D. Rochaix (2002). "The ferredoxin docking site of photosystem I." Biochimica Et Biophysica Acta-Bioenergetics **1555**(1-3): 204-209.

Shen, G., M. L. Antonkine, A. van der Est, I. R. Vassiliev, K. Brettel, R. Bittl, S. G. Zech, J. Zhao, D. Stehlik, D. A. Bryant and J. H. Golbeck (2002). "Assembly of photosystem I. II. Rubredoxin is required for the in vivo assembly of F(X) in Synechococcus sp. PCC 7002 as shown by optical and EPR spectroscopy." J Biol Chem **277**(23): 20355-20366.

Shen, G., J. Zhao, S. K. Reimer, M. L. Antonkine, Q. Cai, S. M. Weiland, J. H. Golbeck and D. A. Bryant (2002). "Assembly of photosystem I. I. Inactivation of the rubA gene encoding a membrane-associated rubredoxin in the cyanobacterium Synechococcus sp. PCC 7002 causes a loss of photosystem I activity." J Biol Chem **277**(23): 20343-20354.

Shinkarev, V. P., B. Zybailov, I. R. Vassiliev and J. H. Golbeck (2002). "Modeling of the P700+ charge recombination kinetics with phylloquinone and plastoquinone-9 in the A1 site of photosystem I." Biophys J **83**(6): 2885-2897.

Singh, S., B. N. Kate and U. C. Banerjee (2005). "Bioactive compounds from cyanobacteria and microalgae: An overview." Critical Reviews in Biotechnology **25**(3): 73-95.

Small, E. W. and S. R. Anderson (1988). "Fluorescence anisotropy decay demonstrates calcium-dependent shape changes in photo-cross-linked calmodulin." Biochemistry **27**(1): 419-428.

Sommer, F., F. Drepper, W. Haehnel and M. Hippler (2006). "Identification of precise electrostatic recognition sites between cytochrome c6 and the photosystem I subunit PsaF using mass spectrometry." J Biol Chem **281**(46): 35097-35103.

Sommer, F., F. Drepper and M. Hippler (2002). "The luminal helix l of PsaB is essential for recognition of plastocyanin or cytochrome c6 and fast electron transfer to photosystem I in Chlamydomonas reinhardtii." J Biol Chem **277**(8): 6573-6581.

Sommer, F., F. Drepper and M. Hippler (2002). "The luminal helix l of PsaB is essential for recognition of plastocyanin or cytochrome c(6) and fast electron transfer to photosystem I in Chlamydomonas reinhardtii." Journal of Biological Chemistry **277**(8): 6573-6581.

Sonoike, K., H. Hatanaka and S. Katoh (1993). "Small subunits of Photosystem I reaction center complexes from Synechococcus elongatus. II. The psaE gene product has a role to promote interaction between the terminal electron acceptor and ferredoxin." Biochim Biophys Acta **1141**(1): 52-57.

Srirangan, K., M. E. Pyne and C. P. Chou (2011). "Biochemical and genetic engineering strategies to enhance hydrogen production in photosynthetic algae and cyanobacteria." Bioresource Technology **102**(18): 8589-8604.

Szczepaniak, A., D. Huang, T. W. Keenan and W. A. Cramer (1991). "Electrostatic destabilization of the cytochrome b6f complex in the thylakoid membrane." EMBO J **10**(10): 2757-2764.

Takabe, T., H. Ishikawa, S. Niwa and S. Itoh (1983). "Electron transfer between plastocyanin and P700 in highly-purified photosystem I reaction center complex. Effects of pH, cations, and subunit peptide composition." J Biochem **94**(6): 1901-1911.

Takahashi, Y., M. Goldschmidt-Clermont, S. Y. Soen, L. G. Franzen and J. D. Rochaix (1991). "Directed chloroplast transformation in Chlamydomonas reinhardtii: insertional inactivation of the psaC gene encoding the iron sulfur protein destabilizes photosystem I." EMBO J **10**(8): 2033-2040.

Takahashi, Y., M. Goldschmidtclermont, S. Y. Soen, L. G. Franzen and J. D. Rochaix (1991). "Directed Chloroplast Transformation in Chlamydomonas-Reinhardtii - Insertional Inactivation of the Psac Gene Encoding the Iron Sulfur Protein Destabilizes Photosystem-I." Embo Journal **10**(8): 2033-2040.

Terasaki, N., N. Yamamoto, M. Hattori, N. Tanigaki, T. Hiraga, K. Ito, M. Konno, M. Iwai, Y. Inoue, S. Uno and K. Nakazato (2009). "Photosensor based on an FET utilizing a biocomponent of photosystem I for use in imaging devices." Langmuir **25**(19): 11969-11974.

Terasaki, N., N. Yamamoto, T. Hiraga, I. Sato, Y. Inoue and S. Yamada (2006). "Fabrication of novel photosystem I-gold nanoparticle hybrids and their photocurrent enhancement." Thin Solid Films **499**(1-2): 153-156.

Terasaki, N., N. Yamamoto, T. Hiraga, Y. Yamanoi, T. Yonezawa, H. Nishihara, T. Ohmori, M. Sakai, M. Fujii, A. Tohri, M. Iwai, Y. Inoue, S. Yoneyama, M. Minakata and I. Enami (2009). "Plugging a Molecular Wire into Photosystem I: Reconstitution of the Photoelectric Conversion System on a Gold Electrode." Angewandte Chemie-International Edition **48**(9): 1585-1587.

Terasaki, N., N. Yamamoto, K. Tamada, M. Hattori, T. Hiraga, A. Tohri, I. Sato, M. Iwai, M. Iwai, S. Taguchi, I. Enami, Y. Inoue, Y. Yamanoi, T. Yonezawa, K. Mizuno, M. Murata, H. Nishihara, S. Yoneyama, M. Minakata, T. Ohmori, M. Sakai and M. Fujii (2007). "Bio-photo sensor: Cyanobacterial photosystem I coupled with transistor via molecular wire." Biochimica Et Biophysica Acta-Bioenergetics **1767**(6): 653-659.

Tiwari, A. and A. Pandey (2012). "Cyanobacterial hydrogen production - A step towards clean environment." International Journal of Hydrogen Energy **37**(1): 139-150.

Tomo, T., Y. Kato, T. Suzuki, S. Akimoto, T. Okubo, T. Noguchi, K. Hasegawa, T. Tsuchiya, K. Tanaka, M. Fukuya, N. Dohmae, T. Watanabe and M. Mimuro (2008). "Characterization of highly purified photosystem I complexes from the chlorophyll d-dominated cyanobacterium Acaryochloris marina MBIC 11017." J Biol Chem **283**(26): 18198-18209.

Toporik, H., I. Carmeli, I. Volotsenko, M. Molotskii, Y. Rosenwaks, C. Carmeli and N. Nelson (2012). "Large Photovoltages Generated by Plant Photosystem I Crystals." Advanced Materials **24**(22): 2988-2991.

Tsinoremas, N. F., A. K. Kutach, C. A. Strayer and S. S. Golden (1994). "Efficient Gene-Transfer in Synechococcus Sp Strains Pcc-7942 and Pcc-6301 by Interspecies Conjugation and Chromosomal Recombination." Journal of Bacteriology **176**(21): 6764-6768.

Tsiotis, G., W. Haase, A. Engel and H. Michel (1995). "Isolation and Structural Characterization of Trimeric Cyanobacterial Photosystem-I Complex with the Help of Recombinant Antibody Fragments." European Journal of Biochemistry **231**(3): 823-830.

Tucker, D. L. and L. A. Sherman (2000). "Analysis of chlorophyll–protein complexes from the cyanobacterium Cyanothece sp. ATCC 51142 by non-denaturing gel electrophoresis." Biochimica et Biophysica Acta (BBA) - Biomembranes **1468**(1–2): 150-160.

Tzfira, T., D. Weinthal, I. Marton, V. Zeevi, A. Zuker and A. Vainstein (2012). "Genome modifications in plant cells by custom-made restriction enzymes." Plant Biotechnology Journal **10**(4): 373-389.

Ullmann, G. M., M. Hauswald, A. Jensen, N. M. Kostic and E. W. Knapp (1997). "Comparison of the physiologically equivalent proteins cytochrome c6 and plastocyanin on the basis of their electrostatic potentials. Tryptophan 63 in cytochrome c6 may be isofunctional with tyrosine 83 in plastocyanin." Biochemistry **36**(51): 16187-16196.

Vermaas, W. (1996). "Molecular genetics of the cyanobacterium Synechocystis sp. PCC 6803: Principles and possible biotechnology applications." Journal of Applied Phycology **8**(4-5): 263-273.

Vermaas, W. F. J. (1994). "Molecular-Genetic Approaches to Study Photosynthetic and Respiratory Electron-Transport in Thylakoids from Cyanobacteria." Biochimica Et Biophysica Acta-Bioenergetics **1187**(2): 181-186.

Wang, B., S. Pugh, D. R. Nielsen, W. W. Zhang and D. R. Meldrum (2013). "Engineering cyanobacteria for photosynthetic production of 3-hydroxybutyrate directly from CO2." Metabolic Engineering **16**: 68-77.

Warden, J. T. and J. H. Golbeck (1986). "Photosystem I charge separation in the absence of centers A and B. II. ESR spectral characterization of center 'X' and correlation with optical signal 'A2'." Biochim Biophys Acta **849**(1): 25-31.

Warren, P. V., J. H. Golbeck and J. T. Warden (1993). "Charge recombination between P700+ and A1- occurs directly to the ground state of P700 in a photosystem I core devoid of FX, FB, and FA." Biochemistry **32**(3): 849-857.

Wedepohl, K. H. (1995). "The Composition of the Continental-Crust." Geochimica Et Cosmochimica Acta **59**(7): 1217-1232.

Weigel, M., P. Pesaresi and D. Leister (2003). "Tracking the function of the cytochrome c6-like protein in higher plants." Trends Plant Sci **8**(11): 513-517.

Widger, W. R., W. A. Cramer, M. Hermodson, D. Meyer and M. Gullifor (1984). "Purification and partial amino acid sequence of the chloroplast cytochrome b-559." J Biol Chem **259**(6): 3870-3876.

Widger, W. R., W. A. Cramer, R. G. Herrmann and A. Trebst (1984). "Sequence homology and structural similarity between cytochrome b of mitochondrial complex III and the chloroplast b6-f complex: position of the cytochrome b hemes in the membrane." Proc Natl Acad Sci U S A **81**(3): 674-678.

Wollman, F. A., L. Minai and R. Nechushtai (1999). "The biogenesis and assembly of photosynthetic proteins in thylakoid membranes1." Biochim Biophys Acta **1411**(1): 21-85.

Wu, X. Q., A. Zarka and S. Boussiba (2000). "A simplified protocol for preparing DNA from filamentous cyanobacteria." Plant Molecular Biology Reporter **18**(4): 385-392.

Xia, Z. C., R. W. Broadhurst, E. D. Laue, D. A. Bryant, J. H. Golbeck and D. S. Bendall (1998). "Structure and properties in solution of PsaD, an extrinsic polypeptide of photosystem I." European Journal of Biochemistry **255**(1): 309-316.

Xu, Q. and P. R. Chitnis (1995). "Organization of photosystem I polypeptides. Identification of PsaB domains that may interact with PsaD." Plant Physiol **108**(3): 1067-1075.

Xu, Q., D. Hoppe, V. P. Chitnis, W. R. Odom, J. A. Guikema and P. R. Chitnis (1995). "Mutational analysis of photosystem I polypeptides in the cyanobacterium Synechocystis sp. PCC 6803. Targeted inactivation of psaI reveals the function of psaI in the structural organization of psaL." J Biol Chem **270**(27): 16243-16250.

Xu, Q., Y. S. Jung, V. P. Chitnis, J. A. Guikema, J. H. Golbeck and P. R. Chitnis (1994). "Mutational analysis of photosystem I polypeptides in Synechocystis sp. PCC 6803. Subunit requirements for reduction of NADP+ mediated by ferredoxin and flavodoxin." J Biol Chem **269**(34): 21512-21518.

Xu, Q., W. R. Odom, J. A. Guikema, V. P. Chitnis and P. R. Chitnis (1994). "Targeted Deletion of Psaj from the Cyanobacterium Synechocystis Sp Pcc-6803 Indicates Structural Interactions between the Psaj and Psaf Subunits of Photosystem-I." Plant Molecular Biology **26**(1): 291-302.

Xu, Q., W. R. Odom, J. A. Guikema, V. P. Chitnis and P. R. Chitnis (1994). "Targeted deletion of psaJ from the cyanobacterium Synechocystis sp. PCC 6803 indicates structural interactions between the PsaJ and PsaF subunits of photosystem I." Plant Mol Biol **26**(1): 291-302.

Xu, Q., L. Yu, V. P. Chitnis and P. R. Chitnis (1994). "Function and organization of photosystem I in a cyanobacterial mutant strain that lacks PsaF and PsaJ subunits." J Biol Chem **269**(5): 3205-3211.

Xu, Q. A., L. A. Yu, V. P. Chitnis and P. R. Chitnis (1994). "Function and Organization of Photosystem-I in a Cyanobacterial Mutant Strain That Lacks Psaf and Psaj Subunits." Journal of Biological Chemistry **269**(5): 3205-3211.

Xu, W., H. Tang, Y. Wang and P. R. Chitnis (2001). "Proteins of the cyanobacterial photosystem I." Biochim Biophys Acta **1507**(1-3): 32-40.

Xu, W., Y. C. Wang, E. Taylor, A. Laujac, L. Y. Gao, S. Savikhin and P. R. Chitnis (2011). "Mutational Analysis of Photosystem I of Synechocystis sp PCC 6803: The Role of Four Conserved Aromatic Residues in the j-helix of PsaB." Plos One **6**(9).

Yehezkeli, O., R. Tel-Vered, D. Michaeli, R. Nechushtai and I. Willner (2013). "Photosystem I (PSI)/Photosystem II (PSII)-based photo-bioelectrochemical cells revealing directional generation of photocurrents." Small **9**(17): 2970-2978.

Yehezkeli, O., O. I. Wilner, R. Tel-Vered, D. Roizman-Sade, R. Nechushtai and I. Willner (2010). "Generation of Photocurrents by Bis-aniline-Cross-Linked Pt Nanoparticle/Photosystem I Composites on Electrodes." Journal of Physical Chemistry B **114**(45): 14383-14388.

You, C. and Y. H. P. Zhang (2013). "Cell-Free Biosystems for Biomanufacturing." Future Trends in Biotechnology **131**: 89-119.

Yu, J. P., L. B. Smart, Y. S. Jung, J. Golbeck and L. Mcintosh (1995). "Absence of Psac Subunit Allows Assembly of Photosystem-I Core but Prevents the Binding of Psad and Psae in Synechocystis Sp Pcc6803." Plant Molecular Biology **29**(2): 331-342.

Zanetti, G. and G. Merati (1987). "Interaction between photosystem I and ferredoxin. Identification by chemical cross-linking of the polypeptide which binds ferredoxin." Eur J Biochem **169**(1): 143-146.

Zhao, J., W. B. Snyder, U. Muhlenhoff, E. Rhiel, P. V. Warren, J. H. Golbeck and D. A. Bryant (1993). "Cloning and Characterization of the Psae Gene of the Cyanobacterium Synechococcus Sp Pcc 7002 - Characterization of a Psae Mutant and Overproduction of the Protein in Escherichia-Coli." Molecular Microbiology **9**(1): 183-194.

Zhao, J. D., P. V. Warren, N. Li, D. A. Bryant and J. H. Golbeck (1990). "Reconstitution of electron transport in photosystem I with PsaC and PsaD proteins expressed in Escherichia coli." FEBS Lett **276**(1-2): 175-180.

Zilber, A. L. and R. Malkin (1988). "Ferredoxin Cross-Links to a 22 kD Subunit of Photosystem I." Plant Physiol **88**(3): 810-814.

Vita

Khoa Dang Nguyen was born in Vietnam in 1984. He moved to the U.S.A. in 1990 and went to school in California. He later moved to Tennessee for high school and eventuall his undergraduate in Microbiology at UT, Knoxville. He later received his doctorate in biochemistry at UT Knoxville in the summer of 2016.